NTNU

Norwegian University of
Science and Technology

Coupled Transport of Heat, Mass and Charge in Ion Exchange Membranes

Aqueous Chloride Systems Relevant for
Harvesting of Low-Grade Waste Heat

Kim Roger Kristiansen

Chemistry
Submission date: May 2018
Supervisor: Signe Kjelstrup, IKJ

Norwegian University of Science and Technology
Department of Chemistry

Abstract

In this thesis, the theory of classical non-equilibrium thermodynamics is used as a tool for the analysis of transport processes in ion exchange membranes, and for designing experiments for the determination of coupling coefficients quantifying the degree of correlation between transport of heat, mass, and charge under operation.

Chapter 1, along with appendix A, give a brief account of the theoretical derivations and assumptions leading to the constitutive relations and an expression for the local entropy production, which are later applied to the special cases considered in chapters 2 and 3.

Chapter 2, along with appendix B, address the case of coupled transport of water and charge carriers across a selection of ion exchange membranes in a variety of aqueous alkali and alkali earth chloride solutions. Appendix B covers the derivation of the regression model needed for analyzing the measured data, which is also a generalization of previous work. It is generally found that the transference coefficient of water, defined as the average number of water molecules transported per unit of elementary charge transferred, decreases in magnitude with the size of the charge carrier. The sign of this coefficient indicates that for all membranes considered, the net transfer of water is in the same direction as the transfer of charge carrier, and correlations are confirmed between water transport and water content of the membranes, and also between water transport and the mass-corrected solvation entropy in external solution. The water permeability, defined as the volume flux of water per unit of pressure difference across the membrane, was also calculated by using the regression model. Although the errors in the permeability estimates are large, likely due to membrane deformation during measurements, the permeability is significantly reduced as the valence of the charge carrier is increased.

In chapter 3, we consider a non-isothermal cell in order to measure the thermoelectric properties of ion exchange membranes. A flow cell was designed and built specifically for these experiments. In order to combat the phenomenon of temperature polarization, the cell potential is measured with membranes stacked together in order to increase the effective membrane thickness. A non-linear model is developed in order to find the Seebeck coefficient, defined as the ratio of cell potential to temperature difference in the stationary state, as a function of the stack thickness. This model is then used for assessing the stack thickness required to eliminate temperature polarization, and to extrapolate to limiting values. The measured values of the Seebeck coefficients are then combined with the water transference coefficients from chapter 2 in order to calculate the transported entropies of the principal charge carriers in each membrane. The results indicate that in both cases considered here, heat is transported along with the charge carrier. The Thomson effect, which is a heat effect due to the temperature dependence of the entropy transfer, was found to be insignificant for all experimental conditions that were considered.

In chapter 4, we present conclusions and perspectives for further work, along with suggestions for improving the experimental techniques. The results of chapter 3 are used for discussing the possibility of enhancing the efficiency of salt power plants by using them as thermoelectric generators. Estimates based on these results indicate that a 40 K temperature difference can increase the cell potential in a typical salt power plant by up to 50 %.

Sammendrag

Dette masterprosjektet omfatter bruken av klassisk irreversibel termodynamikk for å analysere koplede transportprosesser i ionebyttermembraner, og utforming av eksperimenter der målinger av koblingskoeffisientene som beskriver korrelasjonene mellom transport av varme, masse, og ladning er ambisjonen.

Kapittel 1, sammen med appendiks A, gir en kortfattet oversikt over den teoretiske bakgrunnen og de fysiske antagelsene som leder til de grunnleggende transportrelasjonene og et uttrykk for den lokale entropiproduksjonen, som senere spesialiseres i kapittel 2 og 3.

Kapittel 2, sammen med appendiks B, tar for seg korrelasjonen mellom transport av vann og ladningsbærere gjennom en håndfull ionebyttermembraner i et utvalg vandige alkalie- og jordalkaliekloridløsninger. Appendiks B dekker utledningen av regresjonsmodellen som brukes til å analysere eksperimentelle data. Vanntransporttallet, definert som det gjennomsnittlige antall vannmolekyler transportert gjennom membranen per elementærladning, ble funnet å korrelere negativt med størrelsen på ladningsbæreren. Transporttallets fortegn indikerer at i alle tilfeller som ble undersøkt, ble vann i netto transportert i samme retning som den dominerende ladningsbæreren. Det ble i tillegg funnet korrelasjoner mellom transporttallet og både membranenes vanninnhold og massekorrigert solvatiseringsentropi i vandig løsning. Vannpermeabiliteten, definert som det volum av vann transportert per flateareal og trykkdifferanseenhet, ble også beregnet ut fra regresjonsresultater. Usikkerhetene i permeabilitetene er store, antageligvis grunnet deformasjon av membranene under trykkgradienten. Permeabiliteten ble funnet å bli signifikant redusert ved økende valens av ladningsbærer.

I kapittel 3 måles det termoelektriske potensialet over et lite utvalg membraner. Til dette formål, ble en helt ny termocelle tegnet og konstruert. For å redusere effekten av temperaturpolarisering i målingene, ble membranene stablet sammen i tykke stakker, slik at den effektive membrantykkelsen ble økt. En modell ble konstruert for å finne Seebeck-koeffisienten, definert som forholdet mellom cellepotensial og temperaturforskjell ved stasjonær tilstand, som funksjon av stakktykkelsen. Modellen ble brukt til å anslå hvor mange membraner som må stables sammen for å gjøre temperaturpolariseringseffekten neglisjerbar, og til å ekstrapolere til grenseverdier for den observerte Seebeck-koeffisienten. Disse målingene ble kombinert med vanntransporttallene fra kapittel 2 for å beregne den transporterte entropien til de dominerende ladningsbærerene i de forskjellige membranene. Resultatene indikere at i begge tilfellene som ble undersøkt, transporteres varmen i samme retning som ladningsbæreren. Thomsoneffekten, som er en varmeeffekt som følger av temperaturavhengigheten til entropitransporten, ble funnet å ikke være signifikant i noen av tilfellene som ble undersøkt.

I kapittel 4 gis konklusjoner felles for hele masterprosjektet, samt forslag til videre arbeid og eksperimentelle forbedringer. Deriblant diskuteres mulighetene for å øke effektiviteten til saltkraftverk ved å anvende kraftverket som en termoelektrisk generator. Resultatene indikerer at en temperaturforskjell på 40 K kan øke cellepotensialet i et saltkraftverk med opptil 50 %.

Acknowledgement

I thank my supervisor, prof. Signe Kjelstrup, for her sagacious counsel on the subject of classical non-equilibrium thermodynamics, and her contagious enthusiasm for its application in solving important and topical problems on a global scale. Her wise style of supervision allowed me to work in relative autonomy on this thesis work, while keeping herself an available and cardinal resource for its completion.

I thank prof. María Barragán at the University of Complutense in Madrid, Spain, for a fruitful and joyous collaboration. Her tremendous resourcefulness as an experimentalist has provided ample inspiration for the work in this thesis, and for my future endeavours in research.

I would like to thank Astrid F. Gunnarshaug for being an excellent colleague, who provided useful discussions on the subject matter, and valuable feedback on this text.

Special thanks to Geir Solem at the Faculty of Science's mechanical workshop, NTNU, for his help with realizing the design of the thermocell skeleton.

Kim R. Kristiansen

Table of Contents

1 Introduction and General Theory **1**
- 1.1 Background and Motivation . . . 2
- 1.2 The Entropy Production . . . 4
  - 1.2.1 Homogeneous Phases . . . 4
  - 1.2.2 Surfaces . . . 6

2 Streaming Potential and Electroosmosis **11**
- 2.1 Introduction . . . 12
- 2.2 Theory . . . 13
  - 2.2.1 The Aqueous Solution . . . 13
  - 2.2.2 The Membrane . . . 16
  - 2.2.3 The Electrodes . . . 20
  - 2.2.4 The Total Cell Potential . . . 22
  - 2.2.5 Time Dependence of the Electric Potential . . . 22
  - 2.2.6 Volume Flux and Water Permeability . . . 24
  - 2.2.7 Partial Molar Volume of Electrolyte and Dielectric Permittivity 24
- 2.3 Experimental . . . 25
- 2.4 Results and Discussion . . . 27

3 Seebeck Effect and Transported Entropy **39**
- 3.1 Introduction . . . 40
- 3.2 Theory . . . 41
  - 3.2.1 The Aqueous Solution . . . 42
  - 3.2.2 The Membrane . . . 47
  - 3.2.3 The Electrodes and External Circuit . . . 50
  - 3.2.4 The Total Cell Potential . . . 53
  - 3.2.5 Temperature Polarization . . . 54
  - 3.2.6 Concentration and Temperature Dependence . . . 56
  - 3.2.7 Entropy Production and Second Law Efficiency . . . 58
- 3.3 Experimental . . . 60
  - 3.3.1 Apparatus . . . 60
  - 3.3.2 Electrodes and Electrolyte . . . 62
  - 3.3.3 Membranes . . . 62

3.3.4 Measurement Procedures 63
3.4 Results and Discussion 63

4 Conclusions and Future Perspectives **73**
4.1 Streaming Potential Measurements 74
4.2 Thermoelectric Potential Measurements 76
4.3 Combining Salt Power and Waste Heat Harvesting 77

List of Symbols **79**

References **81**

A Microscopic Foundations of the Theory **87**

B Streaming Potential Regression Model **91**
B.1 Analytical Solution 91
B.2 Linear Regression Model 93
B.3 Choosing the Regression Interval 97
B.4 Choice of Model Order 99
B.5 Variance Estimation and Robustness 99

C Thermocell Design **101**

Chapter 1
Introduction and General Theory

We give here the background and motivation for the master thesis work, along with some general theory that will be applied in later chapters. Practical expressions for the entropy production are derived from assumptions of energy and mass conservation, and the second law of thermodynamics. Analogous expressions for the excess entropy production of two-dimensional surfaces, derived in a similar manner, will be useful for analyzing interfaces between bulk phases. A brief account of the statistical foundations of the theory, derived from classical statistical mechanics, is relegated to appendix A.

1.1 Background and Motivation

Among the principal instruments for meeting the growing international energy demands and restraining greenhouse gas emissions is the energy efficiency improvement of industrial processes [1, 2]. An investigation by Cullen and Allwood [3] indicates that low-temperature applications of high quality energy sources, such as electricity and fossil fuels, exhibits a loss of around 40 - 80 % of potentially useful energy in the form of waste heat, with heat exchange processes being the worst off. Further investigations [4] indicate that a substantial fraction (> 60 %) of this occurs as low-grade waste heat at temperatures below 100°C, with the largest share coming from electrical power production. The higher end of these temperatures overlap with the lower end of the temperature range of efficient waste heat harvesting processes such as the Rankine cycle, and the exploitation of thermal gradients at lower temperatures are mainly the domain of thermoelectric generators.

Thermoelectric phenomena are the macroscopic physical manifestations of statistical correlations between transport of heat and electric charge. The dynamical phenomenon is the transfer of heat associated with the transport of charge carriers, known as the Peltier effect. The reciprocal effect, which is the formation of an electric field due to a gradient in temperature, is called the Seebeck effect. The Peltier effect has a wide array of applications e.g. in heating and cooling, where temperature is regulated carefully by controlling heat transfer by means of passing an electric current through a thermoelectric system. The Seebeck effect can be used for extracting electrical work from a temperature difference, using a thermal driving force for an electric current.

Solid-state semiconducting devices are traditionally dominant in applications of thermoelectricity. As thermoelectric generators, their efficiencies typically range from 5 to 8 % of the theoretical maximum demanded by the second law of thermodynamics, and further development is largely restricted to expensive nanoscale-engineering [5]. This becomes one of the motivations for exploring a different concept for thermoelectric generators – the ion exchange membrane. Such membranes are already being used in the development of promising concepts in saline power production, where the energy potential of mixing between sea water and brackish water is exploited in areas such as estuaries, where the two aqueous solutions naturally meet. An interesting question to pose in this context is whether the salt power plants can at the same time be used as thermoelectric generators for extracting work from industrial waste heat. To give a quantitative answer to this question, an account of the thermoelectric properties of the ion exchange membranes in aqueous salt solutions is required.

The degree to which electrical work can be extracted from a temperature difference depends on the amount of heat transferred along with the charge carriers in the thermoelectric generator, called the *heat of transfer* of the relevant charge carrier. A large heat of transfer means that the system can transport a large amount of heat down the temperature gradient by driving the transport of charge carrier. This is a reversible effect that competes with the irreversible Fourier type diffusive heat transport. The loss of work by Joule heating is proportional to the electrical resistivity. An efficient generator in the second law sense is therefore characterized by a low thermal conductivity, a high electrical conductivity, and charge carriers with large heats of transfer. Reported values of the heats of transfer of ions in aqueous solution are typically two orders of magnitude greater than that of electrons in solid state semiconductors [6], and the thermal conductivities and fabrication costs of ion exchange membranes are relatively low [7]. This gives the impression that the prospects for applications of ion exchange membranes in aqueous electrolytes for thermoelectric power generation are resoundingly favourable.

Although the ion exchange membrane may sound like a remarkably good fit for this role so far, it is important to keep in mind that the membrane in aqueous solution constitutes a multi-component system, with several degrees of freedom associated with particle transport. In particular, it is important to keep in mind that the transport of charge carriers through the system couples not only to the transfer of heat, but also to the transport of other, neutral components. The transport of solvent along with charge carriers in a membrane system is known as electroosmosis, and affects the thermoelectric properties of the system because the solvent also carries heat. In order to fully understand the operation of the system as a thermoelectric generator, it is therefore important to also investigate this coupling effect, which is the subject of chapter 2. Combining knowledge of this coupling effect with knowledge of the thermoelectric potential of the system allows the estimation of the heats of transfer of the ions in the membrane, which is the subject of chapter 3.

While we restrict our attention to ion exchange membranes in aqueous solutions of chloride electrolytes in this thesis, the theoretical considerations will be of a general nature with respect to the choice of cation. Experimentally, we will explore water transport using several different cations, but will restrict our attention to sodium in the thermoelectric measurements, as it is the dominant cation in salt power applications. An important question that we seek to answer is whether it is feasible to improve the efficiency of salt power plants by creating temperature differences across their working membranes, e.g. by means of routing waste heat into the plant, and in which direction such a temperature gradient should be applied. Answering this question can be taken to be the principal aim of this thesis. The answer, in light of the theoretical and experimental results of the preceeding chapters, is proposed in chapter 4.

1.2 The Entropy Production

We identify the local entropy production as given by the linear force-flux relations and general conservation laws. In this thesis, we are dealing with gradients in temperature T, pressure P, and electrochemical potential $\tilde{\mu}$. The systems include homogeneous phases separated by surfaces. We will therefore treat couplings between the energy flux $\mathbf{J}_u$, and molar fluxes $\mathbf{J}_j$ of both ionic and neutral components. The notation and methodology presented here follows closely that of the book by Kjelstrup and Bedeaux [8]. In this work, we neglect viscous effects, electromagnetic polarization, and magnetic fields. Central to the theory is the local equilibrium hypothesis, which is the assumption that the system can be divided into microscopic volume elements that can each be treated as an equilibrium system at all times.

1.2.1 Homogeneous Phases

The starting point of our analysis is the differential of the internal energy U

$$\mathrm{d}U = T\mathrm{d}S - P\mathrm{d}V + \sum_j \tilde{\mu}_j \mathrm{d}N_j \tag{1.2.1}$$

with S the entropy, V the volume, and $\tilde{\mu}_j$ and N_j the electrochemical potential and number of particles of j, respectively. We rewrite this in terms of densities

$$V\mathrm{d}u + u\mathrm{d}V = VT\mathrm{d}s + Ts\mathrm{d}V - P\mathrm{d}V + \sum_j \tilde{\mu}_j V \mathrm{d}c_j + \sum_j \tilde{\mu}_j c_j \mathrm{d}V \tag{1.2.2}$$

with s and u the entropy and internal energy densities, and c_j the molar concentration of j. Homogeneity of u implies

$$u = Ts - P + \sum_j \tilde{\mu}_j c_j \tag{1.2.3}$$

such that subtracting $u\mathrm{d}V$ from both sides of the equation, and dividing throughout by V gives

$$\mathrm{d}u = T\mathrm{d}s + \sum_j \tilde{\mu}_j \mathrm{d}c_j \tag{1.2.4}$$

which is the local form of (1.2.1). The local equilibrium hypothesis allows us to identify these local variables with the macroscopic equilibrium quantities. Rearranging and dividing by an infinitesimal time interval $\mathrm{d}t$ gives

$$\frac{\mathrm{d}s}{\mathrm{d}t} = \frac{1}{T}\frac{\mathrm{d}u}{\mathrm{d}t} - \sum_j \frac{\tilde{\mu}_j}{T}\frac{\mathrm{d}c_j}{\mathrm{d}t} \tag{1.2.5}$$

The time derivatives of the different densities can be expressed by local conservation laws. Let $\mathbf{J}_s$ be the entropy flux. Then,

$$\frac{\mathrm{d}}{\mathrm{d}t}\int_\Omega s\mathrm{d}^3\mathbf{x} = \int_\Omega \sigma \mathrm{d}^3\mathbf{x} - \oint_{\partial\Omega} \mathbf{J}_s \cdot \hat{\mathbf{n}} \mathrm{d}^2\mathbf{x} = \int_\Omega (\sigma - \nabla \cdot \mathbf{J}_s)\, \mathrm{d}^3\mathbf{x} \tag{1.2.6}$$

in words, the total change in entropy in any volume element is equal to the total entropy production inside the element minus the total entropy flux out of it. The local form of this conservation law is

$$\frac{\mathrm{d}s}{\mathrm{d}t} + \nabla \cdot \mathbf{J}_s = \sigma \geq 0 \tag{1.2.7}$$

where the inequality expressing the second law has been included. For reversible processes, we have $\sigma = 0$, and entropy is conserved. For irreversible processes, $\sigma > 0$, and the total entropy of an isolated system increases with time.

The total energy is conserved, with the local form of the conservation law

$$\frac{\mathrm{d}u}{\mathrm{d}t} + \nabla \cdot \mathbf{J}_u = 0 \tag{1.2.8}$$

i.e. the total change in internal energy density is equal to minus the energy flux out of the volume element. Finally, conservation of mass gives

$$\frac{\mathrm{d}c_j}{\mathrm{d}t} + \nabla \cdot \mathbf{J}_j = \sum_k r^k \nu_j^k \tag{1.2.9}$$

which states that the total change in concentration of component j is minus the flux out of the element, plus whatever amount of j is produced by all the chemical reactions occuring with reaction rates r^k and stoichiometric coefficients ν_j^k. In the systems considered here, we assume that no chemical reactions occur in the homogeneous phases, and therefore $r^k = 0$ for all k. Inserting (1.2.8) and (1.2.9) into (1.2.5) and applying the product rule gives

$$\frac{\mathrm{d}s}{\mathrm{d}t} = -\nabla \cdot \underbrace{\left(\frac{\mathbf{J}_u - \sum_j \mathbf{J}_j \tilde{\mu}_j}{T} \right)}_{\mathbf{J}_s} + \underbrace{\mathbf{J}_u \cdot \nabla \left(\frac{1}{T} \right) + \sum_j \mathbf{J}_j \cdot \left(-\nabla \left(\frac{\tilde{\mu}_j}{T} \right) \right)}_{\sigma} \tag{1.2.10}$$

where we have identified the entropy flux and the entropy production. We see that the entropy production has the bilinear structure of euclidean dot products between fluxes and their conjugate driving forces, as in (A.13). This form of the entropy production is a fundamental starting point for analyzing homogeneous phases. We note that the energy flux in an electrochemical system is

$$\mathbf{J}_u = \mathbf{J}_q + \psi \mathbf{j} = \mathbf{J}_q + \sum_{j \in \{cc\}} z_j F \psi \mathbf{J}_j \tag{1.2.11}$$

where $\{cc\}$ is the set of charge carriers in the system, each with charge $z_j F$, ψ the electrostatic potential, and $\mathbf{J}_q$ the total heat flux. For deriving expressions defining experimentally available quantities, it is most often more convenient to recast the

entropy production into a form that uses the measurable heat flux $\mathbf{J}'_q := \mathbf{J}_q - \sum_j \mathbf{J}_j H_j$. We write out the electrochemical potentials

$$\nabla\tilde{\mu}_j = \nabla\mu_j + z_j F\nabla\psi \tag{1.2.12}$$

where $z_j = 0$ for neutral components. One can obtain the properly conjugated forces by the following transformation

$$\nabla\mu_j = \nabla\mu_{j,T} + \frac{\partial\mu_j}{\partial T}\nabla T = \nabla\mu_{j,T} + T^2 S_j \nabla\left(\frac{1}{T}\right) \tag{1.2.13}$$

such that

$$\nabla\left(\frac{\mu_j}{T}\right) = \frac{\nabla\mu_{j,T}}{T} + \left(\mu_j + TS_j\right)\nabla\left(\frac{1}{T}\right) = \frac{\nabla\mu_{j,T}}{T} + H_j\nabla\left(\frac{1}{T}\right) \tag{1.2.14}$$

with the result being that the second term from the chemical driving force cancels the enthalpy terms in the heat flux. We define the electric current density

$$\mathbf{j} = \sum_j z_j F\mathbf{J}_j \tag{1.2.15}$$

then, the entropy production is

$$\sigma = \left(\mathbf{J}'_q + \mathbf{j}\psi\right)\cdot\nabla\left(\frac{1}{T}\right) + \mathbf{j}\cdot\left(-\nabla\left(\frac{\psi}{T}\right)\right) + \sum_j \mathbf{J}_j\cdot\left(-\frac{\nabla\mu_{j,T}}{T}\right) \tag{1.2.16}$$

or, applying the product rule

$$\sigma = \mathbf{J}'_q\cdot\nabla\left(\frac{1}{T}\right) + \mathbf{j}\cdot\left(-\frac{\nabla\psi}{T}\right) + \sum_j \mathbf{J}_j\cdot\left(-\frac{\nabla\mu_{j,T}}{T}\right) \tag{1.2.17}$$

from which the conjugate flux-force pairs are easily identified. It is important to note that the measurable cell potential is not a difference in ψ. The measurable potential must be that representing the total work required to move the charge carrier involved in the electrode reactions, and will therefore also include its chemical potential. Rather than give an overly general treatment of this issue, we will obtain the experimentally available potential explicitly for the special cases involved.

1.2.2 Surfaces

In the systems considered in this work, there occur surfaces separating the homogeneous phases, which have thicknesses much smaller than the extent of the surrounding phases. The discrete nature of the surface calls for a slightly modified treatment, and an expression for entropy production of the surface will be derived for easy identification of the properly conjugated forces. We consider only transport normal to the surfaces, assume that the surface is isotropic with respect to coordinates normal to

the surface normal, and that the surfaces have no appreciable curvature. The entropy balance is

$$\frac{\mathrm{d}}{\mathrm{d}t}\int_\Omega s\mathrm{d}^3\mathbf{x} = \int_\Omega (\sigma - \nabla\cdot\mathbf{J}_s)\,\mathrm{d}^3\mathbf{x} \tag{1.2.18}$$

This time, the assumption of isotropy parallel to the surface allows the integration of two degrees of freedom in exchange for a factor of the total membrane surface area A. Furthermore, we define the one-dimensional integrals

$$s^s := \int_0^\delta s\mathrm{d}x \qquad\qquad \sigma^s := \int_0^\delta \sigma\mathrm{d}x \tag{1.2.19}$$

which we call the entropy density per unit surface area, and the entropy production per unit surface area, respectively. Letting $\delta \to 0$, these become *excess* quantities of the dividing surface between two homogeneous phases, which is additional to the entropy density in the bulk phases that meet at the surface. Finally, we apply the fundamental theorem of calculus

$$\int_0^\delta \frac{\partial}{\partial x} J_s\mathrm{d}x = J_s^{o,i} - J_s^{i,o} \tag{1.2.20}$$

which are the entropy fluxes out of the surface at point δ and into the surface at point 0. Scalar fluxes denote the flux components normal to the surface. The combined second law and entropy balance becomes

$$\frac{\mathrm{d}s^s}{\mathrm{d}t} + J_s^{o,i} - J_s^{i,o} = \sigma^s \geq 0 \tag{1.2.21}$$

Similar considerations of energy yield

$$\frac{\mathrm{d}u^s}{\mathrm{d}t} + J_u^{o,i} - J_u^{i,o} = 0 \tag{1.2.22}$$

and of mass

$$\frac{\mathrm{d}\Gamma_j}{\mathrm{d}t} + J_j^{o,i} - J_j^{i,o} = \sum_k r^k \nu_j^k \tag{1.2.23}$$

where Γ_j is the number of particles of j per unit surface area, also called the adsorption of j. Furthermore, we introduce the change in Gibbs energy $\Delta_n G^k$ due to process k, which can be chemical reactions or phase changes at the surface

$$\Delta_n G^k = \sum_j \mu_j^s\left(T^s\right)\nu_j^k \tag{1.2.24}$$

The local internal energy differential is [8]

$$\frac{\mathrm{d}s^s}{\mathrm{d}t} = \frac{1}{T^s}\frac{\mathrm{d}u^s}{\mathrm{d}t} - \sum_j \frac{\tilde{\mu}_j^s\left(T^s\right)}{T^s}\frac{\mathrm{d}\Gamma_j}{\mathrm{d}t} \tag{1.2.25}$$

The use of a thermodynamic formulation for such a small system as a dividing surface has been demonstrated to coincide with molecular dynamics results for as few as 8 particles [8], justifying its use here. Inserting (1.2.22) and (1.2.23) into (1.2.25) and comparing terms with (1.2.21) gives

$$\begin{aligned}\frac{\mathrm{d}s^s}{\mathrm{d}t} &= J_u^{i,o}\left(\frac{1}{T^s}-\frac{1}{T^{i,o}}\right)+J_u^{o,i}\left(\frac{1}{T^{o,i}}-\frac{1}{T^s}\right)+\sum_k r^k\left(-\frac{\Delta_n G^k}{T^s}\right)\\ &+\sum_j J_j^{i,o}\left(\frac{\tilde{\mu}_j^{i,o}\left(T^{i,o}\right)}{T^{i,o}}-\frac{\tilde{\mu}_j^s\left(T^s\right)}{T^s}\right)+\sum_j J_j^{o,i}\left(\frac{\tilde{\mu}_j^s\left(T^s\right)}{T^s}-\frac{\tilde{\mu}_j^{o,i}\left(T^{o,i}\right)}{T^{o,i}}\right)\\ &+\underbrace{\frac{1}{T^{i,o}}\left(J_u^{i,o}-\sum_j J_j^{i,o}\tilde{\mu}_j^{i,o}\left(T^{i,o}\right)\right)}_{J_s^{i,o}}-\underbrace{\frac{1}{T^{o,i}}\left(J_u^{o,i}-\sum_j J_j^{o,i}\tilde{\mu}_j^{o,i}\left(T^{o,i}\right)\right)}_{J_s^{o,i}}\end{aligned} \tag{1.2.26}$$

where the entropy fluxes are clearly identified. An important remark here is that this implies a linear coupling between r^k and the reaction affinities, which only holds very close to equilibrium. See e.g. [9] for a discussion. The entropy production is then made up of the remaining terms. We introduce the difference notation from [8]

$$\begin{aligned}\sigma^s &= J_u^{i,o}\Delta_{i,s}\left(\frac{1}{T}\right)+J_u^{o,i}\Delta_{s,o}\left(\frac{1}{T}\right)+\sum_k r^k\left(-\frac{\Delta_n G^k}{T^s}\right)\\ &+\sum_j J_j^{i,o}\left(-\Delta_{i,s}\left(\frac{\tilde{\mu}_j}{T}\right)\right)+\sum_j J_j^{o,i}\left(-\Delta_{s,o}\left(\frac{\tilde{\mu}_j}{T}\right)\right)\end{aligned} \tag{1.2.27}$$

We would again like to have a form of the entropy production using the measurable heat flux, as was derived for the homogeneous phases. The procedure is similar

$$\begin{aligned}\Delta_{i,s}\left(\frac{\mu_j}{T}\right) &= \frac{\mu_j^s\left(T^s\right)}{T^s}-\frac{\mu_j^{i,o}\left(T^{i,o}\right)}{T^{i,o}}-\frac{\mu_j^{i,o}\left(T^s\right)}{T^s}+\frac{\mu_j^{i,o}\left(T^s\right)}{T^s}\\ &= \frac{\Delta_{i,s}\mu_{j,T}\left(T^s\right)}{T^s}+\frac{\mu_j^{i,o}\left(T^s\right)}{T^s}-\frac{\mu_j^{i,o}\left(T^{i,o}\right)}{T^{i,o}}\end{aligned} \tag{1.2.28}$$

To first order in the temperature difference between one of the homogeneous phases and the surface, we have

$$\frac{\mu_j^{i,o}\left(T^s\right)}{T^s}=\frac{\mu_j^{i,o}\left(T^{i,o}\right)}{T^{i,o}}+\frac{\partial}{\partial T}\left(\frac{\mu_j^{i,o}}{T}\right)\Big|_{T^{i,o}}\left(T^s-T^{i,o}\right) \tag{1.2.29}$$

following the style of being first order in the temperature difference, we obtain by approximating $\left(T^{i,o}\right)^2\approx T^s T^{i,o}$

$$\frac{\partial}{\partial T}\left(\frac{\mu_j^{i,o}}{T}\right)\Big|_{T^{i,o}}=-\frac{T^{i,o}S_j^{i,o}\left(T^{i,o}\right)+\mu_j^{i,o}\left(T^{i,o}\right)}{\left(T^{i,o}\right)^2}\approx-\frac{H_j^{i,o}\left(T^{i,o}\right)}{T^s T^{i,o}} \tag{1.2.30}$$

thus

$$\Delta_{i,s}\left(\frac{\mu_j}{T}\right) \approx \frac{\Delta_{i,s}\mu_{j,T}\left(T^s\right)}{T^s} + H_j^{i,o}\left(T^{i,o}\right)\Delta_{i,s}\left(\frac{1}{T}\right) \tag{1.2.31}$$

where the second term cancels with the enthalpy terms in $J_q^{i,o}$, analogously with how the procedure went in the homogeneous phase. Similar arguments yield the same result for $J_q^{o,i}$, and the entropy production becomes

$$\begin{aligned}\sigma^s = {} & J_q'^{i,o}\Delta_{i,s}\left(\frac{1}{T}\right) + J_q'^{o,i}\Delta_{s,o}\left(\frac{1}{T}\right) + j\left(-\frac{\Delta_{i,o}\psi}{T^s}\right) + \sum_k r^k\left(-\frac{\Delta_n G^k}{T^s}\right) \\ & + \sum_j J_j^{i,o}\left(-\frac{\Delta_{i,s}\mu_{j,T}\left(T^s\right)}{T^s}\right) + \sum_j J_j^{o,i}\left(-\frac{\Delta_{s,o}\mu_{j,T}\left(T^s\right)}{T^s}\right)\end{aligned} \tag{1.2.32}$$

which is the form of the entropy production that will be used for surface contributions.

Chapter 2
Streaming Potential and Electroosmosis

A theoretical expression describing the electric cell potential of an isothermal cell with an ion exchange membrane separating two half-cells of aqueous chloride solution with Ag/AgCl electrodes in response to a pressure difference was derived in the framework of classical non-equilibrium thermodynamics. A linear regression model was developed to fit time-dependent cell potential data, with higher order correction terms than those used by previous workers. Streaming potentials, water permeabilities, and water content were measured on membranes in aqueous solutions of LiCl, NaCl, KCl, $MgCl_2$, $CaCl_2$, and $BaCl_2$ at 0.03 mol/kg, and, additionally, NaCl at 0.10 and 0.60 mol/kg. The membranes used were Nafion 115, Neosepta CMX and AMX, and Fumasep FKS-PET-75 and FAD-PET-75. Observed streaming potentials were found in the range 60 - 260 µV/bar, which is in the lower end of typical results for this type of membrane. Water transference coefficients were estimated by means of Saxen's relation, and range from 2 to 14 in magnitude. The sign of the water transference coefficient was found to be positive for all cation exchange membranes, and negative for the anion exchange membranes. This indicates that water is in each case transported in the same direction as the charge carrier. Water permeabilities were estimated by regression on the time-dependent cell potential, and was found to decrease with cation size in the cation exchange membranes. The water content of the membranes ranged from 10 to 30 mass percent, and was found to decrease with cation size in the cation exchange membranes, and was invariant with respect to the type of cation in the anion exchange membranes. A correlation was confirmed between the water content and the water transference coefficient in the Nafion 115 and Neosepta CMX membranes. A positive correlation is presented between the average number of water molecules transported with cations in the cation exchange membranes, and the Jones-Dole viscosity B-coefficients, which hints at a possible connection between water transport and structural bulk properties in external solution. Much of the data is subject to relatively large errors, likely due to deformation of the membranes under the pressure difference. Suggestions for improving the experimental techniques are proposed in chapter 4.

2.1 Introduction

The coupling process between fluxes of ions and solvent in electrochemical membrane systems is known as *electroosmosis*, which is a reversible transport phenomenon, in contrast to irreversible diffusion processes. In all applications of such systems where an electric current is used for extracting work, it is, for various reasons, important to consider the magnitude and direction of this effect. It affects the potential for moving charge carriers across the system, due to the additional work involved in the co-transport of solvent. Solvent transfer also affects the composition profiles in the membrane and in the external solution. The latter alteration gives a dynamical contribution to the concentration potential of the cell, while the former can manifest itself as a drying out of the membrane under operation, possibly leading to degradation of the membrane material.

Theoretical expressions for the design and interpretation of experiments are derived here in the framework of classical non-equilibrium thermodynamics, and the theoretical basis is grounded in works on thermodynamics such as Kjelstrup & Bedeaux [8] and de Groot & Mazur [9], more fundamentally based on linear response theory in classical non-equilibrium statistical mechanics [10]. The most important assumption in the theory is the local equilibrium hypothesis, which allows at all times the unambiguous definition of thermodynamic variables in the mesoscopic volume elements of the system.

We investigate in this work the electroosmotic transfer of water across ion exchange membranes in aqueous chloride solutions by an indirect method. Rather than measuring the amount of water transferred with electric currents directly, we measure the potential for volume transfer in the system, and relate this to the electroosmotic volume flux by means of an Onsager relation. This is done by measuring the electric cell potential in response to a pressure gradient across the membrane, known as the *streaming potential* of the cell. Notably, this particular Onsager relation, also known as Saxen's relation [9], was shown to hold experimentally by Brun and Vaula [11]. In this, we demonstrate how analysis of the volume changes occuring with the passage of an electric current can be used to estimate the mean number of water molecules transferred per elementary unit of charge passing through the system, called the *water transference coefficient* of the membrane.

The streaming potential method has been used previously by several workers, along with attempts to connect results to structural properties, see e.g. [12, 13, 14, 15, 16, 17, 18]. The dynamical contribution to the cell potential due to volume transfer down the pressure gradient was analyzed by Okada et al. [19], and we give a more general treatment of this problem in appendix B. We show how it is also possible to obtain the water permeability of the membrane by analyzing the time-dependent behaviour of the open circuit electric cell potential under the influence of the pressure gradient,

and give criteria for the validity of the regression model.

2.2 Theory

We consider an isothermal system of two chambers of aqueous metal chloride solution separated by an ion-exchange membrane. Each chamber has its own Ag/AgCl electrode, and the system is initially in global equilibrium. At one instant, the system is perturbed from equilibrium by an abrupt increase in pressure in one of the chambers. We assume that, apart from the electrode reactions, no chemical reactions occur in the system. We express fluxes within the rest frame of the membrane surface, with positive direction of vectorial quantities counter-clockwise in figure 2.1. We divide the system into three subsystems: the aqueous solution, the membrane, and the electrodes along with the external electrical circuit. We will then sum together the different contributions and analyze measurable quantities.

2.2.1 The Aqueous Solution

We treat the aqueous solution as a homogeneous and isotropic medium with no net flux of water, such that there is no pressure gradient in the bulk solution. The entropy production is then only due to fluxes of cations, $\mathbf{J}_{\mathrm{M}^{z+}}$, and of chloride anions, $\mathbf{J}_{\mathrm{Cl}^-}$.

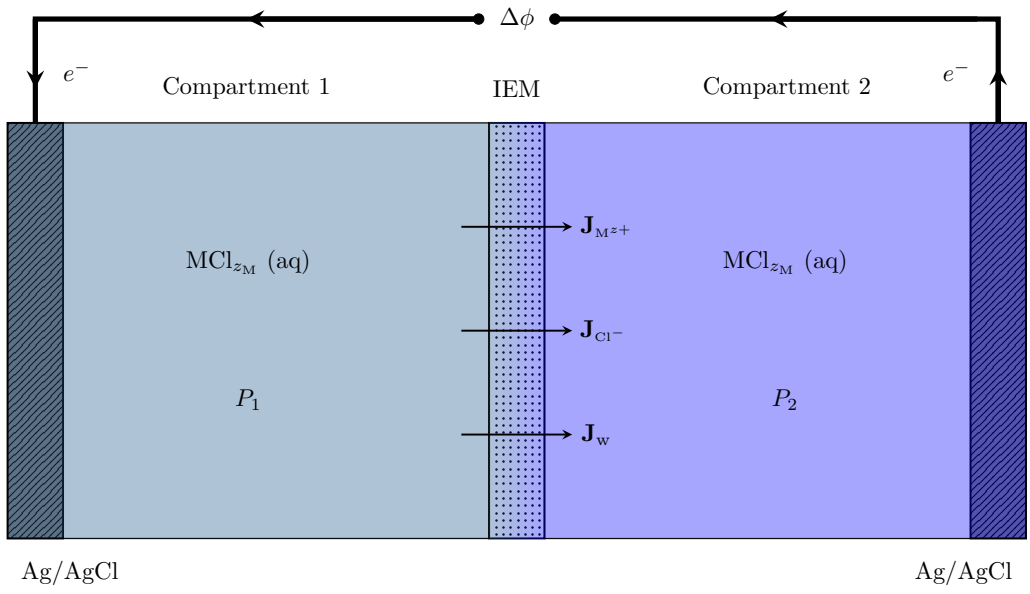

Figure 2.1: Sketch of the system considered in this paper. Two compartments of electrolyte solution are separated by an ion-exchange membrane, and kept at different pressures P_1 and P_2. The resulting fluxes in cation, chloride, and water ($\mathbf{J}_{\mathrm{M}^{z+}}$, $\mathbf{J}_{\mathrm{Cl}^-}$, and $\mathbf{J}_\mathrm{w}$) are indicated. The flux directions indicated are defined as the positive directions.

The entropy production is

$$\sigma_{\text{sol}} = -\frac{1}{T}\mathbf{J}_{\text{M}^{z+}} \cdot \nabla\tilde{\mu}_{\text{M}^{z+}} - \frac{1}{T}\mathbf{J}_{\text{Cl}^-} \cdot \nabla\tilde{\mu}_{\text{Cl}^-} \tag{2.2.1}$$

where T is the cell temperature, and $\tilde{\mu}_i$ is the electrochemical potential of i, which can be written as

$$\tilde{\mu}_i = \mu_i + z_i F\psi \tag{2.2.2}$$

where μ_i is the chemical potential of i, F is Faraday's constant, and ψ is the local electrostatic potential. The charge number z_i is defined such that $z_i F$ is the total charge of one mole of i. Since the system is isothermal, the chemical potentials are understood to be evaluated at the cell temperature.

The entropy production is invariant under the following set of transformations

$$\begin{aligned}
\mathbf{J}_{\text{e}} &= \mathbf{J}_{\text{M}^{z+}} \\
\mathbf{j} &= zF\mathbf{J}_{\text{M}^{z+}} - F\mathbf{J}_{\text{Cl}^-} \\
\mu_{\text{e}} &= \mu_{\text{M}^{z+}} + z\mu_{\text{Cl}^-} \\
\phi &= \psi - \frac{\mu_{\text{Cl}^-}}{F}
\end{aligned} \tag{2.2.3}$$

where $\mathbf{J}_{\text{e}}$ is the net flux of neutral electrolyte in the cell, $\mathbf{j}$ the electric current density, μ_{e} the chemical potential of the neutral electrolyte, z the valence number of the cation, and ϕ the measurable electric potential. The chemical potential of the charge carrier involved in the electrode reactions gives a measurable contribution to the measured electric potential difference between the electrodes. This is due to differences in chemical potential of the charge carrier presenting an additional contribution to the work required to move the particle. The measurable cell potential is therefore the difference in ϕ, and not ψ. Making the transformations in (2.2.3) has the advantage of yielding such measurable quantities. However, the flux of neutral electrolyte is non-local, and has no physical meaning in each subsystem locally. We will therefore use the locally valid form that we started out with to derive the relevant expressions, and then use the transformations in (2.2.3) to find experimentally available quantities.

We confine our interest to one-dimensional transport along the axis x orthogonal to the membrane and electrode surfaces. Applying the linear regression hypothesis [9] gives the following set of equations

$$\begin{bmatrix} J_{\text{M}^{z+}} \\ J_{\text{Cl}^-} \end{bmatrix} = -\frac{1}{T}\begin{bmatrix} L_{++} & L_{+-} \\ L_{-+} & L_{--} \end{bmatrix}\begin{bmatrix} \partial_x\tilde{\mu}_{\text{M}^{z+}} \\ \partial_x\tilde{\mu}_{\text{Cl}^-} \end{bmatrix} \tag{2.2.4}$$

We use (2.2.3) to identify the electric current density

$$\begin{aligned}
j &= -\frac{F}{T}\left(zL_{++} - L_{-+}\right)\partial_x\tilde{\mu}_{\text{M}^{z+}} - \frac{F}{T}\left(zL_{+-} - L_{--}\right)\partial_x\tilde{\mu}_{\text{Cl}^-} \\
&= -\frac{L_{\psi+}}{T}\partial_x\mu_{\text{M}^{z+}} - \frac{L_{\psi-}}{T}\partial_x\mu_{\text{Cl}^-} - \frac{L_{\psi\psi}}{T}\partial_x\psi
\end{aligned} \tag{2.2.5}$$

where the new coefficients are

$$\begin{aligned} L_{\psi+} &= F\left(zL_{++} - L_{-+}\right) & L_{\psi-} &= F\left(zL_{+-} - L_{--}\right) \\ L_{\psi\psi} &= F^2\left[z^2 L_{++} + L_{--} + z\left(L_{-+} + L_{+-}\right)\right] \end{aligned} \tag{2.2.6}$$

which inherit the Onsager symmetry of the original coefficients. We show this for one of the flux equations by writing out the electrochemical potentials

$$J_{\mathrm{M}^{z+}} = -\frac{L_{++}}{T}\partial_x \mu_{\mathrm{M}^{z+}} - \frac{L_{+-}}{T}\partial_x \mu_{\mathrm{Cl}^-} - \frac{1}{T}\underbrace{F\left(zL_{++} - L_{+-}\right)}_{L_{+\psi}}\partial_x \psi \tag{2.2.7}$$

where we see that if $L_{+-} = L_{-+}$, then also $L_{+\psi} = L_{\psi+}$. The same relation can be shown for $L_{-\psi} = L_{\psi-}$. We find from (2.2.5) the open circuit (zero current) electric field

$$\left(\partial_x \psi\right)_{j=0} = -\frac{L_{\psi+}}{L_{\psi\psi}}\partial_x \mu_{\mathrm{M}^{z+}} - \frac{L_{\psi-}}{L_{\psi\psi}}\partial_x \mu_{\mathrm{Cl}^-} \tag{2.2.8}$$

and we can identify the coefficients by exploiting the Onsager symmetries

$$zF\frac{L_{\psi+}}{L_{\psi\psi}} = zF\frac{L_{+\psi}}{L_{\psi\psi}} = zF\left(\frac{J_{\mathrm{M}^+}}{j}\right)_{\mathrm{d}\mu=0} =: t_{\mathrm{M}^{z+}} \tag{2.2.9}$$

where $\mathrm{d}\mu = 0$ means uniform composition in the bulk phase. The coefficient $t_{\mathrm{M}^{z+}}$ is the *transport number* of the cation, and is defined as the fraction of the electric charge transported in the system by the cation. Similarly, we find

$$-F\frac{L_{\psi-}}{L_{\psi\psi}} = -F\frac{L_{-\psi}}{L_{\psi\psi}} = -F\left(\frac{J_{\mathrm{Cl}^-}}{j}\right)_{\mathrm{d}\mu=0} =: t_{\mathrm{Cl}^-} \tag{2.2.10}$$

the transport number of chloride. We have already assumed that these are the only charge carriers in the solution, and therefore obtain from the definition of the electric current density that

$$t_{\mathrm{M}^{z+}} + t_{\mathrm{Cl}^-} = 1 \tag{2.2.11}$$

Using these relations, along with (2.2.3) to identify μ_{e} and ϕ, (2.2.8) becomes

$$\left(\partial_x \phi\right)_{j=0} = -\frac{t_{\mathrm{M}^{z+}}}{zF}\partial_x \mu_{\mathrm{e}} \tag{2.2.12}$$

We introduce the electrolyte activity model in order to obtain a more explicit composition dependence

$$\partial_x \mu_{\mathrm{e}} = \frac{\partial \mu_{\mathrm{e}}}{\partial m_{\mathrm{e}}}\partial_x m_{\mathrm{e}} = \frac{\nu RT}{m_{\mathrm{e}}}\left(1 + \frac{\partial \ln\left(\gamma_{\mathrm{e}}\right)}{\partial \ln\left(m_{\mathrm{e}}\right)}\right)\partial_x m_{\mathrm{e}} = \Gamma \nu RT \partial_x \ln\left(m_{\mathrm{e}}\right) \tag{2.2.13}$$

where m_{e} and γ_{e} are the molality and the mean molal activity coefficient of the electrolyte, R the universal gas constant, and ν the total number of ions per molecule

of neutral electrolyte. We have introduced the thermodynamic factor, Γ, in order to ease the notation. (2.2.12) is then

$$(\partial_x \phi)_{j=0} = -\frac{\Gamma \nu RT t_{\mathrm{M}^{z+}}}{zF} \partial_x \ln(m_{\mathrm{e}}) \tag{2.2.14}$$

For the sake of integration, we parameterize ϕ and m_{e} as mutually independent functions of position, such that

$$\partial_x \phi \mathrm{d}x = \mathrm{d}\phi \qquad \partial_x \ln(m_{\mathrm{e}})\,\mathrm{d}x = \mathrm{d}\ln(m_{\mathrm{e}}) \tag{2.2.15}$$

We will consider small concentration differences in this system. Neglecting the concentration dependence of Γ and $t_{\mathrm{M}^{z+}}$, integration of (2.2.14) is trivial, and the contribution from compartment 1 is

$$\Delta_{1,\ell}\phi = -\frac{\Gamma(P_1)\,\nu RT t_{\mathrm{M}^{z+}}(P_1)}{zF} \ln\left(\frac{m_\ell}{m_1}\right) \tag{2.2.16}$$

where we have introduced the difference notation $\Delta_{i,k} f = f_k - f_i$, and denoted by subscripts 1 and ℓ the positions close to the electrode and close to the membrane surface in compartment 1, respectively. We will denote by subscripts r and 2 the membrane surface and electrode in compartment 2. Equivalently, integration of (2.2.14) over compartment 2 gives

$$\Delta_{r,2}\phi = -\frac{\Gamma(P_2)\,\nu RT t_{\mathrm{M}^{z+}}(P_2)}{zF} \ln\left(\frac{m_2}{m_r}\right) \tag{2.2.17}$$

Neglecting the pressure dependence of Γ and $t_{\mathrm{M}^{z+}}$, and taking $m_1 = m_2$ then adding the two contributions gives a simple expression for the total contribution

$$\Delta\phi_{\mathrm{sol}} = \frac{\Gamma \nu RT t_{\mathrm{M}^{z+}}}{zF} \ln\left(\frac{m_r}{m_\ell}\right) \tag{2.2.18}$$

While we will seek to keep the composition profile as close as possible to uniform, this contribution will be important in practice due to composition changes driven by the pressure difference. This dynamical effect will be discussed in detail in section 2.2.5.

2.2.2 The Membrane

We treat the membrane as a homogeneous phase, separated from the two bulk aqueous solutions by two membrane-solution interfaces. The treatment of the membrane bulk is similar to that of the aqueous solution. Here, we also allow for a net flux of water as a neutral component, by means of a hydrodynamical flow driven by the pressure gradient, and through electroosmotic transfer along with the charge carriers. We will denote by a bar any quantity evaluated in the membrane phase. The entropy production is

$$\sigma_{\mathrm{mem}} = -J_{\mathrm{M}^{z+}} \frac{\partial_x \tilde{\mu}_{\mathrm{M}^{z+}}}{T} - J_{\mathrm{Cl}^-} \frac{\partial_x \tilde{\mu}_{\mathrm{Cl}^-}}{T} - J_{\mathrm{w}} \frac{\partial_x \mu_{\mathrm{w}}}{T} \tag{2.2.19}$$

where the subscript w refers to water. The corresponding flux equations follow predictably

$$\begin{bmatrix} J_{\mathrm{M}^{z+}} \\ J_{\mathrm{Cl}^-} \\ J_{\mathrm{w}} \end{bmatrix} = -\frac{1}{T} \begin{bmatrix} \overline{L}_{++} & \overline{L}_{+-} & \overline{L}_{+\mathrm{w}} \\ \overline{L}_{-+} & \overline{L}_{--} & \overline{L}_{-\mathrm{w}} \\ \overline{L}_{\mathrm{w}+} & \overline{L}_{\mathrm{w}-} & \overline{L}_{\mathrm{ww}} \end{bmatrix} \begin{bmatrix} \partial_x \tilde{\mu}_{\mathrm{M}^{z+}} \\ \partial_x \tilde{\mu}_{\mathrm{Cl}^-} \\ \partial_x \mu_{\mathrm{w}} \end{bmatrix} \tag{2.2.20}$$

Following the same procedure as for the aqueous solution, we identify the electric current density

$$j = -\frac{\overline{L}_{\psi+}}{T}\partial_x \mu_{\mathrm{M}^{z+}} - \frac{\overline{L}_{\psi-}}{T}\partial_x \mu_{\mathrm{Cl}^-} - \frac{\overline{L}_{\psi\mathrm{w}}}{T}\partial_x \mu_{\mathrm{w}} - \frac{\overline{L}_{\psi\psi}}{T}\partial_x \psi \tag{2.2.21}$$

with the coefficients defined similarly to those in the aqueous solution, and can by the same procedure be shown to inherit the Onsager symmetries. The open circuit electric field is then given by

$$(\partial_x \psi)_{j=0} = -\frac{\overline{L}_{\psi+}}{\overline{L}_{\psi\psi}}\partial_x \mu_{\mathrm{M}^{z+}} - \frac{\overline{L}_{\psi-}}{\overline{L}_{\psi\psi}}\partial_x \mu_{\mathrm{Cl}^-} - \frac{\overline{L}_{\psi\mathrm{w}}}{\overline{L}_{\psi\psi}}\partial_x \mu_{\mathrm{w}} \tag{2.2.22}$$

and we find the ionic transport numbers in the membrane phase

$$\begin{aligned} zF\frac{\overline{L}_{\psi+}}{\overline{L}_{\psi\psi}} = zF\frac{\overline{L}_{+\psi}}{\overline{L}_{\psi\psi}} = zF\left(\frac{J_{\mathrm{M}^{z+}}}{j}\right)_{\mathrm{d}\mu=0} =: \bar{t}_{\mathrm{M}^{z+}} \\ -F\frac{\overline{L}_{\psi-}}{\overline{L}_{\psi\psi}} = -F\frac{\overline{L}_{-\psi}}{\overline{L}_{\psi\psi}} = -F\left(\frac{J_{\mathrm{Cl}^-}}{j}\right)_{\mathrm{d}\mu=0} =: \bar{t}_{\mathrm{Cl}^-} \end{aligned} \tag{2.2.23}$$

and the transference coefficient of water

$$F\frac{\overline{L}_{\psi\mathrm{w}}}{\overline{L}_{\psi\psi}} = F\frac{\overline{L}_{\mathrm{w}\psi}}{\overline{L}_{\psi\psi}} = F\left(\frac{J_{\mathrm{w}}}{j}\right)_{\mathrm{d}\mu=0} =: \bar{t}_{\mathrm{w}} \tag{2.2.24}$$

Similarly to the situation in the aqueous solution, the ionic transport numbers are subject to the constraint that their sum equals unity. Using this constraint along with (2.2.3), we find the measurable electric potential

$$(\partial_x \phi)_{j=0} = -\frac{\bar{t}_{\mathrm{M}^{z+}}}{zF}\partial_x \mu_{\mathrm{e}} - \frac{\bar{t}_{\mathrm{w}}}{F}\partial_x \mu_{\mathrm{w}} \tag{2.2.25}$$

Before proceeding to integrate this equation, we note that the flux equation for water gives

$$\partial_x \mu_{\mathrm{w}} = -\frac{\bar{\ell}_{\mathrm{w}+}}{\bar{\ell}_{\mathrm{ww}}}\partial_x \mu_{\mathrm{M}^{z+}} - \frac{\bar{\ell}_{\mathrm{w}-}}{\bar{\ell}_{\mathrm{ww}}}\partial_x \mu_{\mathrm{Cl}^-} - \frac{T}{\bar{\ell}_{\mathrm{ww}}}\left(J_{\mathrm{w}}\right)_{j=0} \tag{2.2.26}$$

where the open circuit coefficients are

$$\bar{\ell}_{ij} := \overline{L}_{ij} - \frac{\overline{L}_{i\psi}\overline{L}_{\psi j}}{\overline{L}_{\psi\psi}} \tag{2.2.27}$$

We now use that water is in excess compared to the electrolyte, such that each moving volume element is dominated by water flux, and the solvated ions are carried along. This allows us to set

$$\begin{aligned}\frac{\overline{\ell}_{\mathrm{w}+}}{\overline{\ell}_{\mathrm{ww}}} &= \frac{\overline{\ell}_{+\mathrm{w}}}{\overline{\ell}_{\mathrm{ww}}} = \left(\frac{J_{\mathrm{M}^{z+}}}{J_{\mathrm{w}}}\right)_{j=0,\mathrm{d}\mu=0} = M_{\mathrm{w}} m_{\mathrm{e}} \\ \frac{\overline{\ell}_{\mathrm{w}-}}{\overline{\ell}_{\mathrm{ww}}} &= \frac{\overline{\ell}_{-\mathrm{w}}}{\overline{\ell}_{\mathrm{ww}}} = \left(\frac{J_{\mathrm{Cl}^-}}{J_{\mathrm{w}}}\right)_{j=0,\mathrm{d}\mu=0} = z M_{\mathrm{w}} m_{\mathrm{e}}\end{aligned} \tag{2.2.28}$$

where M_{w} is the molar mass of water. Furthermore, we assume that the open circuit water flux is mainly driven by the gradient in pressure, such that

$$(J_{\mathrm{w}})_{j=0} \approx -\frac{\overline{\ell}_{\mathrm{ww}}}{T}\overline{V}_{\mathrm{w}}\partial_x P \tag{2.2.29}$$

with $\overline{V}_{\mathrm{w}}$ the molar volume of water in the membrane. Using the relations (2.2.3), we find

$$\partial_x \mu_{\mathrm{w}} = -M_{\mathrm{w}} m_{\mathrm{e}} \partial_x \mu_{\mathrm{e}} + \overline{V}_{\mathrm{w}} \partial_x P \tag{2.2.30}$$

also, we rewrite the gradient in the chemical potential of electrolyte

$$\partial_x \mu_{\mathrm{e}} = \frac{\partial \mu_{\mathrm{e}}}{\partial m_{\mathrm{e}}}\partial_x m_{\mathrm{e}} + \frac{\partial \mu_{\mathrm{e}}}{\partial P}\partial_x P = \frac{\overline{\Gamma}\nu RT}{m_{\mathrm{e}}}\partial_x m_{\mathrm{e}} + \overline{V}_{\mathrm{e}}\partial_x P \tag{2.2.31}$$

such that (2.2.25) becomes

$$\begin{aligned}(\partial_x \phi)_{j=0} = &-\frac{1}{F}\left(\left(\frac{\bar{t}_{\mathrm{M}^{z+}}}{z} - M_{\mathrm{w}} m_{\mathrm{e}} \bar{t}_{\mathrm{w}}\right)\overline{V}_{\mathrm{e}} + \bar{t}_{\mathrm{w}}\overline{V}_{\mathrm{w}}\right)\partial_x P \\ &- \frac{\overline{\Gamma}\nu RT}{F}\left(\frac{\bar{t}_{\mathrm{M}^{z+}}}{z m_{\mathrm{e}}} - M_{\mathrm{w}}\bar{t}_{\mathrm{w}}\right)\partial_x m_{\mathrm{e}}\end{aligned} \tag{2.2.32}$$

We make the approximation $(m_r - m_\ell) \approx \hat{m}\ln(m_r/m_\ell)$, with $\hat{m}$ the mean molality, and define the *apparent* transference coefficient of the electrolyte

$$\bar{t}_a := \frac{\bar{t}_{\mathrm{M}^{z+}}}{z} - M_{\mathrm{w}}\hat{m}\bar{t}_{\mathrm{w}} \qquad t_a := \frac{t_{\mathrm{M}^{z+}}}{z} \tag{2.2.33}$$

We follow again the procedure of parameterizing the profiles in electric potential, pressure, and composition as explicit functions of position only, such that

$$\partial_x \phi \mathrm{d}x = \mathrm{d}\phi \qquad \partial_x P \mathrm{d}x = \mathrm{d}P \qquad \partial_x m_{\mathrm{e}} \mathrm{d}x = \mathrm{d}m_{\mathrm{e}} \tag{2.2.34}$$

We neglect second derivatives of the chemical potentials, and assume that $\bar{t}_{\mathrm{M}^{z+}}$ and $\bar{t}_{\mathrm{w}}$ are constant over the concentration range. Integration over the membrane gives

$$\Delta\phi'_{\mathrm{mem}} = -\frac{1}{F}\left(\bar{t}_a\overline{V}_{\mathrm{e}} + \bar{t}_{\mathrm{w}}\overline{V}_{\mathrm{w}}\right)\Delta P - \frac{\overline{\Gamma}\nu RT}{F}\bar{t}_a \ln\left(\frac{m_r}{m_\ell}\right) \tag{2.2.35}$$

where we see that the potential difference over the membrane has one term similar to the contribution from the aqueous solution, being logarithmic in the concentration difference. It occurs here with the opposite sign, and with the membrane value of the cationic transport number instead. The coupling to water transport is taken into account by the apparent transference coefficient, which will be discussed in more detail in section 2.2.5. Next comes the question of the membrane phase molar volumes and thermodynamic factor. We will now show that we can replace these quantities with those in aqueous solution, by adding the membrane surface contributions to the electric potential. Assuming a continuous temperature profile, the temperature is constant over the surface. The steady state entropy production of one such surface is

$$\sigma_{\text{surf}} = -J_{\text{M}^{z+}} \frac{\Delta_{i,o}\tilde{\mu}_{\text{M}^{z+}}}{T} - J_{\text{Cl}^-} \frac{\Delta_{i,o}\tilde{\mu}_{\text{Cl}^-}}{T} - J_{\text{w}} \frac{\Delta_{i,o}\mu_{\text{w}}}{T} \tag{2.2.36}$$

Following the standard prescription for the flux equations, as was done for the bulk phase, we can again find the electric current density through the surface

$$j = -\frac{L^s_{\psi+}}{T}\Delta_{i,o}\mu_{\text{M}^{z+}} - \frac{L^s_{\psi-}}{T}\Delta_{i,o}\mu_{\text{Cl}^-} - \frac{L^s_{\psi\text{w}}}{T}\Delta_{i,o}\mu_{\text{w}} - \frac{L^s_{\psi\psi}}{T}\Delta_{i,o}\psi \tag{2.2.37}$$

In the exact same manner as for the bulk phase, we find the transference coefficients of the different components at the surface. Continuity of the fluxes demands that these transport numbers are the same as in the membrane bulk, i.e. that there is no accumulation of water or charge at the surfaces in the steady state. The open circuit electric potential across the surface is

$$\left(\Delta_{i,o}\psi\right)_{j=0} = -\frac{\bar{t}_{\text{M}^{z+}}}{zF}\Delta_{i,o}\mu_{\text{M}^{z+}} + \frac{\bar{t}_{\text{Cl}^-}}{F}\Delta_{i,o}\mu_{\text{Cl}^-} - \frac{\bar{t}_{\text{w}}}{F}\Delta_{i,o}\mu_{\text{w}} \tag{2.2.38}$$

then, subtracting the difference in the chemical potential of chloride gives the measurable potential. It is worth noting that if the surface is in equilibrium with the aqueous solution, then all these contributions vanish. Identifying the electrolyte chemical potential and decomposing it to a composition and a pressure term, and also making the same volume flux argument as in (2.2.28), we obtain at the surface in compartment 1

$$\left(\Delta_{i,o}\phi^{(1)}\right)_{j=0} = -\frac{\nu RT}{zF}\bar{t}_a\left(\overline{\Gamma} - \Gamma\right)\ln m_\ell - \frac{P_1}{F}\left(\bar{t}_a\left(\overline{V}_{\text{e}} - V_{\text{e}}\right) + \bar{t}_{\text{w}}\left(\overline{V}_{\text{w}} - V_{\text{w}}\right)\right) \tag{2.2.39}$$

similarly, we obtain the jump across the surface in compartment 2

$$\left(\Delta_{i,o}\phi^{(2)}\right)_{j=0} = \frac{\nu RT}{zF}\bar{t}_a\left(\overline{\Gamma} - \Gamma\right)\ln m_r + \frac{P_2}{F}\left(\bar{t}_a\left(\overline{V}_{\text{e}} - V_{\text{e}}\right) + \bar{t}_{\text{w}}\left(\overline{V}_{\text{w}} - V_{\text{w}}\right)\right) \tag{2.2.40}$$

then, approximating the activity jumps with differences in thermodynamic factors, and adding the two contributions gives

$$\Delta\phi_{\text{surf}} = \frac{\nu RT}{zF}\bar{t}_a\left(\overline{\Gamma} - \Gamma\right)\ln\left(\frac{m_r}{m_\ell}\right) + \frac{\Delta P}{F}\left(\bar{t}_a\left(\overline{V}_{\text{e}} - V_{\text{e}}\right) + \bar{t}_{\text{w}}\left(\overline{V}_{\text{w}} - V_{\text{w}}\right)\right) \tag{2.2.41}$$

Then, adding this to (2.2.35) gives the total membrane contribution. We define the streaming potential of the membrane

$$\beta^{\text{mem}} := -\frac{1}{F}\left(\bar{t}_a V_{\text{e}} + \bar{t}_{\text{w}} V_{\text{w}}\right) \tag{2.2.42}$$

such that

$$\Delta\phi_{\text{mem}} = \beta^{\text{mem}}\Delta P - \frac{\Gamma\nu RT}{F}\bar{t}_a \ln\left(\frac{m_r}{m_\ell}\right) \tag{2.2.43}$$

which is the same expression as in (2.2.35), but with the partial molar volumes and thermodynamic factors of the membrane phase replaced by those in aqueous solution. An important result here is that this expression is exactly the same whether the membrane surface is in equilibrium with the aqueous solution or not. The often-invoked assumption that the surface is in equilibrium with the external solution is therefore superfluous in the steady state case.

2.2.3 The Electrodes

The electrode surfaces host the chemical reactions needed to change charge carrier from chloride in solution to electron in the external circuit. We model this as adsorption of charge carriers to the electrode surface, with a chemical reaction transforming the electrode materials. The entropy production is

$$\sigma_{\text{el}} = -J^i_{\text{Cl}^-}\frac{\Delta_{i,s}\tilde{\mu}_{\text{Cl}^-}}{T} - J^o_{\text{e}^-}\frac{\Delta_{s,o}\tilde{\mu}_{\text{e}^-}}{T} - r^c\frac{\Delta_n G}{T} \tag{2.2.44}$$

where subscript e^- pertains to electrons, r^c is the rate of the chemical reaction, and $\Delta_n G$ is the change in Gibbs energy due to exchange of neutral components in the chemical reaction. The reaction rate is determined by the electric current

$$r^c = j/F \tag{2.2.45}$$

while the fluxes of charge carrier are what make up the electric current

$$J^i_{\text{Cl}^-} = J^o_{\text{e}^-} = -j/F \tag{2.2.46}$$

which means that there is only one independent flux-force pair in the entropy production. The electrochemical potentials are

$$\begin{aligned}\Delta_{i,s}\tilde{\mu}_{\text{Cl}^-} &= \Delta_{i,s}\mu_{\text{Cl}^-} - F\Delta_{i,s}\psi = -F\Delta_{i,s}\phi\\ \Delta_{s,o}\tilde{\mu}_{\text{e}^-} &= \Delta_{s,o}\mu_{\text{e}^-} - F\Delta_{s,o}\psi = -F\Delta_{s,o}\phi\end{aligned} \tag{2.2.47}$$

The entropy production is then

$$\sigma_{\text{el}} = -\frac{j}{T}\left(\Delta_{i,o}\phi + \frac{\Delta_n G}{F}\right) \tag{2.2.48}$$

from which we observe that reversible conditions ($\sigma_{\rm el} = 0$) for $j = 0$. The linear flux-force relation gives

$$\left(\Delta_{i,o}\phi\right)_{j=0} = -\frac{\Delta_n G}{F} \tag{2.2.49}$$

We can now use this equation to assess the electrode contribution to the cell potential. For each Faraday of positive charge transferred from compartment 1 to 2 through the membrane, we have the reaction

$$\mathrm{Ag} + \mathrm{Cl}^- \rightarrow \mathrm{AgCl} + \mathrm{e}^- \tag{2.2.50}$$

compensating for the loss of positive charge in compartment 1, allowing negative charge to be carried by means of the electron from compartment 1 to 2 through the external circuit, with the opposite reaction occuring in compartment 2. The Gibbs energy change due to neutral components in compartment 1 is

$$\Delta_n G^{(1)} = \mu^{(1)}_{\rm AgCl}\left(P_1\right) - \mu^{(1)}_{\rm Ag}\left(P_1\right) \tag{2.2.51}$$

and in compartment 2

$$\Delta_n G^{(2)} = \mu^{(2)}_{\rm Ag}\left(P_2\right) - \mu^{(2)}_{\rm AgCl}\left(P_2\right) \tag{2.2.52}$$

we distinguish the chemical potentials at each electrode in order to take into account that the electrode surfaces can be slightly different, giving rise to a *bias potential*. We denote mean values between electrodes by a hat

$$\hat{\mu}_i := \frac{\mu^{(1)}_i + \mu^{(2)}_i}{2} \tag{2.2.53}$$

and the deviation parameters

$$\varepsilon_i := \hat{\mu}_i - \mu^{(1)}_i = \mu^{(2)}_i - \hat{\mu}_i \tag{2.2.54}$$

The total Gibbs energy change is then, to first order in the pressure difference

$$\Delta_n G = \left(\hat{V}_{\rm Ag} - \hat{V}_{\rm AgCl}\right)\Delta P + 2\left(\varepsilon_{\rm Ag} - \varepsilon_{\rm AgCl}\right) + 2\left(V^{\varepsilon}_{\rm Ag} - V^{\varepsilon}_{\rm AgCl}\right)\Delta P \tag{2.2.55}$$

where the V^{ε}_i is the deviation in molar volume. We will take the electrode materials to be incompressible, such that the volume deviation vanishes. Then

$$\Delta_n G = \left(V_{\rm Ag} - V_{\rm AgCl}\right)\Delta P + \Delta_n G_{\rm bias} \tag{2.2.56}$$

with $\Delta_n G_{\rm bias} = 2\left(\varepsilon_{\rm Ag} - \varepsilon_{\rm AgCl}\right)$ being the Gibbs energy of the electrode bias. We define the electrode streaming potential

$$\beta^{\rm el} := \frac{V_{\rm AgCl} - V_{\rm Ag}}{F} \tag{2.2.57}$$

The electrode contribution to the cell potential is

$$\Delta\phi_{\rm el} = -\frac{\Delta_n G}{F} = \beta^{\rm el}\Delta P + \Delta\phi_{\rm bias} \tag{2.2.58}$$

which gives a measurable contribution to the observed streaming potential, and a bias term that we have assumed to be pressure-independent, such that it can be subtracted by a baseline measurement.

2.2.4 The Total Cell Potential

We now add up the contributions to the observed cell potential. Adding together (2.2.18), (2.2.43), and (2.2.58) gives

$$\Delta\phi = \beta^{\mathrm{obs}}\Delta P - \frac{\Gamma\nu RT}{F}\left(\bar{t}_a - t_a\right)\ln\left(\frac{m_r}{m_\ell}\right) + \Delta\phi_{\mathrm{bias}} \tag{2.2.59}$$

with $\beta^{\mathrm{obs}} = \beta^{\mathrm{mem}} + \beta^{\mathrm{el}}$. For small molality differences, we can make the approximation $m_r - m_\ell \approx m_\ell \ln\left(m_r/m_\ell\right)$. The relative error of this approximation as a function of m_ℓ with m_r constant is shown graphically for the neighborhoods of 0.03 mol/kg and 0.6 mol/kg in figure 2.2. We make the observation that the approximation is a better one for higher salt concentrations, and that the approximated term is still negligible at lower concentrations. This means that unless the accuracy of an experiment is better than a relative error of the order 1 %, this approximation can always be made.

The streaming potential of interest is β^{mem}, which is a material property of the membrane. The observed streaming potential is the sum of the membrane and electrode contributions, such that for a given observed value, we find $\beta^{\mathrm{mem}} = \beta^{\mathrm{obs}} - \beta^{\mathrm{el}}$. Once the streaming potential has been determined experimentally, knowledge of the molar volumes and the ionic transport number yields the water transference coefficient

$$\bar{t}_{\mathrm{w}} = \frac{F\beta^{\mathrm{mem}} + \bar{t}_{\mathrm{M}^{z+}}V_{\mathrm{e}}/z}{M_{\mathrm{w}}\hat{m}V_{\mathrm{e}} - V_{\mathrm{w}}} \tag{2.2.60}$$

Determination of this water transference coefficient will be the main goal of the streaming potential measurements in this work.

2.2.5 Time Dependence of the Electric Potential

While the electrode bias can be eliminated by a baseline measurement, and the first term in (2.2.59) should be observed as a simple jump in the observed potential difference as the pressure is applied, we expect the pressure difference to drive electroneutral mass fluxes through the membrane as time passes. This will alter the compositions of the electrolyte solutions close to the membrane surfaces, and lead to measurable, time-dependent alterations to the observed cell potential. Assuming that the streaming potential, pressure difference, and electrode bias remains constant throughout the measurements, the only time dependence lies in the composition changes driven by the pressure difference. Since the transient period between the initial equilibrium and the steady state is strongly non-equilibrium, we will apply a model with which we can find the streaming potential by extrapolation. In appendix B, we derive a differential equation describing the time evolution of the composition changes, and expand the analytical solution of the form

$$\Delta\phi = a + b\sqrt{t} + ct^{3/2} + dt^{5/2} + \mathcal{O}\left(\left(V_{\mathrm{w}}J_{\mathrm{w}}\sqrt{t/D}\right)^7\right) \tag{2.2.61}$$

with t the time, and D_e the diffusion coefficient of the electrolyte in the aqueous solution. Fitting this model to the experimental data allows the estimation of the initial jump in cell potential, as well as other parameters characterizing the time evolution. The first two terms of the model coincide with the simple model used by Okada et al [19], while the higher order terms are included in case the diffusion processes approach a time scale comparable to the fluxes driven by the pressure difference. All coefficients are in each case checked for statistical significance, and any superfluous terms are discarded. For more details on the statistical treatment of the measurements, see appendix B.

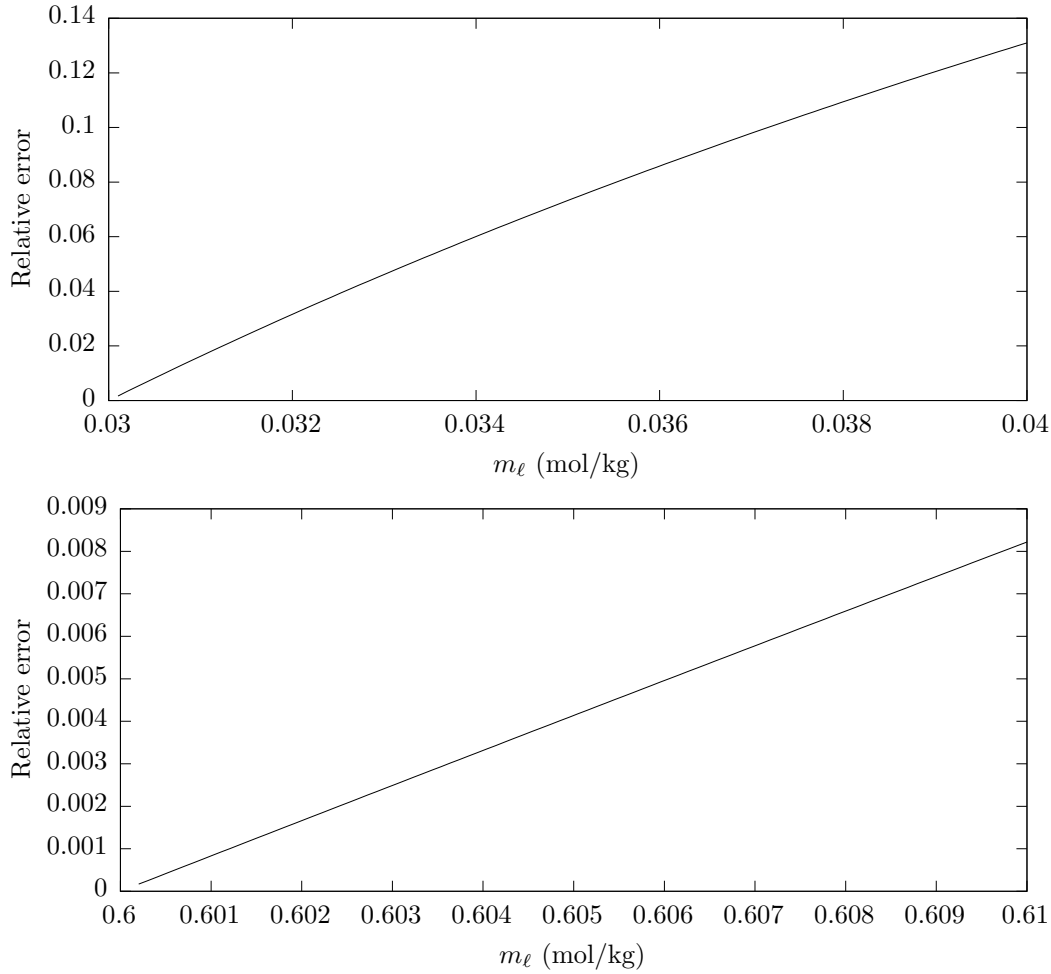

Figure 2.2: Plots of the relative error of the approximation $(m_r - m_\ell) \approx m_\ell \ln(m_r/m_\ell)$ as a function of m_ℓ with m_r held constant at 0.03 mol/kg (top) and 0.6 mol/kg (bottom).

2.2.6 Volume Flux and Water Permeability

The volume flux in the system is $J_{\mathrm{V}} = V_{\mathrm{e}}J_{\mathrm{e}} + V_{\mathrm{w}}J_{\mathrm{w}} + \Delta V_{\mathrm{el}}j/F$. We approximate that most of the open circuit volume flux in the system consists of water, and we obtain an approximate expression for the volume flux by multiplying (2.2.29) by V_{w} and integrating

$$(J_{\mathrm{V}})_{j=0} \approx V_{\mathrm{w}}J_{\mathrm{w}} = -\frac{\bar{\ell}_{\mathrm{ww}}}{Td}V_{\mathrm{w}}^2\Delta P = -L_p\Delta P \tag{2.2.62}$$

where L_{p} is the water permeability of the membrane. Knowledge of the volume flux in response to a pressure difference under open circuit conditions thus allows estimation of the permeability. Using the linear model described in (2.2.61) to fit the time-dependent data, it is possible to estimate the permeability from the regression coefficients. In particular, we find from the coefficient b

$$L_p = \frac{\sqrt{\pi D_{\mathrm{e}}}Fb}{4\Gamma\nu RT\left(t_a - \bar{t}_a\right)\Delta P} = \frac{\sqrt{\pi D_{\mathrm{e}}}zFb}{4\Gamma\nu RT\left(t_{\mathrm{M}^{z+}} + zM_{\mathrm{w}}\hat{m}\bar{t}_{\mathrm{w}} - \bar{t}_{\mathrm{M}^{z+}}\right)\Delta P} \tag{2.2.63}$$

Diffusion coefficients and transport numbers in aqueous solution are generally well investigated in the literature. Knowledge of the ionic transport numbers in the membrane can be combined with the streaming potential estimate of the water transference coefficient to estimate the permeability.

2.2.7 Partial Molar Volume of Electrolyte and Dielectric Permittivity

In order to estimate the molar volume V_{e} of the electrolytes at low concentrations, we employ the well-known Debye-Hückel result (see e.g. [20]) for the activity coefficients of ions

$$\ln(\gamma_i) = -\frac{z_i^2 A\sqrt{wm}}{\sqrt{2} + Ba\sqrt{wm}} \tag{2.2.64}$$

where

$$B = F\sqrt{\frac{\rho_{\mathrm{W}}}{\varepsilon RT/2}} \qquad A = \frac{Fe}{8\pi\varepsilon RT}B \qquad w = \sum_i \nu_i z_i^2$$

where ε is the bulk dielectric permittivity of the solution, R is the gas constant, e is the elementary charge, ρ_{W} the mass density of pure water, ν_i the stoichiometric coefficient of species i in the electrolyte, m the molality, and a is a size parameter, acting as the lower spatial integration limit for the linearized Poisson-Boltzmann equation leading up to the expression. We assume here that no degree of ion-ion association occurs, and that the electrolytes are fully dissociated. The parameter a is purely empirical, and is interpreted as the distance of closest approach of ions. The total activity coefficient of the electrolyte is obtained by

$$\ln(\gamma) = \sum_i \nu_i \ln(\gamma_i) = -\frac{Aw^{\frac{3}{2}}\sqrt{m}}{\sqrt{2} + Ba\sqrt{wm}} \tag{2.2.65}$$

while the pressure derivatives of A and B are

$$\begin{aligned}\partial_P B &= F\sqrt{\frac{\rho_{\mathrm{W}}}{2\varepsilon RT}}\left[\frac{\partial_P V_{\mathrm{W}}}{V_{\mathrm{W}}} - \partial_P \ln(\varepsilon)\right] \\ \partial_P A &= \frac{F^2 e\sqrt{\rho_{\mathrm{W}}}}{8\sqrt{2}\pi(\varepsilon RT)^{\frac{3}{2}}}\left[\frac{\partial_P V_{\mathrm{W}}}{V_{\mathrm{W}}} - 3\partial_P \ln(\varepsilon)\right]\end{aligned} \tag{2.2.66}$$

in which the ratio of the volume derivative and the volume is recognized as the isothermal compressibility of water. The second bracketed term is also available in literature by studying permittivity data at different pressures. Assuming that the size parameter does not vary appreciably with pressure for the relevant experimental conditions, the excess molar volume of the electrolyte can then be estimated by

$$V_{\mathrm{e}}^E = RT\partial_P \ln(\gamma) = RT\frac{aw^2\left(A\partial_P B - B\partial_P A\right)m - \sqrt{2}w^{\frac{3}{2}}\partial_P A\sqrt{m}}{(\sqrt{2} + Ba\sqrt{wm})^2} \tag{2.2.67}$$

and the molar volume of the electrolyte in solution is then estimated as

$$V_{\mathrm{e}} = V_{\mathrm{e}}^0 + V_{\mathrm{e}}^E \tag{2.2.68}$$

where V_{e}^0 is the molar volume at infinite dilution, obtained by extrapolating activity coefficient data. For estimating the dielectric permittivity, we use an empirical equation [21]

$$\varepsilon = \varepsilon_{\mathrm{W}} - \rho_{\mathrm{W}}\varepsilon_0\delta_\varepsilon\hat{m} \tag{2.2.69}$$

where δ_ε is an empirical fitting parameter, ε_{W} is the permittivity of pure water, and ε_0 is the permittivity of vacuum.

2.3 Experimental

The apparatus and experimental methods used were similar to that in a previous work by Barragán et al [22], and a sketch of the apparatus is given in figure 2.3. The cell consists of two glass chambers with an internal volume of approximately 125 cm^3 each, connected by a threaded joint where the membrane was inserted between two plane O-rings. The effective area of an undeformed membrane was 2.27 ± 0.02 cm^2. Each chamber has two inlets, one through which Ag/AgCl electrodes were inserted, and another for pressure control. The low-pressure chamber was maintained at atmospheric pressure by means of a capillary tube. The inlet of the high-pressure chamber was connected to a bottle of pure pressurized air delivered byPraxair through a single stage regulator from Air Liquide. The pressure difference was measured using a Cecomp Electronics DPG1000B15PSIG-5 digital pressure gauge with a resolution of 68.9 Pa (0.01 PSI). The cell voltage was measured with a HP 34401 high resolution multimeter. The entire cell was immersed in a thermostatted bath kept at 25.0 ± 0.1 °C using a Techne RB-12A refrigerated bath with Thermo Scientific

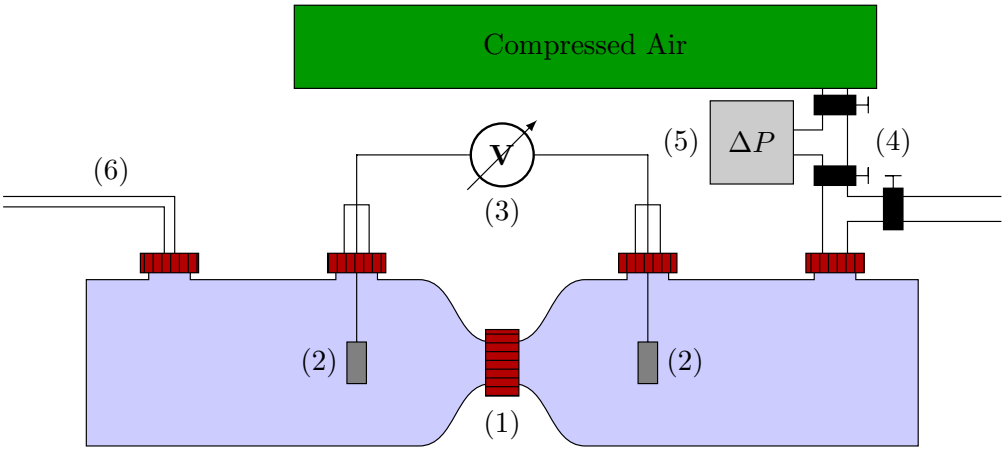

Figure 2.3: A sketch of the apparatus used for measuring the streaming potentials. The membrane sample is locked in a threaded ring joint (1), separating the two chambers of electrolyte solution. Each chamber is equipped with an Ag/AgCl electrode (2), connected to a voltmeter (3). The pressure is regulated by a series of valves (4) connecting one half-cell to a cylinder of compressed air, and is monitored by a manometer (5). The pressure is maintained at ambient in the other half-cell by means of a capillary tube (6).

Haake AC150 heated immersion circulator.

The salt solutions were prepared by weighing appropriate amounts of salt (all Merck analytical grade) for 1 kg of solvent using a high precision Sartorius balance (±0.1 mg) and then dissolving in 1 kg of distilled water. The membranes were pretreated by immersion in the appropriate salt solution at least 48 hours prior to the experiments.

For each measurement series, the electric potential was measured for 6 minutes prior to the application of the pressure gradient. The pressure pulse was prepared by closing the valve at the cell inlet and building up the desired air pressure using the pressure reducer. The gradient was then applied by opening the valve, and the time dependence of the potential was recorded for 3 minutes, after which the pressure was immediately released by opening a valve connecting the high-pressure cell chamber to the atmosphere. The potential was then measured for another 460 seconds before the measurement was terminated. This procedure was for each membrane-electrolyte combination repeated twice at pressure differences of approximately 1 bar, 0.8 bar and 0.6 bar, in that order.

In addition to measuring streaming potentials, the solvent uptake of the different membranes in different salt solutions was also measured. Both the membrane samples used for the streaming potential experiments, and new, unused membrane samples were equilibriated in appropriate salt solutions and weighed once per day until a stable weight was found for at least 3 consecutive days. The samples were then dried

in vacuo at 25°C with activated silica as dessicant. The dried samples were then weighed over the course of several days until a stable weight was found. The solvent uptake was then calculated as the relative mass difference between the wet and dry membranes.

2.4 Results and Discussion

A typical regression result for the streaming potential is plotted in figure 2.4. The observed streaming potentials as calculated by extrapolation are given in table 2.2. The normality and homoscedasticity of the deviations from the fitted curve are demonstrated in figure 2.5. The regression interval was chosen from quantitative criteria on the normality and homoscedasticity of the errors. See appendix B for details. An example of a plot of the observed initial jump in electric potential versus the applied pressure difference is given in figure 2.6. The streaming potential was for each case calculated as the slope of the least squares simple linear fit of initial jump in electric potential as a function of the applied pressure difference.

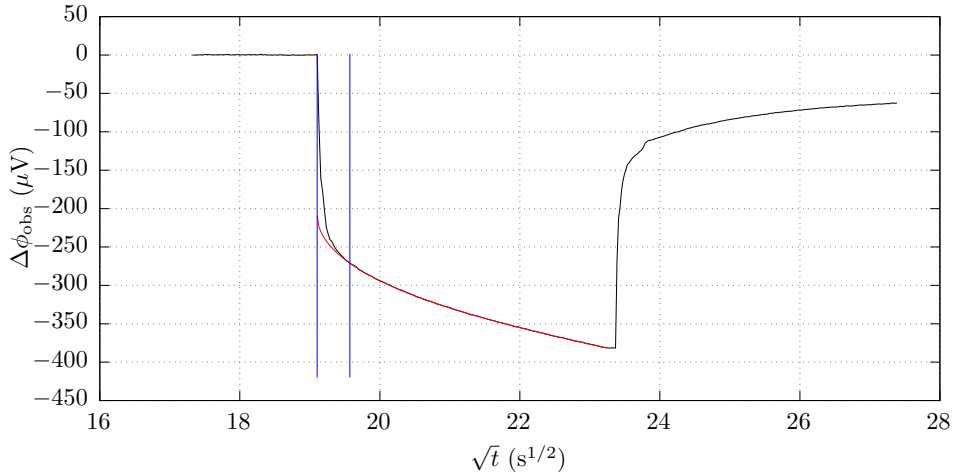

Figure 2.4: The experimentally observed electric potential between the Ag/AgCl electrodes over the course of an experiment using the NAFION 115 cation-exchange membrane in 0.03 mol/kg LiCl solution, plotted against the square root of time. The transient period between equilibrium and steady state is indicated by the blue lines, and the fitted regression curve is plotted in red. The applied pressure difference in the plotted experiment was approximately 1 bar.

For calculating the molar volumes of the electrolytes at 0.03 mol/kg, a water compressibility of 0.45248 GPa^{-1} [23] was used. The pressure derivative of the permittivity was estimated by taking finite differences of permittivity data as a function of pressure [24] and interpolating. The value used is $\partial_P \ln(\varepsilon) = 0.52645$ GPa^{-1}. This value was taken to be approximately the same for all the electrolytes under investiga-

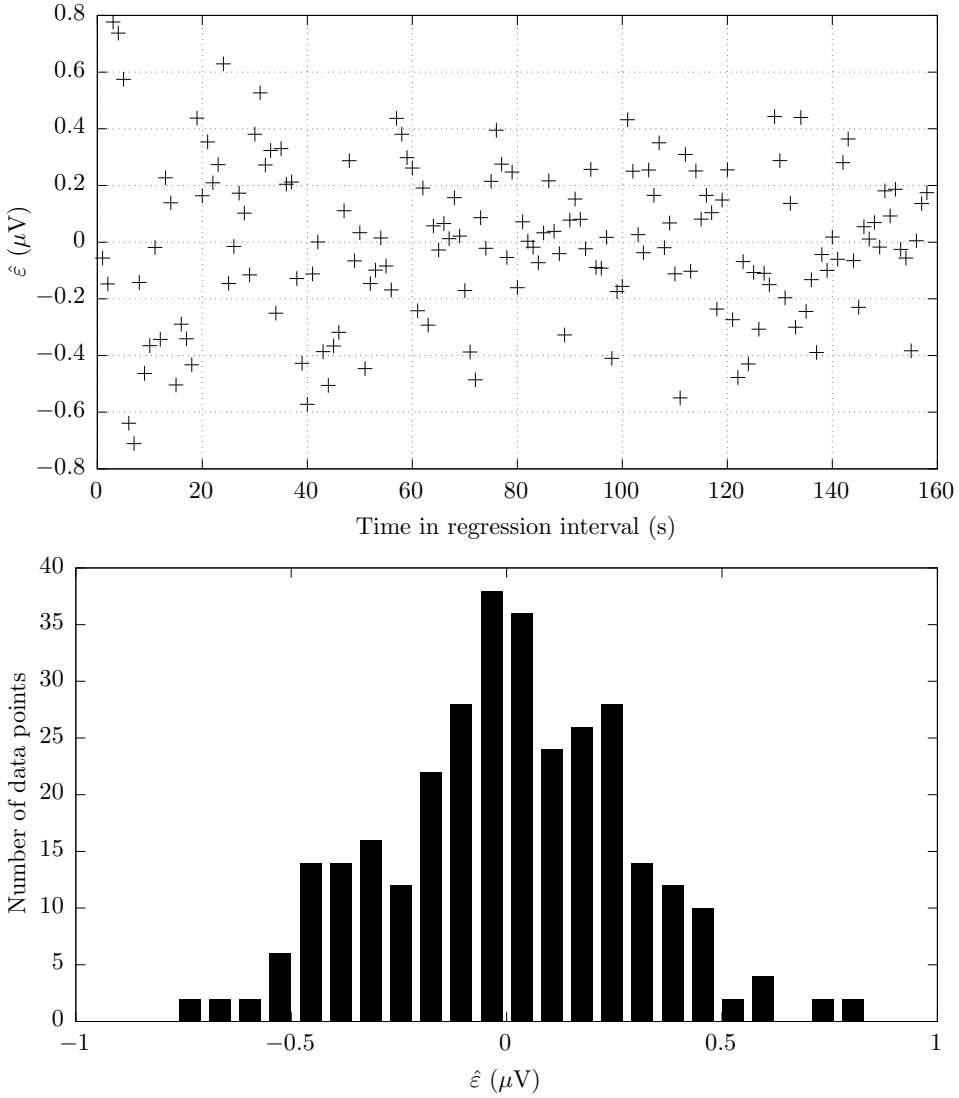

Figure 2.5: **Top:** Deviations from the fitted regression curve in the regression interval after the transient period plotted in figure 2.4. **Bottom:** A histogram showing the frequencies of the observed deviations from the fitted regression curve.

tion. The dielectric permittivity of pure water was taken to be 693.8 pF/m [25], and the permittivities of the salt solutions were calculated according to equation (2.2.69). The excess molar volumes were calculated according to equation (2.2.67), using extrapolated data from [26]. Empirical data gathered from literature, along with the resulting estimates are given in table 2.1.

For calculating the electrode contribution to the observed streaming potential, molar

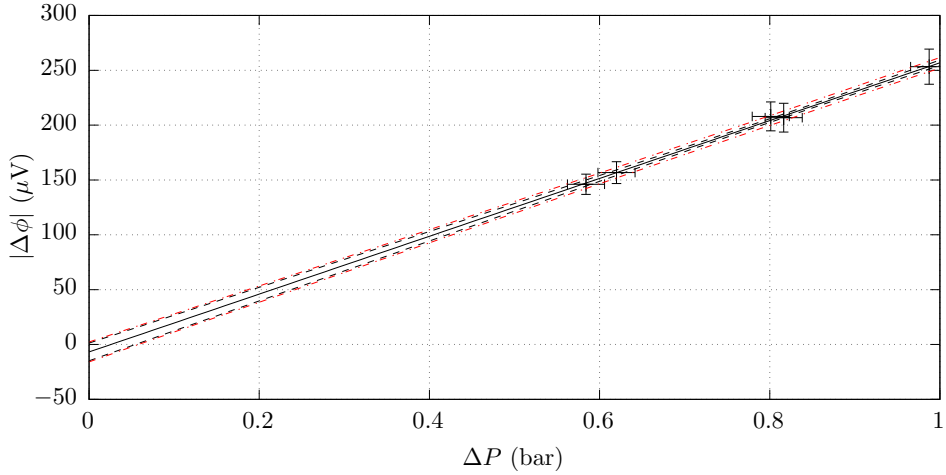

Figure 2.6: Absolute values of observed streaming potentials plotted against pressure applied over the NAFION 115 cation-exchange membrane in 0.03 mol/kg LiCl solution. The black and red dashed lines indicate 95% confidence and prediction bounds, respectively. The observed points lie along a straight line within their error bounds, and the regression result contains the origin within the confidence bounds.

masses of 107.8682 g/mol and 143.321 g/mol [25] were used for Ag and AgCl, respectively. The densities used were respectively 10.49 g/cm^3 [25] and 5.589 g/cm^3 [29]. These values yield molar volumes of 10.283 cm^3/mol for Ag and 25.643 cm^3/mol for AgCl. Together, this gives an electrode contribution of $\beta^{\mathrm{el}} = 15.920$ µV/bar, which is taken to be the same in all experiments. The molar volume of water was taken to be approximately the same as in pure water, and therefore estimated by the ratio of a molar mass of 18.0153 g/mol [25] and a pure water density of 997.047 kg/m^3 [25], giving an estimated molar volume of 18.0686 cm^3/mol. We take all membranes to be perfectly selective at 0.03 mol/kg concentration for all electrolytes, and, in light

Table 2.1: Molar volumes at infinite dilution, Debye-Hückel size parameters, permittivity fitting parameters, and estimated permittivities and molar volumes at 0.03 mol/kg for the relevant electrolytes.

Electrolyte	V_{e}^0[26] (cm^3/mol)	a[27] (pm)	δ_ε[28] (dm^3/mol)	ε (pF/m)	V_{e} (cm^3/mol)
LiCl	17.1	432	13.3	690.3	17.6
NaCl	16.6	397	11.0	690.9	17.1
KCl	26.8	363	9.4	691.3	27.3
$MgCl_2$	15.3	502	24.0	687.5	17.3
$CaCl_2$	18.5	473	27.2	686.6	20.5
$BaCl_2$	23.9	445	22.8	687.8	25.9

Table 2.2: Membrane streaming potentials and water transference coefficients for different combinations of membrane and electrolyte at molality 0.03 mol/kg. Missing values are either pending for measurement or temporarily under revision due to severe lack of precision in raw data.

	Nafion 115		Neosepta CMX	
Electrolyte	β^{mem} (µV/bar)	$\bar{t}_{\mathrm{w}}$	β^{mem} (µV/bar)	$\bar{t}_{\mathrm{w}}$
LiCl	-280 ± 10	14.0 ± 0.5	-129 ± 20	5.9 ± 1.1
NaCl	-207 ± 56	10.1 ± 3.0	-102 ± 8	4.5 ± 0.4
KCl	-121 ± 7	4.9 ± 0.4	-90 ± 18	3.3 ± 1.0
$MgCl_2$	-241 ± 8	12.4 ± 0.4	-	-
$CaCl_2$	-193 ± 19	9.7 ± 1.0	-	-
$BaCl_2$	-119 ± 10	5.6 ± 0.5	-	-
	Fumasep FKS		Fumasep FAD	
LiCl	-141 ± 21	6.6 ± 1.1	-	-
NaCl	-90 ± 9	3.9 ± 0.5	52 ± 18	-2.8 ± 1.0
KCl	-97 ± 14	3.7 ± 0.7	97 ± 23	-5.2 ± 1.2
$MgCl_2$	-169 ± 7	8.5 ± 0.4	68 ± 49	-3.6 ± 2.6
$CaCl_2$	-	-	45 ± 16	-2.4 ± 0.9
$BaCl_2$	-119 ± 5	5.6 ± 0.3	59 ± 58	-3.2 ± 3.1
	Neosepta AMX			
LiCl	64 ± 4	-3.4 ± 0.2		
NaCl	-	-		
KCl	-	-		
$MgCl_2$	-	-		
$CaCl_2$	54 ± 21	-2.9 ± 1.1		
$BaCl_2$	-	-		

of transport number data by Zlotorowicz et al.[30], we also take the FKS and FAD membranes to be perfectly selective also at elevated concentrations of NaCl, introducing an error that is found negligible a posterori in all cases. Unless stated otherwise, all errors are reported as 95 % confidence, under the assumption of normally distributed residuals. Normality is in every case confirmed at the 5 % level by means of an Anderson-Darling test.

We observe that all streaming potentials are in the range $60 - 260$ µV/bar, which is just below the lower range of values reported for Flemion S [32], which are found in the range $0.3 - 1$ mV/bar, and 3 orders of magnitude smaller than values reported for Cyclopore filtration membranes [33]. The magnitudes of the water transference coefficients found in these experiments are typical. To the precision in these experiments, we cannot conclude that $\bar{t}_{\mathrm{w}}$ of the anion exchange membranes change with cation. For the cation exchange membranes, we observe a tendency for $\bar{t}_{\mathrm{w}}$ to decrease with cation size. A plot of $\bar{t}_{\mathrm{w}}$ against the ratio of the cationic charge number to the

Table 2.3: Streaming potentials and water transference coefficients of the FUMASEP membranes for different molalities of NaCl. The molar volumes at 0.10 and 0.60 mol/kg were obtained by interpolating experimental data by Dunn [31]. The streaming potentials are given in µV/bar.

$\overline{m}_e$	V_e	FKS		FAD	
(mol/kg)	(cm^3/mol)	β^{mem}	$\bar{t}_w$	β^{mem}	$\bar{t}_w$
0.03	17.1	-90 ± 9	3.9 ± 0.5	52 ± 18	-2.8 ± 1.0
0.10	17.4	-78 ± 17	3.2 ± 0.9	92 ± 11	-4.9 ± 0.6
0.60	18.0	-97 ± 14	4.2 ± 0.7	150 ± 92	-8.1 ± 4.9

crystallographic radii of the cations is given in figure 2.7. This ratio is an estimate of the magnitude of the local electric potential due to the electric field of the cationic monopole at the distance of closest approach, and thus indicates the depth of the potential well of the solvating water molecules. We observe that there are two different trends – one for the monovalent cations, and one for the divalent cations. For each separate trend, we see a monotonous increase with the charge-radius ratio. Xie and Okada [13] found that $\bar{t}_w$ increases with the size of the cation in NAFION membranes, likely due to a size exclusion effect pumping the water along with the ions. This effect becomes more appreciable when the volume of the cation is made up of hydrophobic groups, contrary to our situation in these experiments. The strong tendency of $\bar{t}_w$ in table 2.2 to decrease with ion size suggests that the ion-dipole interaction dominates the water transport in these cases.

The aqueous solution cation transport numbers, $t_{M^{z+}}$, were found by interpolating experimental data found in the literature. Data was found for LiCl, NaCl and KCl [34]; $CaCl_2$ [35]; $MgCl_2$ [36] and $BaCl_2$ [37]. Diffusion coefficients were found by interpolation of data from [36, 38, 39, 40, 41, 42, 43, 44], and thermodynamic factors were estimated by finite differences on interpolation of activity data from [25]. All data are given in tables 2.4 and 2.5. Water permeabilities were estimated using equation (2.2.63), and data for different electrolytes and different concentrations are given in tables 2.6 and 2.7, respectively.

The measured water content for all membranes in different electrolyte solutions are given in tables 2.8 and 2.9. Although the error in much of the data is sizeable, the numbers indicate that the water content of the anion exchange membranes is insensitive to the type of cation in the solution, while the water content of the cation exchange membranes seems to decrease with increasing cation size and charge. For the cation exchange membranes, there appears to be a correlation between the water content and the water transference coefficient. Due to the large error in the FKS data, however, only the correlations for the NAFION 115 and NEOSEPTA CMX membranes are significant, and a plot is shown in figure 2.8. Such correlations have been found previously by other workers, see e.g. [17], and suggest that part of the water trans-

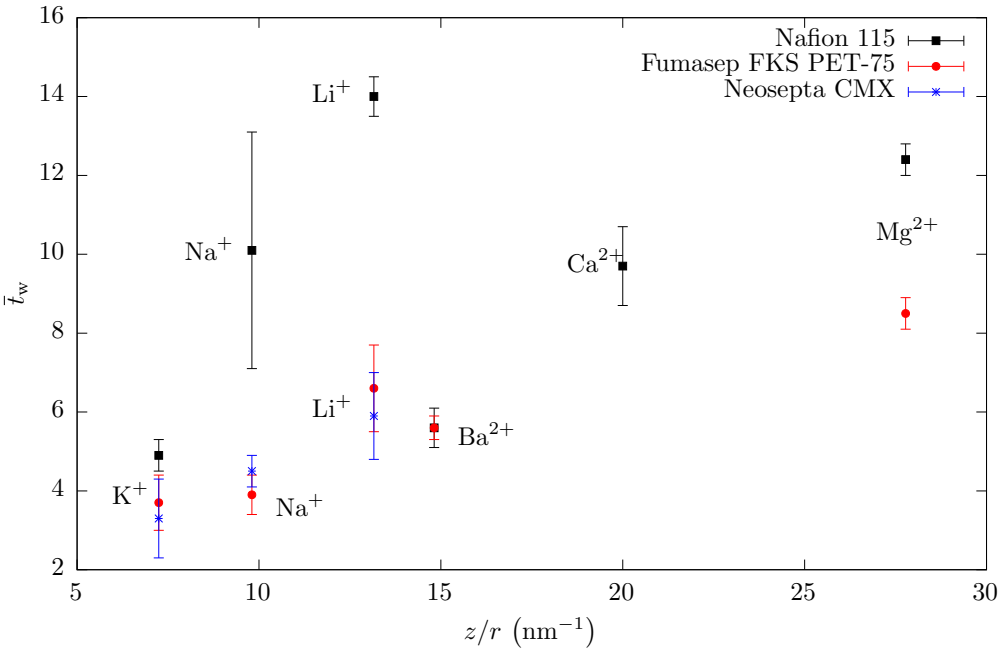

Figure 2.7: Plot of water transference coefficients against the ratio of cationic charge numbers, z, and the crystallographic radii at coordination number 6, r.

Table 2.4: Aqueous solution transport numbers, diffusion coefficients, and thermodynamic factors obtained by interpolating literature data at 0.03 mol/kg and 25°C.

Electrolyte	$t_{M^{z+}}$	D_e (10^{-9} m^2/s)	Γ
LiCl	0.324	1.29	0.942
NaCl	0.389	1.52	0.937
KCl	0.490	1.89	0.932
$MgCl_2$	0.380	1.10	0.864
$CaCl_2$	0.419	1.15	0.853
$BaCl_2$	0.430	1.21	0.836

Table 2.5: Aqueous solution transport numbers, diffusion coefficients and thermodynamic factors of NaCl obtained by interpolating literature data at different concentrations and 25°C.

Molality	$t_{M^{z+}}$	D_e(10^{-9}m^2/s)	Γ
0.03	0.389	1.52	0.937
0.10	0.386	1.48	0.922
0.60	0.376	1.47	0.939

Table 2.6: Water permeabilities L_p at 0.03 mol/kg, calculated from diffusion slopes using values from table 2.4 and assuming zero electrolyte flux and perfect ionic selectivity. The values are all given in units of nm s^{-1} bar^{-1}.

Electrolyte	Nafion 115	Neosepta CMX	Fumasep FKS
LiCl	6.3 ± 0.4	7 ± 15	6.3 ± 1.2
NaCl	7.0 ± 1.6	0.9 ± 0.9	3.4 ± 1.6
KCl	4.2 ± 1.2	2.1 ± 1.4	2.3 ± 0.6
$MgCl_2$	1.9 ± 0.9	-	1.6 ± 1.0
$CaCl_2$	6.2 ± 5.4	-	-
$BaCl_2$	1.9 ± 1.9	-	1.0 ± 1.3
	Fumasep FAD	Neosepta AMX	
LiCl	-	1.6 ± 3.0	
NaCl	9.5 ± 4.7	-	
KCl	9.1 ± 1.6	-	
$MgCl_2$	11.5 ± 7.6	-	
$CaCl_2$	12.2 ± 4.1	1.1 ± 2.3	
$BaCl_2$	17.0 ± 4.2	-	

Table 2.7: Water permeabilities calculated for different concentrations of NaCl. The values are all given in units of nm s^{-1} bar^{-1}.

Molality	Fumasep FKS	Fumasep FAD
0.03	3.4 ± 1.6	9.5 ± 4.7
0.10	2.6 ± 0.1	6.1 ± 1.1
0.60	2.6 ± 0.7	6.3 ± 3.7

Table 2.8: Measured water content in mass percent for unused membranes immersed in 0.03 mol/kg aqueous salt solutions.

Electrolyte	Nafion 115	Neosepta CMX	Fumasep FKS
LiCl	19.2 ± 0.4	23.7 ± 0.6	17.7 ± 1.4
NaCl	16.8 ± 0.4	21.3 ± 0.5	17.7 ± 0.8
KCl	9.2 ± 1.3	20.5 ± 0.4	14.1 ± 1.1
$MgCl_2$	15.3 ± 0.4	19.6 ± 0.6	17.4 ± 1.3
$CaCl_2$	14.4 ± 0.5	19.8 ± 1.0	15.6 ± 2.1
$BaCl_2$	10.3 ± 0.7	14.2 ± 0.6	14.1 ± 2.7
	Fumasep FAD	Neosepta AMX	
LiCl	23.5 ± 2.1	16.2 ± 0.6	
NaCl	22.3 ± 0.5	17.2 ± 0.7	
KCl	24.5 ± 1.4	14.6 ± 0.8	
$MgCl_2$	25.5 ± 2.1	16.9 ± 1.0	
$CaCl_2$	26.7 ± 1.1	16.9 ± 1.4	
$BaCl_2$	24.3 ± 1.5	15.8 ± 1.0	

port is bulk transport of loosely bound water in the membrane, which is additional to that transported by electrostriction due to the ion-dipole interaction. Interestingly, the water content of the FAD membrane appears to decrease with concentration of NaCl, though the effect is small.

The water content of membranes that were used for streaming potential measurements, and thus exposed to a pressure difference of approximately 1 bar, is given in table 2.10. The deformation of the membranes made removal of surface solution from the wet membranes less reliable, and caused some increase in the error. We can see, however, that the general tendency is for the water content to decrease in all membranes after deformation. This is possibly an effect of structural collapse in the membrane, such that it can accomodate only a smaller volume of water than prior to the deformation. Since the correlation between water content and water transport is positive, it is possible that this effect serves to shift our estimates for the water transference coefficients to a lower value than the true value of the undeformed membrane. If this is true, then we expect that the water transference coefficients of the cation exchange membranes are underestimated by a value of up to around 1, according to the correlations given in figure 2.8.

An interesting connection can be made to the effect of the ions on the solvent structure. An empirical measure of the ion-solvent interaction is the B-coefficient of the Jones-Dole equation. For details, see the original paper [45], or e.g. [46]. It was shown by Nightingale [47] that there exists a direct correlation between the B-coefficients

Table 2.9: Measured water content in mass percent for unused membranes immersed in aqueous NaCl at different concentrations.

Molality	Fumasep FKS	Fumasep FAD
0.03	17.7 ± 0.8	22.3 ± 0.5
0.10	18.8 ± 0.6	21.3 ± 0.7
0.60	17.0 ± 0.6	20.9 ± 0.7

Table 2.10: Measured water content in mass percent for membranes immersed in 0.03 mol/kg aqueous salt solutions after exposure to a pressure difference of 1 bar.

Electrolyte	Nafion 115	Neosepta CMX	Fumasep FKS
LiCl	16.8 ± 0.9	22.0 ± 1.0	19.5 ± 2.7
NaCl	15.5 ± 1.2	18.5 ± 1.5	14.7 ± 1.8
KCl	10.1 ± 0.9	18.0 ± 0.9	14.9 ± 3.1
$MgCl_2$	13.3 ± 1.1	16.5 ± 1.5	14.1 ± 2.4
$CaCl_2$	14.4 ± 1.2	17.1 ± 1.2	15.7 ± 1.9
$BaCl_2$	10.1 ± 0.6	16.5 ± 1.4	17.4 ± 4.8
	Fumasep FAD	Neosepta AMX	
LiCl	22.2 ± 2.6	14.3 ± 1.6	
NaCl	21.9 ± 2.6	13.3 ± 2.0	
KCl	21.0 ± 3.4	13.7 ± 2.0	
$MgCl_2$	18.7 ± 1.7	12.9 ± 1.5	
$CaCl_2$	19.9 ± 2.6	13.4 ± 2.2	
$BaCl_2$	21.0 ± 1.0	15.0 ± 1.4	

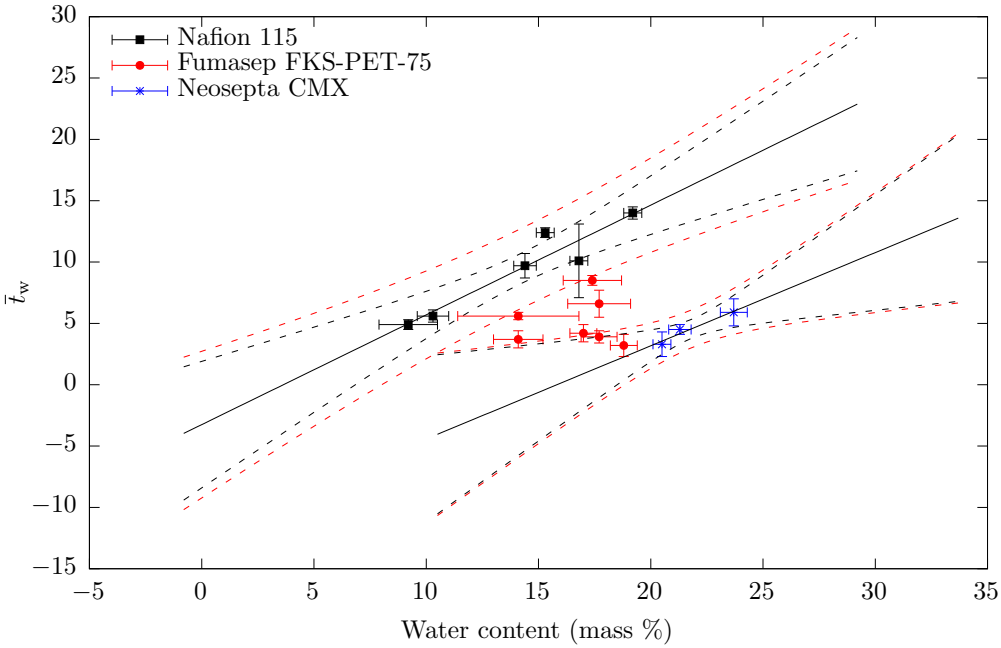

Figure 2.8: Plot of water transference coefficients against water content of the cation exchange membranes, obtained by changing the cation of a 0.03 mol/kg aqueous chloride solution. The black and red dashed lines indicate 95 % confidence and prediction, respectively.

and the mass-corrected partial entropy of solvation. The average number of water molecules transported *per ion* is $z\bar{t}_w$. In figure 2.9, we show a strong correlation between $z\bar{t}_w$ and the B-coefficients. We observe that the water transport through the membrane is correlated with the effect of the cation on the solvent structure in free solution. For NAFION 115, the correlation is not monotonous, which may be due to an effect of the ion in the membrane structure. The fixed charge groups are monovalent, which means that a divalent cation requires the proximity of two such groups to achieve electroneutral conditions. It is possible that this strong monopole interaction between a divalent cation and two sulfonic acid groups strains the polymer structure so as to alter the water transport properties of the membrane. This hypothesis is supported by the trend in water permeability in table 2.6. We observe that, apart from the highly uncertain estimate in calcium chloride solution, the permeability is significantly lower in solution with divalent cations than with monovalent cations. This indicates that the divalent cations strain the membrane structure such that the nanopores are more constricted. The correlation also further supports the hypothesis that the water transport is dominated by ion-dipole interactions, rather than the pumping effect seen with hydrophobic cations.

The water transport through the FKS membrane appears to be insensitive to the

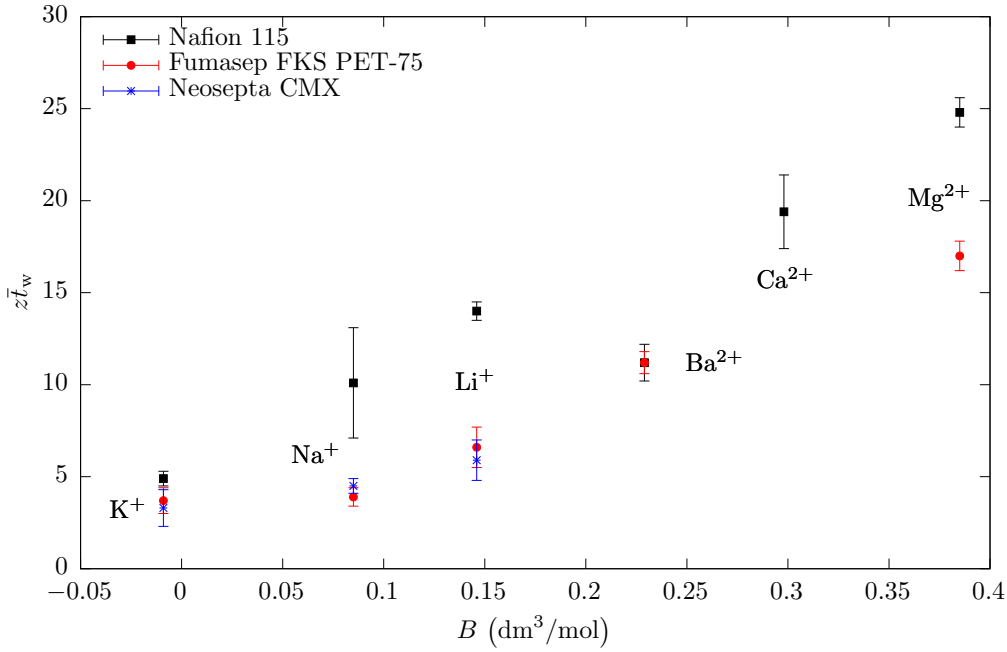

Figure 2.9: Plot of the product of cation valence number and water transference coefficient against the Jones-Dole B-coefficients of the cations in aqueous solution.

concentration of NaCl in the range 0.03 - 0.60 mol/kg, while that of the FAD membrane increases in magnitude with the concentration. This is contrary to findings by Trivijitkasem and Østvold [18], who found for all membranes they investigated that the magnitude of $\bar{t}_w$ either decreased with or was insensitive to electrolyte concentration. The permeabilities of both membranes appear to be insensitive to the concentration, though the estimates are quite uncertain. Several of the streaming potential measurements suffer from large errors, which is due to observed perturbations to the cell potential after application of the pressure difference. These perturbations are postulated to occur due to mechanical deformation of the membrane. Interesting investigations have been made on the viscoelastic response of such membranes to a pressure gradient [48], which may lead to interesting results relevant for applications of non-isobaric membrane systems. Previously mentioned workers applying the streaming potential method have used a perforated support plate for their measurements to avoid deformation. Investigations on finite size effects of the perforations have not yet been performed to a satisfactory degree, however, and we suggest a completely different method in chapter 4.

Chapter 3
Seebeck Effect and Transported Entropy

A theoretical expression describing the measured electric potential difference over an ion exchange membrane in contact with a nonisothermal aqueous metal chloride solution with Ag/AgCl electrodes was derived in the framework of classical non-equilibrium thermodynamics. The expression includes the effects of temperature polarization, Thomson effect, and concentration polarization. The effect of stacking membranes together to diminish the polarization effects is discussed, and an empirical model is applied. A thermocell was designed and built for measuring the Seebeck coefficient of ion exchange membranes experimentally. The Seebeck coefficient was measured for the FuMA-Tech FKS-PET-75 and FAD-PET-75 membranes in sodium chloride solutions with molalities 0.03, 0.1, and 0.6 mol/kg, with temperature differences spanning from -20 to 20 Kelvin, and with membranes stacked together in numbers ranging from 1 to 20. The arithmetic mean temperature of the cell was kept at 25 °C. A regression model was used to fit the observed Seebeck coefficient of the total system as a function of the membrane stack thickness. In both cases, the Seebeck coefficient converged towards a limiting value with increasing thickness, suggesting that the polarization effects vanish. The Seebeck coefficient of the two membranes were found to range from 1.41 to 0.98 mV/K, and 0.56 to 0.48 mV/K for the FKS and FAD membranes in stacks of 20, as the NaCl concentration was increased. From the experimental data, estimates of the transported entropies of the ions in the membranes were obtained. The Thomson effect was found to be insignificant in all cases. A theoretical bound for the Seebeck coefficient, given by the second law of thermodynamics, is also discussed. A figure of merit of a thermoelectric generator is derived and related directly to the second law efficiency. The transported entropy of Na^+ in the FKS membrane was found to be insensitive to the composition of the aqueous solution, and remains around 300 J/mol K. The transported entropy of Cl^- in the FAD membrane appears to increase with salt concentration, ranging from 250 to 600 J/mol K. The errors are, however, large, due to large errors in the estimates of the water transference coefficients. More accurate methods for determining the water transference coefficients are needed in order to obtain better estimates of the transported entropies.

3.1 Introduction

A complete description of a non-isothermal system with electric currents includes considerations of the coupling of heat and charge transfer, known as the Peltier effect. Even isothermal systems can become non-isothermal under operation due to this effect, which carries heat along with or in the opposite direction of the electric flux. This coupling allows the extraction of electrical work from non-isothermal systems, by allowing the temperature gradient to act as a driving force for the electric current, an effect known in the literature as the Seebeck effect. The Peltier and Seebeck effects are mutually reciprocal, and are related by an Onsager relation in the local equilibrium theory.

Notable experimental work on the thermoelectric potential of ion exchange membranes was done by a Japanese group [6, 49, 50, 51, 52, 53]. Although parts of their theory could have been more transparent regarding the physical origin of the potential that is being measured, their results do provide valuable insight. They demonstrated that the potential was dependent on the flow rate in their cell, suggesting an effect of the diffusion layers adjacent to the membrane. This was further investigated by Barragán et al. [54], who also investigated the effect of changing the mean temperature of the cell [55]. More recent investigations have focused on the explicit application of such systems to harvest waste heat, see e.g. [56, 57].

In the experiments presented here, we investigate the cell potential as the temperature difference between the two compartments is varied, measuring the *Seebeck coefficient* of the cell. We apply the Onsager reciprocity theorem to relate this to the Peltier heat, quantified by the *transported entropy* of the charge carrier in the ion exchange membrane. Agar [58] provided a review on the transported entropy of ions in aqueous solutions, which are typically much larger than those of electrons and holes in conventional semiconducting thermoelectric generators. Estimating and reporting the transported entropies of ions in ion exchange membranes from Seebeck coefficients appears to be the standard in the literature.

We develop here theoretical expressions describing the measurable cell potential of a non-isothermal cell made up of two compartments with Ag/AgCl electrodes in aqueous chloride electrolyte, separated by an ion exchange membrane, in the framework of non-equilibrium thermodynamics. We follow closely the conventions of workers such as Kjelstrup & Bedeaux [8], and de Groot & Mazur [9]. The theoretical considerations are somewhat general with respect to choice of cation, and we restrict experiments to the case of NaCl, which is the most relevant for non-isothermal salt power applications. See chapter 4 for more details on this particular application.

3.2 Theory

We consider an electrochemical cell, where two compartments of an aqueous chloride solution are separated by an ion exchange membrane. Each compartment has its own Ag/AgCl electrode, and the electrodes are connected through an outer circuit by means of metallic conductors. The system is nonisothermal, and there will therefore be a net heat conduction through the membrane. The membrane also allows for transfer of ions and solvent. A sketch of the system is given in figure 3.1. The temperatures close to the electrodes in compartment 1 and 2 are T_1 and T_2, and the corresponding temperatures close to the membrane surfaces are T_ℓ and T_r. We define positive fluxes to be counter-clockwise in figure 3.1, using the rest frame of the membrane as reference. We will divide the cell into distinct sub-systems, treating the aqueous solution, the membrane, and the electrodes with external circuit separately, and finally sum their contributions to obtain an expression for the total cell potential.

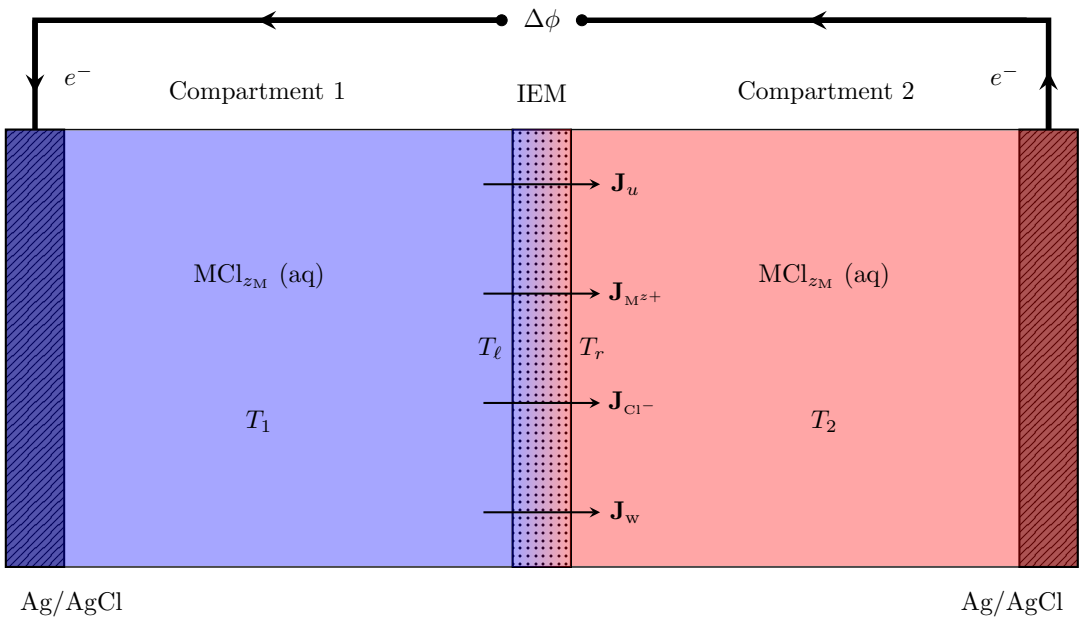

Figure 3.1: Sketch of the system considered in this work. The system is assumed to have mirror symmetry with respect to membrane plane before the application of a temperature gradient. The temperature difference $T_2 - T_1$ acts as a driving force for fluxes of energy, cations, chloride, and water, denoted $\mathbf{J}_u$, $\mathbf{J}_{\mathrm{M}^{z+}}$, $\mathbf{J}_{\mathrm{Cl}^-}$, and $\mathbf{J}_\mathrm{w}$, respectively. Charge transfer is facilitated by reactions at the electrodes, which are at electric potentials ϕ_1 and ϕ_2. The temperatures T_ℓ and T_r close to the membrane are also indicated.

3.2.1 The Aqueous Solution

We treat the electrolyte solution as a continuum where fluxes of energy, $\mathbf{J}_u$, cation, $\mathbf{J}_{\mathrm{M}^{z+}}$, and chloride, $\mathbf{J}_{\mathrm{Cl}^-}$ occur. With this, we assume that there is no net flux of water in the bulk solution. We give the entropy production, σ, in terms of the conjugate flux-force pairs

$$\sigma = \mathbf{J}_u \cdot \nabla\left(\frac{1}{T}\right) - \mathbf{J}_{\mathrm{M}^{z+}} \cdot \nabla\left(\frac{\tilde{\mu}_{\mathrm{M}^{z+}}}{T}\right) - \mathbf{J}_{\mathrm{Cl}^-} \cdot \nabla\left(\frac{\tilde{\mu}_{\mathrm{Cl}^-}}{T}\right) \tag{3.2.1}$$

where $\tilde{\mu}_i$ is the electrochemical potential of i, defined as

$$\tilde{\mu}_i := \mu_i + z_i F \psi \tag{3.2.2}$$

with μ_i the chemical potential, F Faraday's constant, and ψ the electrostatic potential. The charge number z_i, is defined such that $z_i e$ is the charge of a particle of i, with e the charge of a proton (i.e. the elementary charge unit). The linear flux-force relations prescribed by the linear regression hypothesis are

$$\begin{aligned}
\mathbf{J}_u &= L_{uu}\nabla\left(\frac{1}{T}\right) - L_{u+}\nabla\left(\frac{\tilde{\mu}_{\mathrm{M}^{z+}}}{T}\right) - L_{u-}\nabla\left(\frac{\tilde{\mu}_{\mathrm{Cl}^-}}{T}\right) \\
\mathbf{J}_{\mathrm{M}^{z+}} &= L_{+u}\nabla\left(\frac{1}{T}\right) - L_{++}\nabla\left(\frac{\tilde{\mu}_{\mathrm{M}^{z+}}}{T}\right) - L_{+-}\nabla\left(\frac{\tilde{\mu}_{\mathrm{Cl}^-}}{T}\right) \\
\mathbf{J}_{\mathrm{Cl}^-} &= L_{-u}\nabla\left(\frac{1}{T}\right) - L_{-+}\nabla\left(\frac{\tilde{\mu}_{\mathrm{M}^{z+}}}{T}\right) - L_{--}\nabla\left(\frac{\tilde{\mu}_{\mathrm{Cl}^-}}{T}\right)
\end{aligned} \tag{3.2.3}$$

where we have used scalar conductivities under the assumption that the solution is sufficiently isotropic. A connection can be made to the Kedem-Katchalsky formulation, which instead includes the net flux of neutral electrolyte, $\mathbf{J}_{\mathrm{e}}$, and the electric current density, $\mathbf{j}$. This, however, requires the introduction of constraints from the global properties of the system. In our case, the electrodes are reversible to the chloride anion, and the net electrolyte flux can only occur with net flux of cation through the membrane. The transformations are, therefore,

$$\begin{aligned}
\mathbf{J}_{\mathrm{e}} &= \mathbf{J}_{\mathrm{M}^{z+}} \\
\mathbf{j} &= zF\mathbf{J}_{\mathrm{M}^{z+}} - F\mathbf{J}_{\mathrm{Cl}^-} \\
\mu_{\mathrm{e}} &= \mu_{\mathrm{M}^{z+}} + z\mu_{\mathrm{Cl}^-} \\
\phi &= \psi - \mu_{\mathrm{Cl}^-}/F
\end{aligned} \tag{3.2.4}$$

where μ_{e} is the chemical potential of the electrolyte MCl_z, z is the valence number of the cation, and ϕ is the measurable electric cell potential. This formulation has the disadvantage of using a non-local electrolyte flux, which complicates local treatment. It does, however, include measurable quantities, such as μ_{e} and ϕ. We will use the formulation with electrochemical potentials in order to derive the local contributions to the cell potential, and use the relations (3.2.4) to reformulate the expressions in

terms of measurable quantities.

We now restrict our attention to one-dimensional transport along the axis x orthogonal to the membrane surfaces, such that (3.2.3) becomes

$$\begin{bmatrix} J_u \\ J_{\mathrm{M}^{z+}} \\ J_{\mathrm{Cl}^-} \end{bmatrix} = \begin{bmatrix} L_{uu} & L_{u+} & L_{u-} \\ L_{+u} & L_{++} & L_{+-} \\ L_{-u} & L_{-+} & L_{--} \end{bmatrix} \begin{bmatrix} \partial_x (1/T) \\ -\partial_x (\tilde{\mu}_{\mathrm{M}^{z+}}/T) \\ -\partial_x (\tilde{\mu}_{\mathrm{Cl}^-}/T) \end{bmatrix} \tag{3.2.5}$$

We use (3.2.4) to find the electric current density in terms of the flux equations for the ion fluxes

$$j = L_{\psi u}\partial_x \left(\frac{1}{T}\right) - L_{\psi +}\partial \left(\frac{\mu_{\mathrm{M}^{z+}}}{T}\right) - L_{\psi -}\partial_x \left(\frac{\mu_{\mathrm{Cl}^-}}{T}\right) - L_{\psi\psi}\partial_x \left(\frac{\psi}{T}\right) \tag{3.2.6}$$

where we have used the relations for j and ψ in (3.2.4), and defined the coefficients

$$\begin{aligned} L_{\psi u} &= F\left(zL_{+u} - L_{-u}\right) & L_{\psi +} &= F\left(zL_{++} - L_{-+}\right) \\ L_{\psi -} &= F\left(zL_{+-} - L_{--}\right) & L_{\psi\psi} &= F^2\left(z^2 L_{++} + L_{--}\right) - zF\left(L_{-+} + L_{+-}\right) \end{aligned} \tag{3.2.7}$$

for which the Onsager symmetry $L_{\psi j} = L_{j\psi}$ also holds if it holds for the original coefficients. This can for instance be shown by rewriting one of the other flux equations, say

$$J_u = L_{uu}\partial_x \left(\frac{1}{T}\right) - L_{u+}\partial_x \left(\frac{\mu_{\mathrm{M}^{z+}}}{T}\right) - L_{u-}\partial_x \left(\frac{\mu_{\mathrm{Cl}^-}}{T}\right) - \underbrace{F\left(zL_{u+} - L_{u-}\right)}_{L_{u\psi}} \partial_x \left(\frac{\psi}{T}\right) \tag{3.2.8}$$

where we see that if $L_{u+} = L_{+u}$ and $L_{u-} = L_{-u}$, then $L_{u\psi} = L_{\psi u}$. The same can easily be shown for the remaining cross coefficients. Imposing the open circuit condition, $j = 0$, we find from (3.2.6)

$$\left(\partial_x \left(\frac{\psi}{T}\right)\right)_{j=0} = \frac{L_{\psi u}}{L_{\psi\psi}}\partial_x \left(\frac{1}{T}\right) - \frac{L_{\psi +}}{L_{\psi\psi}}\partial_x \left(\frac{\mu_{\mathrm{M}^{z+}}}{T}\right) - \frac{L_{\psi -}}{L_{\psi\psi}}\partial_x \left(\frac{\mu_{\mathrm{Cl}^-}}{T}\right) \tag{3.2.9}$$

from which we can now exploit the symmetries among the coefficients to identify the ionic transport numbers

$$\begin{aligned} zF\frac{L_{\psi +}}{L_{\psi\psi}} = zF\frac{L_{+\psi}}{L_{\psi\psi}} = zF\left(\frac{J_{\mathrm{M}^{z+}}}{j}\right)_{\mathrm{d}T=0,\mathrm{d}\mu=0} &=: t_{\mathrm{M}^{z+}} \\ -F\frac{L_{\psi -}}{L_{\psi\psi}} = -F\frac{L_{-\psi}}{L_{\psi\psi}} = -F\left(\frac{J_{\mathrm{Cl}^-}}{j}\right)_{\mathrm{d}T=0,\mathrm{d}\mu=0} &=: t_{\mathrm{Cl}^-} \end{aligned} \tag{3.2.10}$$

which are linearly dependent through the definition of the electric current density, such that

$$t_{\mathrm{M}^{z+}} + t_{\mathrm{Cl}^-} = 1 \tag{3.2.11}$$

The energy flux can be expressed as

$$J_u = J'_q + H_{\mathrm{M}^{z+}} J_{\mathrm{M}^{z+}} + H_{\mathrm{Cl}^-} J_{\mathrm{Cl}^-} + j\psi \tag{3.2.12}$$

where J'_q is the *measurable heat flux*, and H_i is the partial molar enthalpy of i, such that the three first terms give the total heat flux. The fourth term is the electrical work contribution to the energy transfer. We express the measurable heat flux in terms of entropy

$$\begin{aligned} J'_q &= TJ_s - TS_{\mathrm{M}^{z+}} J_{\mathrm{M}^{z+}} - TS_{\mathrm{Cl}^-} J_{\mathrm{Cl}^-} \\ &= T\left[\left(S^*_{\mathrm{M}^{z+}} - S_{\mathrm{M}^{z+}}\right) J_{\mathrm{M}^{z+}} + \left(S^*_{\mathrm{Cl}^-} - S_{\mathrm{Cl}^-}\right) J_{\mathrm{Cl}^-}\right] \end{aligned} \tag{3.2.13}$$

where S_i is the partial molar entropy of i, and we have introduced the *transported entropy* S^*_i of i to represent the contribution of i to the total entropy transfer. Using that $\mu_i = H_i - TS_i$, we obtain

$$J_u = \left(TS^*_{\mathrm{M}^{z+}} + \mu_{\mathrm{M}^{z+}}\right) J_{\mathrm{M}^{z+}} + \left(TS^*_{\mathrm{Cl}^-} + \mu_{\mathrm{Cl}^-}\right) J_{\mathrm{Cl}^-} + j\psi \tag{3.2.14}$$

such that, by the Onsager symmetry

$$F\frac{L_{\psi u}}{L_{\psi\psi}} = F\left(\frac{J_u}{j}\right)_{\mathrm{d}T=0,\mathrm{d}\mu=0} = \frac{t_{\mathrm{M}^{z+}}}{z}\left(TS^*_{\mathrm{M}^{z+}} + \mu_{\mathrm{M}^{z+}}\right) - t_{\mathrm{Cl}^-}\left(TS^*_{\mathrm{Cl}^-} + \mu_{\mathrm{Cl}^-}\right) + F\psi \tag{3.2.15}$$

and (3.2.9) becomes

$$\begin{aligned} \left(\partial_x\left(\frac{\psi}{T}\right)\right)_{j=0} = {} & \frac{t_{\mathrm{M}^{z+}}}{zF}\left[\left(TS^*_{\mathrm{M}^{z+}} + \mu_{\mathrm{M}^{z+}}\right)\partial_x\left(\frac{1}{T}\right) - \partial_x\left(\frac{\mu_{\mathrm{M}^{z+}}}{T}\right)\right] \\ & - \frac{t_{\mathrm{Cl}^-}}{F}\left[\left(TS^*_{\mathrm{Cl}^-} + \mu_{\mathrm{Cl}^-}\right)\partial_x\left(\frac{1}{T}\right) - \partial_x\left(\frac{\mu_{\mathrm{Cl}^-}}{T}\right)\right] + \psi\partial_x\left(\frac{1}{T}\right) \end{aligned} \tag{3.2.16}$$

we use that

$$\psi\partial_x\left(\frac{1}{T}\right) = \partial_x\left(\frac{\psi}{T}\right) - \frac{1}{T}\partial_x\psi \qquad \text{and} \qquad \partial_x\left(\frac{\mu_i}{T}\right) = \mu_i\partial_x\left(\frac{1}{T}\right) + \frac{1}{T}\partial_x\mu_i \tag{3.2.17}$$

so that (3.2.16) can be rewritten to

$$\left(\partial_x\psi\right)_{j=0} = -\frac{t_{\mathrm{M}^{z+}}}{zF}\left[S^*_{\mathrm{M}^{z+}}\partial_x T + \partial_x\mu_{\mathrm{M}^{z+}}\right] + \frac{t_{\mathrm{Cl}^-}}{F}\left[S^*_{\mathrm{Cl}^-}\partial_x T + \partial_x\mu_{\mathrm{Cl}^-}\right] \tag{3.2.18}$$

subtracting $\partial_x\mu_{\mathrm{Cl}^-}/F$ from both sides, and applying (3.2.4) and (3.2.11), we obtain the measurable potential

$$\left(\partial_x\phi\right)_{j=0} = -\frac{1}{F}\left[\frac{t_{\mathrm{M}^{z+}}}{z}S^*_{\mathrm{M}^{z+}} - t_{\mathrm{Cl}^-}S^*_{\mathrm{Cl}^-}\right]\partial_x T - \frac{t_{\mathrm{M}^{z+}}}{zF}\partial_x\mu_{\mathrm{e}} \tag{3.2.19}$$

and the temperature dependence of the chemical potential can be separated from the composition dependence to first order as

$$\partial_x\mu_{\mathrm{e}} = \partial_x\mu_{\mathrm{e},T} + \frac{\partial\mu_{\mathrm{e}}}{\partial T}\partial_x T = \partial_x\mu_{\mathrm{e},T} - S_{\mathrm{e}}\partial_x T \tag{3.2.20}$$

where the subscript T indicates that the chemical potential is evaluated at the temperature around which the expansion is taken. We employ the activity model for the composition dependence of the chemical potential

$$\partial_x \mu_{\mathrm{e},T} = \frac{\partial \mu_{\mathrm{e},T}}{\partial a_{\mathrm{e},T}} \partial_x a_{\mathrm{e},T} = \nu R T_0 \partial_x \ln\left(a_{\mathrm{e},T}\right) \tag{3.2.21}$$

where R is the universal gas constant, $a_{\mathrm{e},T}$ the isothermal activity of the electrolyte, ν the number of ions per molecule of electrolyte, and T_0 the temperature from which the temperature dependence is expanded. The activity can be expressed as the product $\gamma_{\mathrm{e}} m_{\mathrm{e}}$, where γ_{e} is the mean molal activity coefficient, and m_{e} is the molality of the electrolyte. The gradient in electric potential can finally be expressed as

$$\left(\partial_x \phi\right)_{j=0} = \frac{1}{F}\left[\frac{t_{\mathrm{M}^{z+}}}{z}\left(S_{\mathrm{e}} - S^*_{\mathrm{M}^{z+}}\right) + t_{\mathrm{Cl}^-} S^*_{\mathrm{Cl}^-}\right]\partial_x T - \frac{\nu R T_0 t_{\mathrm{M}^{z+}}}{zF}\partial_x \ln\left(a_{\mathrm{e},T}\right) \tag{3.2.22}$$

Before proceeding to integrate (3.2.22), we make explicit the temperature dependence of the entropies

$$\begin{aligned} S_i\left(T\right) &= S_i\left(\hat{T}\right) + \int_{\hat{T}}^{T} \frac{c_{p,i}}{T}\mathrm{d}T = S_i\left(\hat{T}\right) + c_{p,i}\ln\left(\frac{T}{\hat{T}}\right) \\ S^*_i\left(T\right) &= S^*_i\left(\hat{T}\right) + \int_{\hat{T}}^{T} \frac{\tau_i}{T}\mathrm{d}T = S^*_i\left(\hat{T}\right) + \tau_i \ln\left(\frac{T}{\hat{T}}\right) \end{aligned} \tag{3.2.23}$$

where $c_{p,i}$ and τ_i are the partial molar heat capacity, and the Thomson coefficient of i, respectively. We have here neglected the temperature dependence of these quantities in performing the integration in (3.2.23), and have introduced the mean temperature of the cell, $\hat{T} = (T_1 + T_2)/2$. We will neglect the composition dependence of the transported entropies and transport numbers. We take the steady state profiles in composition, temperature, and electric potential to be explicit functions of position only, and form the integration measures

$$\partial_x \phi \mathrm{d}x = \mathrm{d}\phi \qquad \partial_x T \mathrm{d}x = \mathrm{d}T \qquad \partial_x \ln\left(a_{\mathrm{e},T}\right)\mathrm{d}x = \mathrm{d}\ln\left(a_{\mathrm{e},T}\right) \tag{3.2.24}$$

In order to ease notation, we define the partial Seebeck coefficient of the solution, and its corresponding Thomson coefficient

$$\begin{aligned} \eta^{\mathrm{sol}}_{\mathrm{S}} &= \frac{1}{F}\left[\frac{t_{\mathrm{M}^{z+}}}{z}\left(S_{\mathrm{e}} - S^*_{\mathrm{M}^{z+}}\right) + t_{\mathrm{Cl}^-} S^*_{\mathrm{Cl}^-}\right] \\ \tau^{\mathrm{sol}} &= \frac{1}{F}\left[\frac{t_{\mathrm{M}^{z+}}}{z}\left(c_{p,\mathrm{e}} - \tau_{\mathrm{M}^{z+}}\right) + t_{\mathrm{Cl}^-}\tau_{\mathrm{Cl}^-}\right] \end{aligned} \tag{3.2.25}$$

Unless otherwise stated, all quantities are evaluated at temperature $\hat{T}$. The integral of (3.2.22) over compartment 1 is then

$$\begin{aligned} \int_{\phi_1}^{\phi_\ell} \mathrm{d}\phi = \Delta_{1,\ell}\phi &= \int_{T_1}^{T_\ell}\left[\eta^{\mathrm{sol}}_{\mathrm{S}} + \tau^{\mathrm{sol}}\ln\left(\frac{T}{\hat{T}}\right)\right]\mathrm{d}T - \int_{a^1_{\mathrm{e}}(T_1)}^{a^\ell_{\mathrm{e}}(T_1)} \frac{\nu R T_1 t_{\mathrm{M}^{z+}}}{zF a_{\mathrm{e},T}}\mathrm{d}a_{\mathrm{e},T} \\ &= \left[\eta^{\mathrm{sol}}_{\mathrm{S}} + \tau^{\mathrm{sol}} f\left(T_1, T_\ell\right)\right]\Delta_{1,\ell}T - \frac{\nu R T_1 t_{\mathrm{M}^{z+}}}{zF}\ln\left(\frac{a^\ell_{\mathrm{e}}\left(T_1\right)}{a^1_{\mathrm{e}}\left(T_1\right)}\right) \end{aligned} \tag{3.2.26}$$

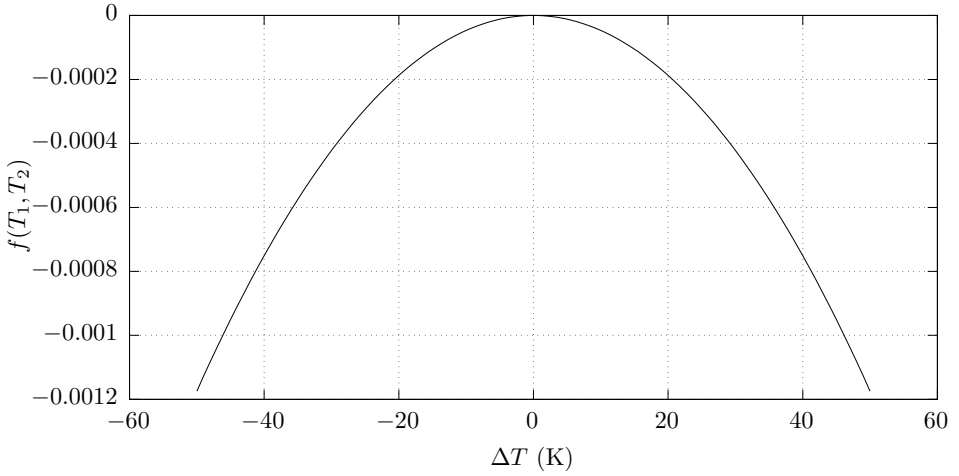

Figure 3.2: Plot of the function f defined in (3.2.27) as a function of the temperature difference when the mean temperature is kept constant equal to 298.15 K.

where we have introduced the difference notation, $\Delta_{j,k}F = F_k - F_j$, and the function

$$f\left(T_j, T_k\right) = \frac{T_k \ln\left(T_k/\hat{T}\right) - T_j \ln\left(T_j/\hat{T}\right)}{T_k - T_j} - 1 \tag{3.2.27}$$

A plot of the function f is given in figure 3.2. We observe that for a mean temperature of 298.15 K, the order of magnitude of f remains at 10^{-4} up to a temperature difference of about 40 K. Thomson coefficients in aqueous solution are typically on the same order of magnitude as their corresponding Seebeck coefficients [8, 58], and we therefore expect the nonlinear dependence of the cell potential on the temperature difference to be important at the third or fourth decimal.

Equivalently, we perform the integration over compartment 2, expanding the chemical potential around the temperature T_2

$$\Delta_{r,2}\phi = \left[\eta_{\mathrm{S}}^{\mathrm{sol}} + \tau^{\mathrm{sol}} f\left(T_r, T_2\right)\right] \Delta_{r,2}T - \frac{\nu R T_2 t_{\mathrm{M}^{z+}}}{zF} \ln\left(\frac{a_{\mathrm{e}}^2\left(T_2\right)}{a_{\mathrm{e}}^r\left(T_2\right)}\right) \tag{3.2.28}$$

The total contribution from the aqueous solution is obtained by adding (3.2.26) and (3.2.28)

$$\begin{aligned}\Delta\phi_{\mathrm{sol}} = {} & \eta_{\mathrm{S}}^{\mathrm{sol}}\left(\Delta_{1,\ell}T + \Delta_{r,2}T\right) + \tau^{\mathrm{sol}}\left[f\left(T_1, T_\ell\right)\Delta_{1,\ell}T + f\left(T_r, T_2\right)\Delta_{r,2}T\right] \\ & - \frac{\nu R t_{\mathrm{M}^{z+}}}{zF}\left[T_1 \ln\left(\frac{a_{\mathrm{e}}^\ell\left(T_1\right)}{a_{\mathrm{e}}^1\left(T_1\right)}\right) + T_2 \ln\left(\frac{a_{\mathrm{e}}^2\left(T_2\right)}{a_{\mathrm{e}}^r\left(T_2\right)}\right)\right]\end{aligned} \tag{3.2.29}$$

which is a sum of a thermoelectric contribution, represented by the Seebeck coefficient, and two isothermal Nernstian potentials due to nonuniform composition profiles between the electrodes and the membrane surfaces.

3.2.2 The Membrane

The treatment of the homogeneous phase is very similar to that of the aqueous solution. A principal difference is that, in the membrane, electroosmotic transport of water as a neutral component may occur. Let the subscript w denote quantities pertaining to water, and denote by a bar all quantities evaluated in the membrane phase. The flux-force relations are

$$\begin{bmatrix} J_u \\ J_{\mathrm{M}^{z+}} \\ J_{\mathrm{Cl}^-} \\ J_{\mathrm{w}} \end{bmatrix} = \begin{bmatrix} \overline{L}_{uu} & \overline{L}_{u+} & \overline{L}_{u-} & \overline{L}_{u\mathrm{w}} \\ \overline{L}_{+u} & \overline{L}_{++} & \overline{L}_{+-} & \overline{L}_{+\mathrm{w}} \\ \overline{L}_{-u} & \overline{L}_{-+} & \overline{L}_{--} & \overline{L}_{-\mathrm{w}} \\ \overline{L}_{\mathrm{w}u} & \overline{L}_{\mathrm{w}+} & \overline{L}_{\mathrm{w}-} & \overline{L}_{\mathrm{ww}} \end{bmatrix} \begin{bmatrix} \partial_x \left(1/T\right) \\ -\partial_x \left(\tilde{\mu}_{\mathrm{M}^{z+}}/T\right) \\ -\partial_x \left(\tilde{\mu}_{\mathrm{Cl}^-}/T\right) \\ -\partial_x \left(\mu_{\mathrm{w}}/T\right) \end{bmatrix} \tag{3.2.30}$$

Again, we can identify the electric current density

$$j = \overline{L}_{\psi u}\partial_x\left(\frac{1}{T}\right) - \overline{L}_{\psi +}\partial_x\left(\frac{\mu_{\mathrm{M}^{z+}}}{T}\right) - \overline{L}_{\psi -}\partial_x\left(\frac{\mu_{\mathrm{Cl}^-}}{T}\right) - \overline{L}_{\psi \mathrm{w}}\partial_x\left(\frac{\mu_{\mathrm{w}}}{T}\right) - \overline{L}_{\psi\psi}\partial_x\left(\frac{\psi}{T}\right) \tag{3.2.31}$$

where $\overline{L}_{\psi\mathrm{w}} = F(z\overline{L}_{+\mathrm{w}} - \overline{L}_{-\mathrm{w}})$, and the remaining coefficients are defined exactly as in (3.2.7). The open circuit condition gives

$$\left(\partial_x\left(\frac{\psi}{T}\right)\right)_{j=0} = \frac{\overline{L}_{\psi u}}{\overline{L}_{\psi\psi}}\partial_x\left(\frac{1}{T}\right) - \frac{\overline{L}_{\psi +}}{\overline{L}_{\psi\psi}}\partial_x\left(\frac{\mu_{\mathrm{M}^{z+}}}{T}\right) - \frac{\overline{L}_{\psi -}}{\overline{L}_{\psi\psi}}\partial_x\left(\frac{\mu_{\mathrm{Cl}^-}}{T}\right) - \frac{\overline{L}_{\psi \mathrm{w}}}{\overline{L}_{\psi\psi}}\partial_x\left(\frac{\mu_{\mathrm{w}}}{T}\right) \tag{3.2.32}$$

The ionic transport numbers are found in the same manner as in the aqueous solution,

$$\begin{aligned} zF\frac{\overline{L}_{\psi +}}{\overline{L}_{\psi\psi}} = zF\frac{\overline{L}_{+\psi}}{\overline{L}_{\psi\psi}} &= zF\left(\frac{J_{\mathrm{M}^{z+}}}{j}\right)_{\mathrm{d}T=0,\mathrm{d}\mu=0} =: \bar{t}_{\mathrm{M}^{z+}} \\ -F\frac{\overline{L}_{\psi -}}{\overline{L}_{\psi\psi}} = -F\frac{\overline{L}_{-\psi}}{\overline{L}_{\psi\psi}} &= -F\left(\frac{J_{\mathrm{Cl}^-}}{j}\right)_{\mathrm{d}T=0,\mathrm{d}\mu=0} =: \bar{t}_{\mathrm{Cl}^-} \end{aligned} \tag{3.2.33}$$

and, similarly, the water transference coefficient

$$F\frac{\overline{L}_{\psi\mathrm{w}}}{\overline{L}_{\psi\psi}} = F\frac{\overline{L}_{\mathrm{w}\psi}}{\overline{L}_{\psi\psi}} = \left(\frac{J_{\mathrm{w}}}{j}\right)_{\mathrm{d}T=0,\mathrm{d}\mu=0} =: \bar{t}_{\mathrm{w}} \tag{3.2.34}$$

The energy balance proceeds in a manner similar to that of the aqueous solution. The energy flux is

$$J_u = \left(T\overline{S}^*_{\mathrm{M}^{z+}} + \overline{\mu}_{\mathrm{M}^{z+}}\right)J_{\mathrm{M}^{z+}} + \left(T\overline{S}^*_{\mathrm{Cl}^-} + \overline{\mu}_{\mathrm{Cl}^-}\right)J_{\mathrm{Cl}^-} + \overline{\mu}_{\mathrm{w}}J_{\mathrm{w}} + j\psi \tag{3.2.35}$$

where we have neglected the transported entropy of neutral water, as the electroosmotic water transport is a reversible effect which should not contribute to the entropy production. See e.g. [8] for a discussion on this. The electric field strength is

$$\left(\partial_x\psi\right)_{j=0} = -\frac{\bar{t}_{\mathrm{M}^{z+}}}{zF}\left[\overline{S}^*_{\mathrm{M}^{z+}}\partial_x T + \partial_x\mu_{\mathrm{M}^{z+}}\right] + \frac{\bar{t}_{\mathrm{Cl}^-}}{F}\left[\overline{S}^*_{\mathrm{Cl}^-}\partial_x T + \partial_x\mu_{\mathrm{Cl}^-}\right] - \frac{\bar{t}_{\mathrm{w}}}{F}\partial_x\mu_{\mathrm{w}} \tag{3.2.36}$$

Subtracting $\partial_x \mu_{\mathrm{Cl}^-}/F$ from both sides and using that $\bar{t}_{\mathrm{M}^{z+}} + \bar{t}_{\mathrm{Cl}^-} = 1$, and identifying the chemical potential of electrolyte, this becomes

$$(\partial_x \phi)_{j=0} = -\frac{1}{F}\left[\frac{\bar{t}_{\mathrm{M}^{z+}}}{z}\overline{S}^*_{\mathrm{M}^{z+}} - \bar{t}_{\mathrm{Cl}^-}\overline{S}^*_{\mathrm{Cl}^-}\right]\partial_x T - \frac{\bar{t}_{\mathrm{M}^{z+}}}{zF}\partial_x \mu_{\mathrm{e}} - \frac{\bar{t}_{\mathrm{w}}}{F}\partial_x \mu_{\mathrm{w}} \tag{3.2.37}$$

Using (3.2.20) and (3.2.21), this is

$$\begin{aligned}(\partial_x \phi)_{j=0} = \frac{1}{F}&\left[\frac{\bar{t}_{\mathrm{M}^{z+}}}{z}\left(\overline{S}_{\mathrm{e}} - \overline{S}^*_{\mathrm{M}^{z+}}\right) + \bar{t}_{\mathrm{Cl}^-}\overline{S}^*_{\mathrm{Cl}^-} + \bar{t}_{\mathrm{w}}\overline{S}_{\mathrm{w}}\right]\partial_x T \\ &- \frac{\nu R T_0 \bar{t}_{\mathrm{M}^{z+}}}{zF}\partial_x \ln\left(a_{\mathrm{e},T}\right) - \frac{R T_0 \bar{t}_{\mathrm{w}}}{F}\partial_x \ln\left(a_{\mathrm{w},T}\right)\end{aligned} \tag{3.2.38}$$

where $a_{\mathrm{w},T}$ is the isothermal activity of water. We define the Seebeck and Thomson coefficients

$$\begin{aligned}\eta_{\mathrm{S}}^{\text{`mem}} &:= \frac{1}{F}\left[\frac{\bar{t}_{\mathrm{M}^{z+}}}{z}\left(\overline{S}_{\mathrm{e}} - \overline{S}^*_{\mathrm{M}^{z+}}\right) + \bar{t}_{\mathrm{Cl}^-}\overline{S}^*_{\mathrm{Cl}^-} + \bar{t}_{\mathrm{w}}\overline{S}_{\mathrm{w}}\right] \\ \tau^{\text{`mem}} &:= \frac{1}{F}\left[\frac{\bar{t}_{\mathrm{M}^{z+}}}{z}\left(\overline{c}_{p,\mathrm{e}} - \overline{\tau}_{\mathrm{M}^{z+}}\right) + \bar{t}_{\mathrm{Cl}^-}\overline{\tau}_{\mathrm{Cl}^-} + \bar{t}_{\mathrm{w}}\overline{c}_{p,\mathrm{w}}\right]\end{aligned} \tag{3.2.39}$$

We choose to expand the temperature around the mean temperature, $\hat{T}$. More pedagogically, this can be obtained by expanding around both T_ℓ and T_r, and taking the symmetric combination of the two expansions, assuming that $\hat{T}$ is also the mean temperature of T_r and T_ℓ. Upon constructing the integration measures as in (3.2.24), integration of (3.2.38) leaves

$$\begin{aligned}\Delta\phi'_{\mathrm{mem}} = &\left[\eta_{\mathrm{S}}^{\text{`mem}} + \tau^{\text{`mem}} f\left(T_\ell, T_r\right)\right]\Delta_{\ell,r} T \\ &- \frac{\nu R \hat{T} \bar{t}_{\mathrm{M}^{z+}}}{zF}\ln\left(\frac{\overline{a}^r_{\mathrm{e}}\left(\hat{T}\right)}{\overline{a}^\ell_{\mathrm{e}}\left(\hat{T}\right)}\right) - \frac{R\hat{T}\bar{t}_{\mathrm{w}}}{F}\ln\left(\frac{\overline{a}^r_{\mathrm{w}}\left(\hat{T}\right)}{\overline{a}^\ell_{\mathrm{w}}\left(\hat{T}\right)}\right)\end{aligned} \tag{3.2.40}$$

We will now show that adding to this the electric potential jumps at the interfaces between aqueous solution and bulk membrane will eliminate membrane phase state variables in favour of those in aqueous solution, while the kinetic variables, such as the transported entropies, will remain specific to the membrane. Assuming that there is no jump in temperature at the interface in the steady state, the steady state entropy production of one such interface is

$$\sigma_{\mathrm{surf}} = -J_{\mathrm{M}^{z+}}\frac{\Delta_{i,o}\tilde{\mu}_{\mathrm{M}^{z+}}}{T} - J_{\mathrm{Cl}^-}\frac{\Delta_{i,o}\tilde{\mu}_{\mathrm{Cl}^-}}{T} - J_{\mathrm{w}}\frac{\Delta_{i,o}\mu_{\mathrm{w}}}{T} \tag{3.2.41}$$

where we note that all driving forces are zero if the interface is in equilibrium with the external solution, and there will be no net contribution to the electric potential. Rather than assume that the interfaces are in equilibrium with the solution, we derive

an expression for the steady state contribution. From the same arguments as in the bulk phase, we obtain the electric current density through the interface

$$j = -\frac{L^s_{\psi+}}{T}\Delta_{i,o}\mu_{\mathrm{M}^{z+}} - \frac{L^s_{\psi-}}{T}\Delta_{i,o}\mu_{\mathrm{Cl}^-} - \frac{L^s_{\psi\mathrm{w}}}{T}\Delta_{i,o}\mu_{\mathrm{w}} - \frac{L^s_{\psi\psi}}{T}\Delta_{i,o}\psi \tag{3.2.42}$$

The transference coefficients and transport numbers derived from these coefficients must, by the steady state constraint that there is no accumulation of charge or water at the interfaces, be equal to the membrane bulk phase coefficients. The open circuit electric potential jump is therefore

$$(\Delta_{i,o}\psi)_{j=0} = -\frac{\overline{t}_{\mathrm{M}^{z+}}}{zF}\Delta_{i,o}\mu_{\mathrm{M}^{z+}} + \frac{\overline{t}_{\mathrm{Cl}^-}}{F}\Delta_{i,o}\mu_{\mathrm{Cl}^-} - \frac{\overline{t}_{\mathrm{w}}}{F}\Delta_{i,o}\mu_{\mathrm{w}} \tag{3.2.43}$$

Correcting for the chemical potential of chloride, and identifying the electrolyte chemical potential, the jump in measurable electric potential is

$$(\Delta_{i,o}\phi)_{j=0} = -\frac{\overline{t}_{\mathrm{M}^{z+}}}{zF}\Delta_{i,o}\mu_{\mathrm{e}} - \frac{\overline{t}_{\mathrm{w}}}{F}\Delta_{i,o}\mu_{\mathrm{w}} \tag{3.2.44}$$

Made explicit in compartment 1, expanding the chemical potentials around $\hat{T}$

$$\begin{aligned}\Delta\phi^{(1)}_{\mathrm{surf}} =& -\frac{\overline{t}_{\mathrm{M}^{z+}}}{zF}\left[\left(\overline{H}^\ell_{\mathrm{e}} - H^\ell_{\mathrm{e}}\right) - T_\ell\left(\overline{S}^\ell_{\mathrm{e}} - S^\ell_{\mathrm{e}}\right) + \left(\overline{c}_{p,\mathrm{e}} - c_{p,\mathrm{e}}\right)\left(T_\ell - \hat{T} - T_\ell\ln\left(T_\ell/\hat{T}\right)\right)\right] \\ & - \frac{\overline{t}_{\mathrm{w}}}{F}\left[\left(\overline{H}^\ell_{\mathrm{w}} - H^\ell_{\mathrm{w}}\right) - T_\ell\left(\overline{S}^\ell_{\mathrm{e}} - S^\ell_{\mathrm{e}}\right) + \left(\overline{c}_{p,\mathrm{w}} - c_{p,\mathrm{w}}\right)\left(T_\ell - \hat{T} - T_\ell\ln\left(T_\ell/\hat{T}\right)\right)\right]\end{aligned} \tag{3.2.45}$$

and similarly for the interface in compartment 2

$$\begin{aligned}\Delta\phi^{(2)}_{\mathrm{surf}} =& \frac{\overline{t}_{\mathrm{M}^{z+}}}{zF}\left[\left(\overline{H}^r_{\mathrm{e}} - H^r_{\mathrm{e}}\right) - T_r\left(\overline{S}^r_{\mathrm{e}} - S^r_{\mathrm{e}}\right) + \left(\overline{c}_{p,\mathrm{e}} - c_{p,\mathrm{e}}\right)\left(T_r - \hat{T} - T_r\ln\left(T_r/\hat{T}\right)\right)\right] \\ & + \frac{\overline{t}_{\mathrm{w}}}{F}\left[\left(\overline{H}^r_{\mathrm{w}} - H^r_{\mathrm{w}}\right) - T_r\left(\overline{S}^r_{\mathrm{e}} - S^r_{\mathrm{e}}\right) + \left(\overline{c}_{p,\mathrm{w}} - c_{p,\mathrm{w}}\right)\left(T_r - \hat{T} - T_r\ln\left(T_r/\hat{T}\right)\right)\right]\end{aligned} \tag{3.2.46}$$

We now introduce activities again by noticing that e.g.

$$\overline{H}^\ell_{\mathrm{e}} - H^\ell_{\mathrm{e}} - T_\ell\left(\overline{S}^\ell_{\mathrm{e}} - S^\ell_{\mathrm{e}}\right) \approx \overline{\mu}^\ell_{\mathrm{e}} - \mu^\ell_{\mathrm{e}} - \left(T_\ell - \hat{T}\right)\left(\overline{S}_{\mathrm{e}} - S_{\mathrm{e}}\right) \tag{3.2.47}$$

and similarly for the remaining terms. We have neglected the composition dependence of the entropies, as we expect these variations to be small. Adding the two contributions then gives the measurable contribution to the electric potential

$$\begin{aligned}&\frac{\overline{t}_{\mathrm{M}^{z+}}}{zF}\left\{\left[\left(S_{\mathrm{e}} - \overline{S}_{\mathrm{e}}\right) + \left(c_{p,\mathrm{e}} - \overline{c}_{p,\mathrm{e}}\right)f\left(T_\ell, T_r\right)\right]\Delta_{\ell,r}T + \nu R\hat{T}\left[\ln\left(\frac{\overline{a}^r_{\mathrm{e}}}{\overline{a}^\ell_{\mathrm{e}}}\right) - \ln\left(\frac{a^r_{\mathrm{e}}}{a^\ell_{\mathrm{e}}}\right)\right]\right\} \\ &+ \frac{\overline{t}_{\mathrm{w}}}{F}\left\{\left[\left(S_{\mathrm{w}} - \overline{S}_{\mathrm{w}}\right) + \left(c_{p,\mathrm{w}} - \overline{c}_{p,\mathrm{w}}\right)f\left(T_\ell, T_r\right)\right]\Delta_{\ell,r}T + R\hat{T}\left[\ln\left(\frac{\overline{a}^r_{\mathrm{w}}}{\overline{a}^\ell_{\mathrm{w}}}\right) - \ln\left(\frac{a^r_{\mathrm{w}}}{a^\ell_{\mathrm{w}}}\right)\right]\right\}\end{aligned} \tag{3.2.48}$$

where activities are evaluated at temperature $\hat{T}$. One may notice that adding this to the bulk contribution in (3.2.40) simply replaces membrane phase thermodynamic entropies and activities with those in aqueous solution. We therefore define new coefficients

$$\begin{aligned}\eta_{\mathrm{S}}^{\mathrm{mem}} &:= \frac{1}{F}\left[\frac{\overline{t}_{\mathrm{M}^{z+}}}{z}\left(S_{\mathrm{e}} - \overline{S}^{*}_{\mathrm{M}^{z+}}\right) + \overline{t}_{\mathrm{Cl}^{-}}\overline{S}^{*}_{\mathrm{Cl}^{-}} + \overline{t}_{\mathrm{w}}S_{\mathrm{w}}\right] \\ \tau^{\mathrm{mem}} &:= \frac{1}{F}\left[\frac{\overline{t}_{\mathrm{M}^{z+}}}{z}\left(c_{p,\mathrm{e}} - \overline{\tau}_{\mathrm{M}^{z+}}\right) + \overline{t}_{\mathrm{Cl}^{-}}\overline{\tau}_{\mathrm{Cl}^{-}} + \overline{t}_{\mathrm{w}}c_{p,\mathrm{w}}\right]\end{aligned} \tag{3.2.49}$$

the total contribution from the membrane and its interfaces is

$$\Delta\phi_{\mathrm{mem}} = \left[\eta_{\mathrm{S}}^{\mathrm{mem}} + \tau^{\mathrm{mem}} f\left(T_\ell, T_r\right)\right]\Delta_{\ell,r}T - \frac{\nu R\hat{T}\overline{t}_{\mathrm{M}^{z+}}}{zF}\ln\left(\frac{a_{\mathrm{e}}^{r}}{a_{\mathrm{e}}^{\ell}}\right) - \frac{R\hat{T}\overline{t}_{\mathrm{w}}}{F}\ln\left(\frac{a_{\mathrm{w}}^{r}}{a_{\mathrm{w}}^{\ell}}\right) \tag{3.2.50}$$

which remains the same under steady state conditions, regardless of whether or not the membrane surfaces are in equilibrium with the external solution.

3.2.3 The Electrodes and External Circuit

We have thus far described the membrane and the aqueous solution, and have referenced the electrodes at each subsystem through the relations (3.2.4). We will now describe the contributions due to the chemical reactions at the electrode surfaces, and any contribution that may occur in the external circuit. We assume again a continuous steady state temperature profile. At the electrode surfaces, the charge carrier changes from chloride in aqueous solution, to electrons in metallic silver. This can be described as transport of chloride (i, s) into the layer of silver chloride, a chemical reaction transforming metallic silver to silver chloride, and transport of electrons out of the silver chloride layer into the metallic silver (s, o). The entropy production is

$$\sigma_{\mathrm{chem}} = -J^{i}_{\mathrm{Cl}^{-}}\frac{\Delta_{i,s}\tilde{\mu}_{\mathrm{Cl}^{-}}}{T} - J^{o}_{\mathrm{e}^{-}}\frac{\Delta_{s,o}\tilde{\mu}_{\mathrm{e}^{-}}}{T} - r^{c}\frac{\Delta_{n}G}{T} \tag{3.2.51}$$

with r^c the chemical reaction rate, $\Delta_n G$ the Gibbs energy contribution of silver and silver chloride in the electrode reaction, and J_{e^-} the electron flux. We take the reaction rate to be constrained by the electric current

$$r^{c} = j/F \tag{3.2.52}$$

and the other fluxes are those making up the electric current

$$J^{i}_{\mathrm{Cl}^{-}} = J^{o}_{\mathrm{e}^{-}} = -j/F \tag{3.2.53}$$

and the electrochemical potentials are

$$\begin{aligned}\Delta_{i,s}\tilde{\mu}_{\mathrm{Cl}^{-}} &= \Delta_{i,s}\mu_{\mathrm{Cl}^{-}} - F\Delta_{i,s}\psi = -F\Delta_{i,s}\phi \\ \Delta_{s,o}\tilde{\mu}_{\mathrm{e}^{-}} &= \Delta_{s,o}\mu_{\mathrm{e}^{-}} - F\Delta_{s,o}\psi = -F\Delta_{s,o}\phi\end{aligned} \tag{3.2.54}$$

there is thus only one independent flux-force pair in the entropy production

$$\sigma_{\text{chem}} = -\frac{j}{T}\left(\Delta_{i,o}\phi + \frac{\Delta_n G}{F}\right) \tag{3.2.55}$$

then, the linear flux-force relation gives

$$\left(\Delta_{i,o}\phi\right)_{j=0} = -\frac{\Delta_n G}{F} \tag{3.2.56}$$

which is the Nernst equation from equilibrium thermodynamics. We can now use this relation to find the electrode contribution to the measurable electric potential. In compartment 1, the transference of 1 Faraday of positive charge from compartment 1 to 2 through the membrane is compensated by the reaction

$$\text{Cl}^- + \text{Ag} \rightarrow \text{AgCl} + \text{e}^- \tag{3.2.57}$$

while the opposite reaction occurs at the electrode in compartment 2. The reaction Gibbs energy contribution from the neutral components in compartment 1 is

$$\Delta_n G^{(1)} = \mu^{(1)}_{\text{AgCl}}\left(T_1\right) - \mu^{(1)}_{\text{Ag}}\left(T_1\right) \tag{3.2.58}$$

and in compartment 2

$$\Delta_n G^{(2)} = \mu^{(2)}_{\text{Ag}}\left(T_2\right) - \mu^{(2)}_{\text{AgCl}}\left(T_2\right) \tag{3.2.59}$$

We use the superscripts to distinguish the states of the electrode materials at the different electrodes. The reason for this distinction is the practical challenge of making the electrodes similar enough that their structural differences do not give rise to a measurable difference in electric potential, known in the literature as a *bias potential*. We will assume that these differences are small, and use mean values at temperature $\hat{T}$ as reference

$$\hat{\mu}_i := \frac{\mu^{(1)}_i + \mu^{(2)}_i}{2} \tag{3.2.60}$$

then,

$$\begin{aligned} \mu^{(1)}_i &= \hat{\mu}_i - \varepsilon_i \\ \mu^{(2)}_i &= \hat{\mu}_i + \varepsilon_i \end{aligned} \tag{3.2.61}$$

with $\varepsilon_i = \mu^{(2)}_i - \hat{\mu}_i = \hat{\mu}_i - \mu^{(1)}_i$ introduced as the deviation parameter between the electrodes. Adding together the Gibbs energies of the two electrode reactions, and using the mean chemical potentials and their temperature dependencies, we obtain

$$\Delta_n G = \left[\hat{S}_{\text{AgCl}} - \hat{S}_{\text{Ag}} + \left(\hat{c}_{p,\text{AgCl}} - \hat{c}_{p,\text{Ag}}\right) f\left(T_1, T_2\right)\right] \Delta_{1,2} T + \Delta_n G_{\text{bias}} \tag{3.2.62}$$

where we have to second order in the temperature difference

$$\Delta_n G_{\text{bias}} = 2\varepsilon + \frac{1}{4}\frac{\partial^2 \varepsilon}{\partial T^2}\bigg|_{T=\hat{T}} \left(\Delta_{1,2} T\right)^2 \qquad \text{with} \quad \varepsilon = \varepsilon_{\text{Ag}} - \varepsilon_{\text{AgCl}} \tag{3.2.63}$$

which gives rise to the measurable bias potential of the electrodes

$$\Delta\phi_{\text{bias}} = -\frac{\Delta_n G_{\text{bias}}}{F} \tag{3.2.64}$$

The total contribution from the electrode reactions is then

$$\Delta\phi_{\text{chem}} = \frac{1}{F}\left[\hat{S}_{\text{Ag}} - \hat{S}_{\text{AgCl}} + (\hat{c}_{p,\text{Ag}} - \hat{c}_{p,\text{AgCl}})\, f\left(T_1, T_2\right)\right]\Delta_{1,2}T + \Delta\phi_{\text{bias}} \tag{3.2.65}$$

An important note is that the bias will generally depend on the temperature difference, due to the second order term which corresponds to deviations in the heat capacities. It is therefore important that the differences between the electrodes are small, so as not to give a significant thermoelectric contribution. We will assume that if the isothermal bias potential is small, then its influence on the thermoelectric potential is negligible.

The silver electrodes are connected to the external circuit via platinum wires. Assuming local equilibrium at the silver-platinum interfaces gives

$$F\left(\Delta\phi_{\text{jun}}\right)_{j=0} = \pm\left(\tilde{\mu}_{\text{e}^-}^{(\text{Ag})} - \tilde{\mu}_{\text{e}^-}^{(\text{Pt})}\right) = 0 \tag{3.2.66}$$

so that the junctions do not contribute to the cell potential. We also assume that all equipment in the external circuit is kept at room temperature, such that we need only consider thermoelectric effects in the platinum wires. The entropy production in such a wire is

$$\sigma^w = J_u\partial_x\left(\frac{1}{T}\right) - J_{\text{e}^-}\partial_x\left(\frac{\tilde{\mu}_{\text{e}^-}}{T}\right) \tag{3.2.67}$$

We have

$$J_u = \left(TS_{\text{e}^-}^{*(\text{Pt})} + \mu_{\text{e}^-}\right)J_{\text{e}^-} + j\psi \qquad J_{\text{e}^-} = -j/F \qquad \tilde{\mu}_{\text{e}^-} = \mu_{\text{e}^-} - F\psi \tag{3.2.68}$$

which gives

$$F\left(\partial_x\left(\frac{\psi}{T}\right)\right)_{j=0} = -\left(\frac{J_u}{J_{\text{e}^-}}\right)_{\text{d}T=0}\partial_x\left(\frac{1}{T}\right) + \partial_x\left(\frac{\mu_{\text{e}^-}}{T}\right) \tag{3.2.69}$$

evaluating the energy flux gives

$$\left(\frac{J_u}{J_{\text{e}^-}}\right)_{\text{d}T=0} = -F\left(\frac{J_u}{j}\right)_{\text{d}T=0} = TS_{\text{e}^-}^{*(\text{Pt})} + \mu_{\text{e}^-} - F\psi \tag{3.2.70}$$

which makes (3.2.69)

$$\begin{aligned} F\left(\partial_x\psi\right)_{j=0} &= -T\left(TS_{\text{e}^-}^{*(\text{Pt})} + \mu_{\text{e}^-}\right)\partial_x\left(\frac{1}{T}\right) + T\partial_x\left(\frac{\mu_{\text{e}^-}}{T}\right) \\ &= S_{\text{e}^-}^{*(\text{Pt})}\partial_x T + \partial_x\mu_{\text{e}^-} \end{aligned} \tag{3.2.71}$$

the measurable potential is obtained by subtracting $\partial_x \mu_{\mathrm{e}^-}/F$ from the electrostatic potential, thus

$$(\partial_x \phi)_{j=0} = \frac{S^{*(\mathrm{Pt})}_{\mathrm{e}^-}}{F} \partial_x T \tag{3.2.72}$$

Integrating by the standard procedure from T_2 to T_1 gives

$$\Delta\phi_{\mathrm{ext}} = -\frac{1}{F}\left[S^{*(\mathrm{Pt})}_{\mathrm{e}^-} + \tau^{(\mathrm{Pt})}_{\mathrm{e}^-} f\left(T_1, T_2\right)\right] \Delta_{1,2} T \tag{3.2.73}$$

the total contribution from the electrodes and the external circuit is then obtained by adding (3.2.65) and (3.2.73). We define the coefficients

$$\begin{aligned} \eta^{\mathrm{el}}_{\mathrm{S}} &= \frac{1}{F}\left[\hat{S}_{\mathrm{Ag}} - \hat{S}_{\mathrm{AgCl}} - S^{*(\mathrm{Pt})}_{\mathrm{e}^-}\right] \\ \tau^{\mathrm{el}} &= \frac{1}{F}\left[\hat{c}_{p,\mathrm{Ag}} - \hat{c}_{p,\mathrm{AgCl}} - \tau^{(\mathrm{Pt})}_{\mathrm{e}^-}\right] \end{aligned} \tag{3.2.74}$$

then,

$$\Delta\phi_{\mathrm{el}} = \left[\eta^{\mathrm{el}}_{\mathrm{S}} + \tau^{\mathrm{el}} f\left(T_1, T_2\right)\right] \Delta_{1,2} T + \Delta\phi_{\mathrm{bias}} \tag{3.2.75}$$

is the contribution of the electrodes and external circuit to the measurable cell potential.

3.2.4 The Total Cell Potential

We will now gather all the terms contributing to the total cell potential, and investigate some limits. The total cell potential is found by adding (3.2.29), (3.2.50), and (3.2.75)

$$\begin{aligned} \Delta\phi = {} & \eta^{\mathrm{sol}}_{\mathrm{S}} \left(\Delta_{1,\ell} T + \Delta_{r,2} T\right) + \tau^{\mathrm{sol}} \left[f\left(T_1, T_\ell\right) \Delta_{1,\ell} T + f\left(T_r, T_2\right) \Delta_{r,2} T\right] \\ & + \left[\eta^{\mathrm{mem}}_{\mathrm{S}} + \tau^{\mathrm{mem}} f\left(T_\ell, T_r\right)\right] \Delta_{\ell,r} T + \left[\eta^{\mathrm{el}}_{\mathrm{S}} + \tau^{\mathrm{el}} f\left(T_1, T_2\right)\right] \Delta_{1,2} T \\ & - \frac{\nu R}{zF}\left\{ t_{\mathrm{M}^{z+}} \left[T_1 \ln\left(\frac{a^{\ell}_{\mathrm{e}}\left(T_1\right)}{a^{1}_{\mathrm{e}}\left(T_1\right)}\right) + T_2 \ln\left(\frac{a^{2}_{\mathrm{e}}\left(T_2\right)}{a^{r}_{\mathrm{e}}\left(T_2\right)}\right)\right] + \bar{t}_{\mathrm{M}^{z+}} \hat{T} \ln\left(\frac{a^{r}_{\mathrm{e}}\left(\hat{T}\right)}{a^{\ell}_{\mathrm{e}}\left(\hat{T}\right)}\right)\right\} \\ & - \frac{R\hat{T}\bar{t}_{\mathrm{w}}}{F} \ln\left(\frac{a^{r}_{\mathrm{w}}\left(\hat{T}\right)}{a^{\ell}_{\mathrm{w}}\left(\hat{T}\right)}\right) + \Delta\phi_{\mathrm{bias}} \end{aligned} \tag{3.2.76}$$

One limit of interest is the compartment-wise isothermal limit, where $T_\ell \to T_1$, and $T_r \to T_2$. The expression reduces to

$$\begin{aligned}\Delta\phi = &\left[\eta_{\mathrm{S}}^{\mathrm{mem}} + \tau^{\mathrm{mem}} f\left(T_1, T_2\right)\right] \Delta_{1,2} T + \left[\eta_{\mathrm{S}}^{\mathrm{el}} + \tau^{\mathrm{el}} f\left(T_1, T_2\right)\right] \Delta_{1,2} T \\ &- \frac{\nu R}{zF}\left\{ t_{\mathrm{M}^{z+}} \left[T_1 \ln\left(\frac{a_{\mathrm{e}}^{\ell}\left(T_1\right)}{a_{\mathrm{e}}^{1}\left(T_1\right)}\right) + T_2 \ln\left(\frac{a_{\mathrm{e}}^{2}\left(T_2\right)}{a_{\mathrm{e}}^{r}\left(T_2\right)}\right)\right] + \bar{t}_{\mathrm{M}^{z+}} \hat{T} \ln\left(\frac{a_{\mathrm{e}}^{r}\left(\hat{T}\right)}{a_{\mathrm{e}}^{\ell}\left(\hat{T}\right)}\right)\right\} \\ &- \frac{R\hat{T}\bar{t}_{\mathrm{w}}}{F} \ln\left(\frac{a_{\mathrm{w}}^{r}\left(\hat{T}\right)}{a_{\mathrm{w}}^{\ell}\left(\hat{T}\right)}\right) + \Delta\phi_{\mathrm{bias}}\end{aligned} \tag{3.2.77}$$

Taking the isothermal limit, $T_1 \to \hat{T}$ and $T_2 \to \hat{T}$, the thermoelectric potentials vanish, and we are left with

$$\Delta\phi = -\frac{\nu R\hat{T}}{zF}\left(\bar{t}_{\mathrm{M}^{z+}} - t_{\mathrm{M}^{z+}}\right) \ln\left(\frac{a_{\mathrm{e}}^{r}\left(\hat{T}\right)}{a_{\mathrm{e}}^{\ell}\left(\hat{T}\right)}\right) - \frac{R\hat{T}\bar{t}_{\mathrm{w}}}{F} \ln\left(\frac{a_{\mathrm{w}}^{r}\left(\hat{T}\right)}{a_{\mathrm{w}}^{\ell}\left(\hat{T}\right)}\right) + \Delta\phi_{\mathrm{bias}} \tag{3.2.78}$$

which is just the standard isothermal concentration potential of a membrane system. Taking the limit of uniform composition, only the electrode bias remains. If, instead of the isothermal limit, we take uniform composition, we have

$$\Delta\phi = \left[\eta_{\mathrm{S}}^{\mathrm{mem}} + \eta_{\mathrm{S}}^{\mathrm{el}} + \left(\tau^{\mathrm{mem}} + \tau^{\mathrm{el}}\right) f\left(T_1, T_2\right)\right] \Delta_{1,2} T + \Delta\phi_{\mathrm{bias}}\left(\Delta_{1,2} T, \hat{T}\right) \tag{3.2.79}$$

We will discuss conditions for the both the compartment-wise isothermal limit and the limit of uniform composition in section 3.2.5. Further assuming that all Thomson effects can be neglected, this reduces to

$$\Delta\phi = \left(\eta_{\mathrm{S}}^{\mathrm{mem}} + \eta_{\mathrm{S}}^{\mathrm{el}}\right) \Delta_{1,2} T + \Delta\phi_{\mathrm{bias}} \tag{3.2.80}$$

which is an assumption that can be checked by checking whether the observed potential deviates significantly from a straight line as a function of the temperature difference. This will be discussed in further detail in section 3.2.6.

3.2.5 Temperature Polarization

In our full expression (3.2.76) for the total cell potential, the thermoelectric contributions stem from both an effect due to transport across the membrane, and for transport through the external solution. In taking the compartment-wise isothermal limit to obtain (3.2.77), the solutions terms are neglected, and the temperature difference across the membrane is assumed to be sufficiently close to the temperature difference between the bulk solutions. In practice, however, the typical situation is that diffusion layers formed close to the membrane surface have significantly non-uniform temperature profiles. This gives measurable alterations to the observed electric potential,

as it provides thermoelectric potentials in the diffusion layers as well as across the membrane proper, and also alters the thermoelectric potential over the membrane by altering the temperature difference across the membrane itself. This effect is commonly known as *temperature polarization* in the literature [54]. An example of how a steady state temperature profile may look like is illustrated in figure 3.3.

The experimental difficulties associated with measuring the temperatures T_ℓ and T_r, without disturbing the transport processes, call for a more practical approach. We introduce the mean temperature gradients in solution and membrane

$$\overline{\partial_x^{\mathrm{s}} T} = \frac{\Delta_{1,\ell} T + \Delta_{r,2} T}{d_{\mathrm{s}}} \qquad \overline{\partial_x^{\mathrm{m}} T} = \frac{\Delta_{\ell,r} T}{d_{\mathrm{m}}} \tag{3.2.81}$$

where d_{s} is two times the mean thickness of the diffusion layers, and d_{m} is the thickness of the membrane. The total temperature difference can then be expressed as

$$\Delta T := \Delta_{1,2} T = \overline{\partial_x^{\mathrm{s}} T} d_{\mathrm{s}} + \overline{\partial_x^{\mathrm{m}} T} d_{\mathrm{m}} \tag{3.2.82}$$

Neglecting the Thomson effect, and the dependence of the composition profiles in the diffusion layers on the temperature difference, the observed Seebeck coefficient of the system is

$$\eta_{\mathrm{S}}^{\mathrm{obs}} = \frac{\Delta\phi}{\Delta T} \propto \frac{\eta_{\mathrm{S}}^{\mathrm{sol}} \overline{\partial_x^{\mathrm{s}} T} d_{\mathrm{s}} + \eta_{\mathrm{S}}^{\mathrm{mem}} \overline{\partial_x^{\mathrm{m}} T} d_{\mathrm{m}}}{\overline{\partial_x^{\mathrm{s}} T} d_{\mathrm{s}} + \overline{\partial_x^{\mathrm{m}} T} d_{\mathrm{m}}} = \frac{\eta_{\mathrm{S}}^{\mathrm{sol}}}{1 + \rho \frac{d_{\mathrm{m}}}{d_{\mathrm{s}}}} + \frac{\eta_{\mathrm{S}}^{\mathrm{mem}} \rho \frac{d_{\mathrm{m}}}{d_{\mathrm{s}}}}{1 + \rho \frac{d_{\mathrm{m}}}{d_{\mathrm{s}}}} \tag{3.2.83}$$

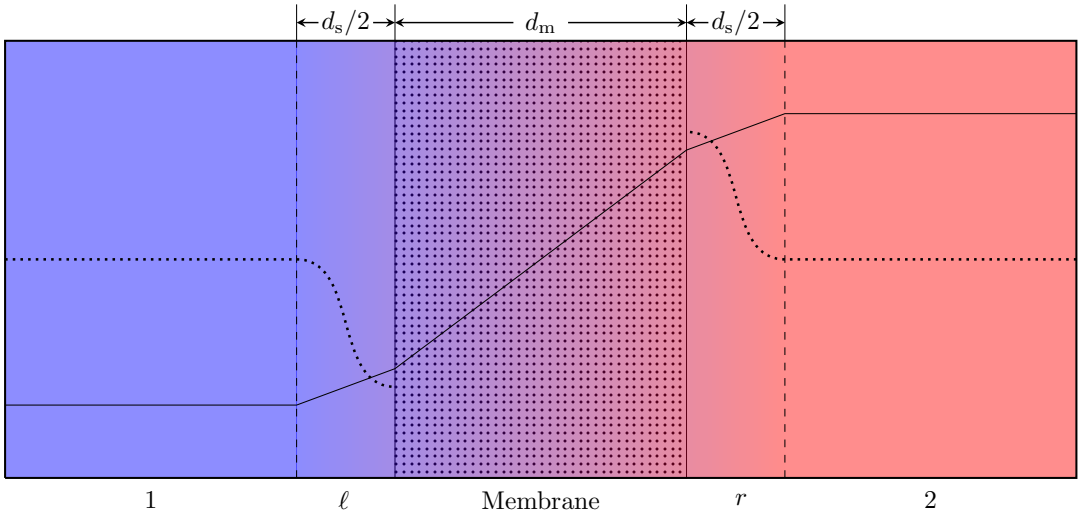

Figure 3.3: An illustration of a possible combination of temperature and composition profile in the system. The dashed lines indicate the diffusion layers ℓ and r, and the solid lines indicate the membrane-solution interfaces. The solid curve indicates the temperature profile, and the dotted curve the electrolyte concentration.

where ρ is the ratio of the mean temperature gradient in the membrane to the mean temperature gradient in the diffusion layers. We see that the dependence on the ratio $d_\mathrm{m}/d_\mathrm{s}$ is such that, provided that ρ is independent of this ratio, only the membrane contribution remains when this ratio is large enough. Experimentally, we will increase the membrane thickness by stacking membranes together. We will then assume that the effective membrane thickness is

$$d_\mathrm{m} = nd \tag{3.2.84}$$

where d is the thickness of a single membrane, and n is the number of membranes stacked together. We furthermore assume that the ratio d/d_s is independent of the number of membranes in the stack, and define the parameter

$$r := \rho\frac{d}{d_\mathrm{s}} \tag{3.2.85}$$

The model for the observed Seebeck coefficient is then

$$\eta_\mathrm{S}^\mathrm{obs} \propto \frac{\eta_\mathrm{S}^\mathrm{sol}}{1+nr} + \frac{\eta_\mathrm{S}^\mathrm{mem}}{1+\frac{1}{nr}} \tag{3.2.86}$$

We will use this model to analyze the dependence of the observed Seebeck coefficient on the number of stacked membranes. As a generalization, we may assume that r is not constant, but varies slowly with n. In this case, we may expand about $n = 1$

$$r(n) \approx r(1) + \left.\frac{\partial r}{\partial n}\right|_{n=1}(n-1) \tag{3.2.87}$$

in which case we define the coefficients

$$a := \left.\frac{\partial r}{\partial n}\right|_{n=1} \qquad\qquad b := r(1) - \left.\frac{\partial r}{\partial n}\right|_{n=1} \tag{3.2.88}$$

so that (3.2.86) becomes

$$\eta_\mathrm{S}^\mathrm{obs} \propto \frac{\eta_\mathrm{S}^\mathrm{sol}}{1+bn+an^2} + \frac{\eta_\mathrm{S}^\mathrm{mem}}{1+\frac{1}{bn+an^2}} \tag{3.2.89}$$

we will use this model to check whether a is significant, and revert to (3.2.86) if it is not. The purpose of this model is to assess whether enough membranes are stacked together such that the effect of temperature polarization may be neglected.

3.2.6 Concentration and Temperature Dependence

When deriving the full expression for the observed cell potential, we neglected the composition dependence of the entropies, arguing that the composition profile of the

cell does not deviate much from uniform. However, if measurements taken at significantly different overall electrolyte concentrations are to be compared, this dependence can no longer be neglected. In order to assess the concentration dependence of the observed potential, we neglect the composition dependence of the transported entropies of the ions, and assume the following concentration dependence for the partial molar entropies of neutral components

$$S_{\mathrm{e}} \propto -\nu R\left(\ln\left(a_{\mathrm{e}}\right)+\frac{\partial \ln\left(\gamma_{\mathrm{e}}\right)}{\partial \ln\left(T\right)}\right) \qquad S_{\mathrm{w}} \propto -R\left(\ln\left(a_{\mathrm{w}}\right)+\frac{\partial \ln\left(y_{\mathrm{w}}\right)}{\partial \ln\left(T\right)}\right) \tag{3.2.90}$$

where a_i is the activity of i, which can be found from tabulated data in the literature. Neglecting the contribution from the aqueous solution, and the concentration dependence of the heat capacities, we obtain

$$\eta_{\mathrm{S}}^{\mathrm{obs}} \propto -\frac{\nu R\bar{t}_{\mathrm{M}^{z+}}}{zF}\left(\ln\left(a_{\mathrm{e}}\right)+\xi_{\mathrm{e}}\right)-\frac{R\bar{t}_{\mathrm{w}}}{F}\left(\ln\left(a_{\mathrm{w}}\right)+\xi_{\mathrm{w}}\right) \tag{3.2.91}$$

where ξ_i are the logarithmic temperature derivatives of the activity coefficients, i.e. the second terms in the brackets of (3.2.90). Since the prefactor to the electrolyte activity term consists of strictly positive quantities, we expect that increasing the electrolyte activity leads to a more negative Seebeck coefficient. However, the transference coefficient of water may take any sign, and is typically on the order of unity or greater. The effect of changing the water activity thus depends on the direction of electroosmotic water transfer. For anion-exchange membranes, we expect the first term to be small if the membrane is highly selective. We expect that both transport numbers may vary with the electrolyte concentration, and the observed Seebeck coefficient therefore has a nonlinear activity dependence in general.

Since the activities are typically well-known in the literature, then $\bar{t}_{\mathrm{M}^{z+}}$ and $\bar{t}_{\mathrm{w}}$ are typically the only unknown quantities in (3.2.91). Therefore, measuring the Seebeck coefficient at different electrolyte concentrations can allow the estimation of the transference coefficients. If the transference coefficient of water is measured by a different method, e.g. by measuring the streaming potential of the membrane, then this is a possible method for measuring the cationic transport number. We will, however, not assume that the transported entropies are independent of electrolyte concentration, and use (3.2.90) to evaluate the thermodynamic entropies at different concentrations in order to calculate the transported entropies.

As for the dependence of the Seebeck coefficient on the mean temperature of the system, we again neglect the effect of temperature polarization, and the temperature dependence of the electrode bias, and draw out the $\hat{T}$-dependence, keeping all

temperature differences in the system the same

$$\eta_{\mathrm{S}}^{\mathrm{obs}} \propto \left(\tau^{\mathrm{mem}} + \tau^{\mathrm{el}}\right) \left[\frac{T_2 \ln\left(T_2/\hat{T}\right) - T_1 \ln\left(T_1/\hat{T}\right)}{T_2 - T_1} - 1\right] - \frac{\hat{T}}{T_2 - T_1} \left[\frac{\Gamma \nu R}{zF} \left(\bar{t}_{\mathrm{M}^{z+}} - t_{\mathrm{M}^{z+}}\right) \ln\left(\frac{m_r}{m_\ell}\right) + \frac{\alpha_{\mathrm{w}} R \bar{t}_{\mathrm{w}}}{F} \ln\left(\frac{c_r}{c_\ell}\right)\right] \tag{3.2.92}$$

We can further assume that the experimental conditions where temperature polarization may be neglected are the same for which the composition difference can also be neglected, thus we can neglect the second term as well. We may expand the logarithms

$$T_i \ln\left(\frac{T_i}{\hat{T}}\right) = T_i - \hat{T} + \frac{1}{2T_i}\left(\hat{T} - T_i\right)^2 + \mathcal{O}\left(\left(\hat{T} - T_i\right)^3\right) \tag{3.2.93}$$

then,

$$\frac{T_2 \ln\left(T_2/\hat{T}\right) - T_1 \ln\left(T_1/\hat{T}\right)}{T_2 - T_1} - 1 \approx \frac{1}{2}\left(1 - \frac{\hat{T}^2}{T_1 T_2}\right) \tag{3.2.94}$$

so that what determines the dependence of the Seebeck coefficient on the mean temperature is the relative deviation of the arithmetic mean temperature from the geometric mean. We may expect a small quadratic dependence on $\hat{T}$ for a given temperature difference. With a mean temperature around room temperature, this term is on the order of 10^{-4}, and its absolute value increases when the mean temperature is decreased. However, if the Thomson effect is sufficiently large, we may compare experiments taken at different mean temperatures to estimate the Thomson coefficients.

If the Thomson effect cannot be neglected, then (3.2.79) becomes, in light of (3.2.94)

$$\Delta\phi = \left[\eta_{\mathrm{S}}^{\mathrm{mem}} + \eta_{\mathrm{S}}^{\mathrm{el}} + \frac{1}{2}\left(\tau^{\mathrm{mem}} + \tau^{\mathrm{el}}\right)\right] \Delta T + \frac{\hat{T}^2}{2}\left(\tau^{\mathrm{mem}} + \tau^{\mathrm{el}}\right) \Delta\frac{1}{T} + \Delta\phi_{\mathrm{bias}} \tag{3.2.95}$$

which means that the linear coefficient in ΔT is not the total Seebeck coefficient, but a combination of the Seebeck and Thomson coefficients. This is not a problem, however, as we can extend the model to include a linear term in the difference of inverse temperature. In this extended model, we may obtain estimates of both the Seebeck and Thomson coefficients. If the inverse temperature term is found to be insignificant, then we can also neglect the contribution of the Thomson coefficients to the ΔT-term, and use the simpler model in (3.2.80).

3.2.7 Entropy Production and Second Law Efficiency

In order to quantify the second law efficiency of the membrane as a thermoelectric generator, we will express the second law in terms of measurable quantities. Assuming

that there is no concentration difference across the membrane, the entropy production in the membrane can be written as

$$\sigma_{\text{mem}} = J_q' \partial_x \left(\frac{1}{T}\right) - \frac{j}{T}\partial_x \phi \geq 0 \tag{3.2.96}$$

with the corresponding flux equations

$$\begin{bmatrix} J_q' \\ j \end{bmatrix} = -\frac{1}{T}\begin{bmatrix} \overline{L}_{qq} & \overline{L}_{q\phi} \\ \overline{L}_{\phi q} & \overline{L}_{\phi\phi} \end{bmatrix}\begin{bmatrix} \partial_x \ln(T) \\ \partial_x \phi \end{bmatrix} \tag{3.2.97}$$

We will express the coefficients in terms of measurable quantities. From the analysis in the membrane phase, neglecting the Thomson effect, it can be concluded that

$$\frac{\overline{L}_{\phi q}}{\overline{L}_{\phi\phi}} = \frac{\overline{L}_{q\phi}}{\overline{L}_{\phi\phi}} = -T\eta_{\text{S}}^{\text{mem}} \tag{3.2.98}$$

we also identify the Ohm's law ionic conductivity, which can be measured under isothermal conditions

$$\overline{\kappa} := -\left(\frac{j}{\partial_x \phi}\right)_{\text{d}T=0} = \frac{\overline{L}_{\phi\phi}}{T} \tag{3.2.99}$$

and the short-circuit thermal conductivity, which can be measured when the cell is short-circuited

$$\overline{\lambda} := -\left(\frac{J_q'}{\partial_x T}\right)_{\text{d}\phi=0} = \frac{\overline{L}_{qq}}{T^2} \tag{3.2.100}$$

The second law demands that the determinant of the conductivity matrix is nonnegative. This means, using $\overline{L}_{q\phi} = \overline{L}_{\phi q}$, that

$$\frac{\overline{L}_{qq}}{\overline{L}_{\phi\phi}} \geq \left(\frac{\overline{L}_{q\phi}}{\overline{L}_{\phi\phi}}\right)^2 \tag{3.2.101}$$

which means that the absolute value of the Seebeck coefficient has an upper bound given in terms of the ionic and thermal conductivities

$$|\eta_{\text{S}}^{\text{mem}}| \leq \sqrt{\frac{\overline{\lambda}}{T\overline{\kappa}}} \tag{3.2.102}$$

where equality minimizes the entropy production. The coupling of heat and charge transfer reduces the amount of lost work in the system, by performing work on the ions in order to transfer heat. A practical quantity for assessing the second law efficiency of the system is obtained by normalizing (3.2.102), called the figure of merit, $\mathcal{F}$

$$\mathcal{F} := \frac{\overline{\kappa}}{\overline{\lambda}}(\eta_{\text{S}}^{\text{mem}})^2 \leq \frac{1}{T} \tag{3.2.103}$$

which is nonnegative due to second law constraints on $\overline{\lambda}$ and $\overline{\kappa}$, and because $\eta_{\mathrm{S}}^{\mathrm{mem}}$ is an observable quantity and therefore real. One can thus assess how close the system is to achieving maximum efficiency by calculating the number $T\mathcal{F}$ for a given operating temperature. No values for $\mathcal{F}$ will be reported in this thesis, as the thermal conducitvity will not be measured. We wish to express the important point of specifying under which conditions the conductivities are measured. Occasionally, figures of merit are reported in the literature [59] which appear to violate (3.2.103), but this is most likely due to disregard of experimental specification.

3.3 Experimental

3.3.1 Apparatus

A polycarbonate cell was designed specifically for the experiments, with cell units according to the drawings in figure 3.4. See appendix C for larger figures. Membranes were squeezed between two such unit cells, each having its own inlet and outlet to allow for tangential flow of solution. Each cell unit also had three ports to accomo-

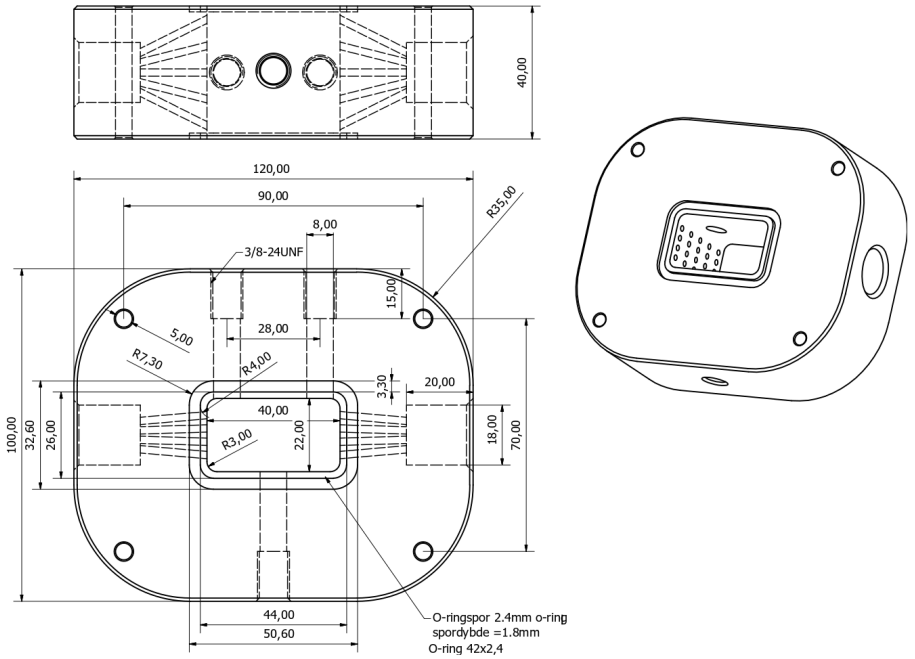

Figure 3.4: Sketch of the cell unit designed for the thermoelectric measurements. The membrane sample is squeezed between two such modules, through which solution is pumped horizontally. There are additionally three openings to accomodate electrodes, temperature sensors and pressure control. All measurements are in millimeters. For a larger version of this figure, see appendix C.

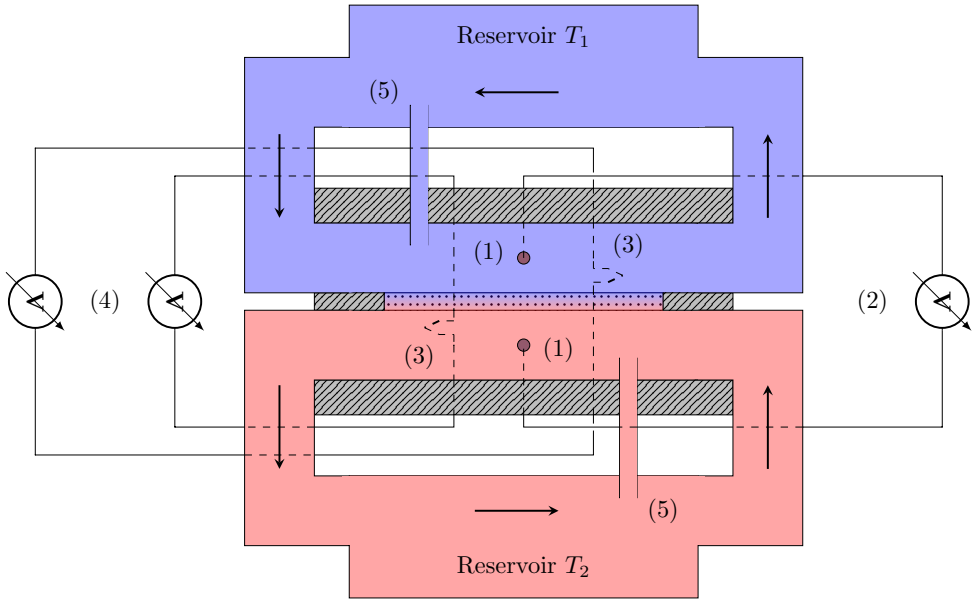

Figure 3.5: Sketch of the experimental setup for thermoelectric measurements. Solutions are thermostatted and pumped through the thermocell by means of thermostatted reservoirs and pumps. Electrodes (1) are connected via a voltmeter (2) to measure the cell potential, and the temperature is monitored by means of thermocouples (3) connected to their own compensated voltmeters (4). Excess pressure is relieved close to the cell inlets by means of tubing (5) back into the reservoirs.

date an electrode, a temperature sensor, and pressure control. The ends of the cell units were capped with polycarbonate walls. All sensor and control equipment was fitted with glass tubing of 8mm outer diameter, and were mounted into the cell units using appropriately dimensioned fittings from Swagelok. The compartment volume is approximately 35 mL, and the exposed membrane area was approximately 8.8 cm^2. A sketch of the experimental setup is given in figure 3.5.

The temperature sensors used were K-type precision fine wire thermocouples from Omega, immersed in glycerol in glass tubing for stability. The thermocouples were calibrated by immersion in a manually stirred ice bath until readings were stable. Magnetic stirring was avoided in due to electromagnetic induction effects disrupting the thermocouple readings. The solution reservoirs were a Grant ecocool LT 100 and a Grant R2 with complementary pump heads and thermostatting spirals. Pressure between chambers was equalized by allowing flow of excess solution back to the reservoirs at the cell inlets, and the reservoirs were kept at the same height to within centimeter precision. The flow in each pressure relief loop was measured to approximately 2 L/min each, such that specifications from Grant imply a tangential flow of 15 L/min at the membranes, which translates to an average velocity of 28 cm/s. All temperature and potential measurements were recorded using an Agilent 34970A data acquisition unit with a 34901A module.

3.3.2 Electrodes and Electrolyte

The electrodes were prepared by winding $40 \times 10 \times 0.5$ mm^3 plates of polished, pure Ag onto Pt wires, activating the Ag surface by immersion in a 3 molar solution of HNO_3, and depositing a fine layer of AgCl by immersing the electrodes in a 1 molar solution of HCl, and sending small electric currents (≈ 1 µA) against a Pt reference electrode for at least 5 hours. The electrodes were then stored in a dark 0.01 molar solution of HCl with grains of AgCl for at least 3 days before use. The bias of the electrodes was measured by immersing them in aqueous 0.03 mol/kg solution of NaCl at room temperature. If the bias exceeded 100 µV, the electrodes were refreshed. Refreshing of electrodes was done by immersion in conc. NH_3 for at least 2 hours, to remove the old chloride layer, and the silver was polished again. A new layer of AgCl was deposited by the same procedure as with new electrodes.

The solutions were prepared by weighing of distilled water, and adding the appropriate amount of salt. The electrical conductivity of the pure water did not exceed 1.5 µS/cm, and the salt used was AnalaR NORMAPUR NaCl from VWR Chemicals. The salt was weighed to a worst case accuracy of 0.02 %, using a Pioneer PA214C analytical balance.

3.3.3 Membranes

The membranes tested in the experiments were Fumasep FKS PET-75 and Fumasep FAD PET-75 reinforced homogeneous ion exchange membranes from FuMA-Tech, both with thicknesses of 75 ± 5 µm according to specifications. The FKS cation exchange membranes were delivered in H^+-form, and the FAD anion exchange membranes in Cl^--form. The FKS membranes were converted to Na^+-form by mounting them in the thermocell under isothermal conditions, and driving an electric current through the membranes using a HP 6181B DC current source at 25°C. The current was driven through the membranes in both directions, using the circuit given in figure 3.6. The switching of the current direction was facilitated by using a simple MT2-relay controlled by an Arduino Uno microcontroller, and the current was monitored using a Fluke 117 true RMS multimeter, and observed to be stable throughout the treatment process.

All membranes were pre-treated by immersion in the solution for which the measurements were to be made, and degassed using a Branson 3510 ultrasound bath. The membranes were stored in closed containers kept at 25 ± 1°C in a Fermaks oven. For the first week of pre-treatment, the solution in each container was changed every 2 days, from which point the solution was changed once per week.

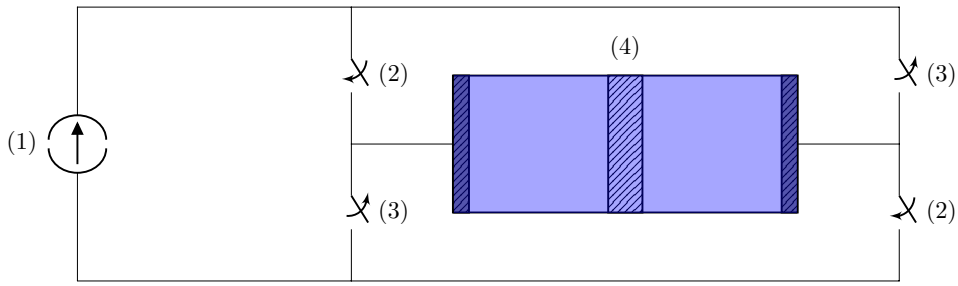

Figure 3.6: The circuit used for electro-treatment of cation exchange membranes. A current source (1) drives an electric current through the electrochemical cell (4). The direction of the current is controlled by opening and closing the sets (2) and (3) of mechanical switches.

3.3.4 Measurement Procedures

The measurements were performed by squeezing the membrane stack between two cell units, and letting the system relax under conditions as close as possible to isothermal, until a stable voltage was read between the electrodes. Great care was taken to eliminate the any bubbles formed between the layers in the stack, as they would severely disrupt the measurements. The temperature gradients were applied by changing the thermostat settings on the reservoirs, and measurements were taken with temperature differences of 10 and 20 K in both directions. Whenever a stable voltage was reached, one such measurement series was taken over at least 15 minutes, before changing the temperature difference again. The time required to reach a stable voltage was typically between 15 minutes to several hours, depending on the type of membrane and stack size. For each case, an isothermal measurement series was taken to eliminate any isothermal bias in the system.

These measurement procedures were carried out for membrane stacks consisting of 1-10 membranes at 0.03 mol/kg concentration, and with 20 membranes at 0.03, 0.1, and 0.6 mol/kg concentration. All membrane samples were cut from the same production batch from FuMA-Tech, and the samples in each stack was selected pseudo-randomly from the entire population. Between each measurement, the cell and reservoirs were disassembled and thoroughly cleaned with distilled water. The electrodes were stored in dark 0.01 molar HCl with AgCl grains, and were short-circuited during storage to eliminate bias.

3.4 Results and Discussion

For all measurement series scanning over the range of temperature differences, the model (3.2.95) was applied using linear least squares. In all cases considered here,

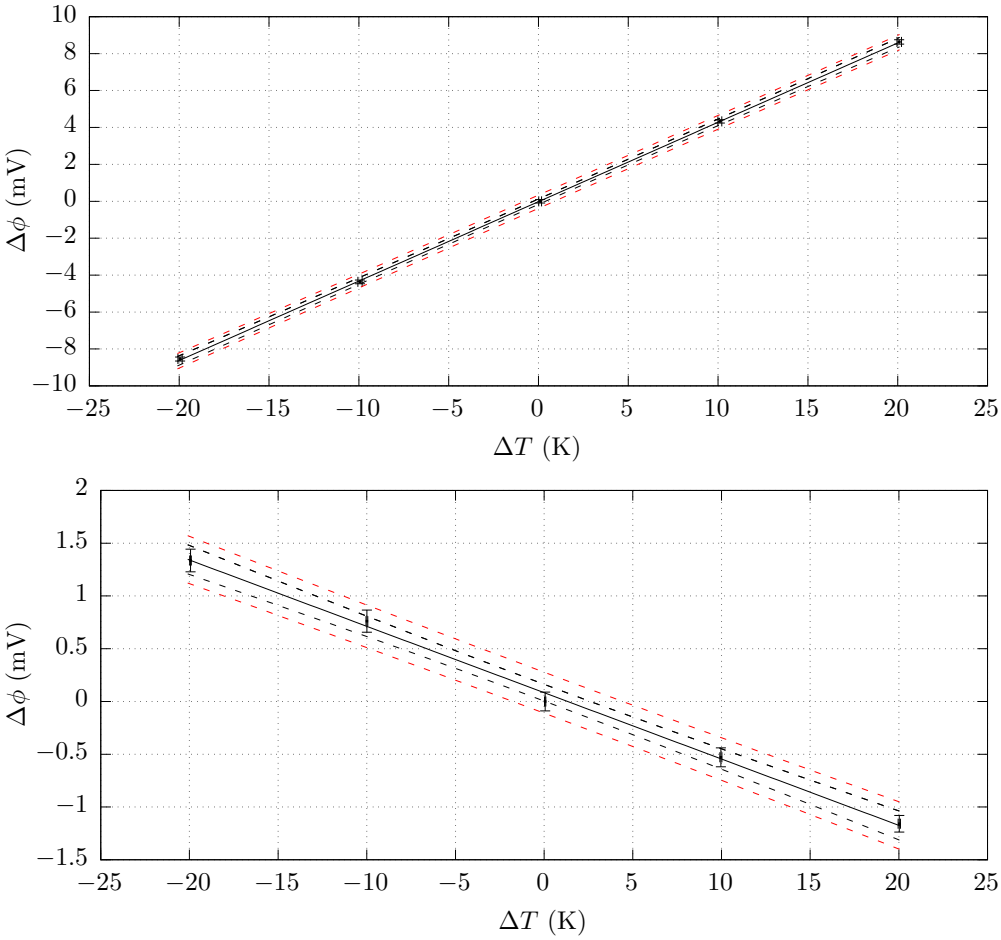

Figure 3.7: Plot of the observed electric potential difference $\Delta\phi$ against the applied temperature difference ΔT over a stack of 20 FKS cation exchange membranes (top), and a stack of 20 FAD anion exchange membranes (bottom) in 0.6 mol/kg aqueous NaCl solution.

the Thomson effect was found to be insignificant, and the observed potential followed a straight line as a function of the temperature difference. The problem of numerical singularity of the covariance matrix of the full model was treated by a singular value decomposition of the information matrix. As examples, plots of the observed potential against the temperature difference for stacks of 20 FKS cation exchange membranes and 20 FAD anion exchange membranes in 0.6 mol/kg solution are given in fig 3.7. The lack of significance of the Thomson effect was expected, as Thomson coefficients are typically on the same order of magnitude as the Seebeck coefficients, and thus the product τf is expected to be four orders of magnitude smaller than η_{S}.

A nonlinear regression algorithm was written to fit the observed Seebeck coefficient

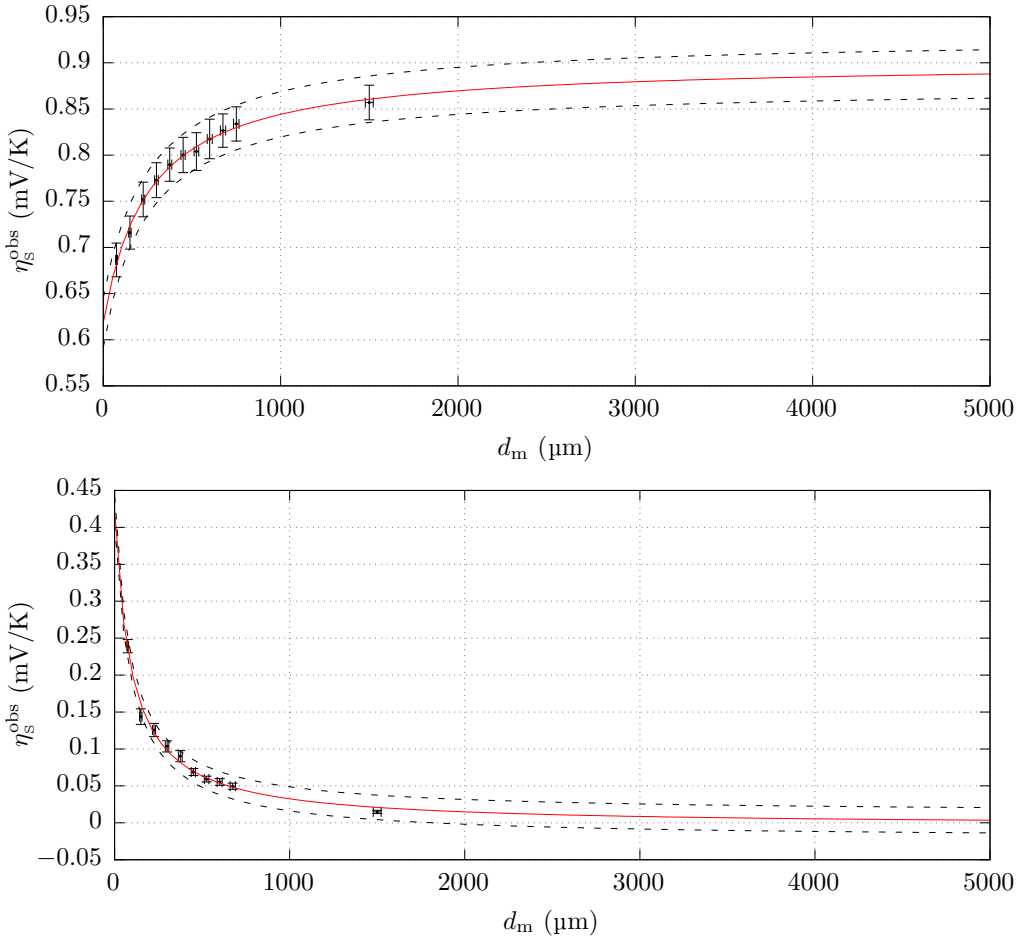

Figure 3.8: Plots of the observed Seebeck coefficients against the stack thickness of FKS (top) and FAD (bottom) membranes in 0.03 mol/kg solution of NaCl. The dashed lines indicate 95 % confidence estimated by residual resampling.

as a function of membrane stack thickness for both types of membranes. Plots of the observed values along with the least squares fitted model are given in figure 3.8. We observe that, in both cases, convergence to within experimental error occurs beyond a stack size of 10, and larger stacks are required to sufficiently eliminate the polarization effects. The limits of the fitted models as $n \to \infty$ can be taken as estimates of $\eta_S^{mem} + \eta_S^{el}$, though at the cost of a large extrapolation uncertainty. This uncertainty can be reduced by adding more data points in the region beyond 10 membranes, where the model approaches convergence to within experimental errors.

The observed values are comparable to results on membranes studied in the literature, having the same order of magnitude as e.g. the FLEMION S cation exchange

Table 3.1: Activity coefficients of aqueous NaCl interpolated from data by Truesdell [60], and their estimated logarithmic temperature derivatives at 25°C, ξ_{NaCl}, along with water activities at 25°C estimated from osmotic coefficients [61]. The error in the water activity was calculated to be in all cases negligible.

	Molality (mol/kg)		
T (°C)	0.03	0.10	0.60
15	0.854 ± 0.002	0.781 ± 0.001	0.671 ± 0.001
25	0.851 ± 0.001	0.778 ± 0.001	0.676 ± 0.001
38	0.849 ± 0.001	0.774 ± 0.001	0.669 ± 0.001
50	0.845 ± 0.001	0.770 ± 0.001	0.671 ± 0.001
ξ_{NaCl}	-0.082 ± 0.005	-0.116 ± 0.005	0.013 ± 0.005
a_{w}	0.999	0.997	0.980

membrane [53]. Most of the previous experimental work was done using calomel electrodes kept at equal temperatures, with a temperature difference across a salt bridge. Their idea appears to have been to neglect the thermoelectric contribution of the salt bridge, assessing that the junction potential did not exceed 0.1 mV. The reported value of 0.261 mV/K for the Seebeck coefficient of Flemion S in 0.1 mol/kg NaCl is a factor 4 smaller than that found for the FKS membrane, and the activity dependence appears to be logarithmic, as predicted in this work as well as by the authors [53]. Similarly, the Seebeck coefficient of the Ionics 61 CZL 386 cation exchange membrane extrapolated to infinite stirring rate in 1 mol/m^3 NaCl was reported to be 0.66 mV/K by Barragán et al [54], who also reported a logarithmic concentration dependence in this limit. We interpret the limit of infinite stirring rate reported by Barragán et al to be equivalent to our own limit of infinite membrane thickness, as in both cases the limit means that the effects of the diffusion layers vanish, while the temperature difference across the membrane is maximized.

As for the concentration dependence of the Seebeck coefficients, activity coefficients at different temperatures and molalities were obtained by Truesdell [60]. The activity data were interpolated using a quadratic linear regression model of the activity coefficients as functions of the logarithm of the molality in the neighborhood of the molalities of interest. The interpolated data were then further interpolated as the logarithm of the activity coefficients as functions of the logarithm of the absolute temperature, and the slope was estimated by a finite difference. Interpolated data are given in table 3.1.

Using values of 42.6 J/K mol and 96.1 J/K mol for S_{Ag} and S_{AgCl}, respectively [25], neglecting the transported entropy of electrons in platinum gives $\eta_{\mathrm{S}}^{\mathrm{el}} = -0.545$ mV/K, which is common to all experiments. The fact that the Seebeck coefficients of both membranes approach a positive value in the limit $n \to 0$ indicates that $\eta_{\mathrm{S}}^{\mathrm{sol}}$ is large and positive. Since the dependence of the cell potential on the activity difference in

NaCl is proportional to the cationic transport number, and the water activity does not change very much in comparison, we expect the anion exchange membrane to be far less sensitive to concentration polarization than the cation exchange membrane. Therefore, the similar rates of change in thermoelectric potential as a function of effective membrane thickness indicates that the dominant effect must be temperature polarization. This indicates that, for the sake of this analysis, we may neglect the effect of concentration polarization on the cell potential.

Using values of 86 and 118 J/mol K for $S^*_{Na^+}$ and $S^*_{Cl^-}$, respectively, which were reported for an NaCl concentration of 10 mol/m^3 [8], and a value of 0.389 for t_{Na^+} [34], along with data given in table 3.1, we obtain $\eta_S^{sol} \approx 0.61$ mV/K. This is indeed positive, and greater in magnitude than the electrode contribution. The results indicate that this contribution is slightly larger in the present experiments, in the neighborhood of 1 mV/K. This is smaller than the calculated Seebeck coefficient of the FKS membrane, and greater than that of the FAD membrane. This can be taken to explain the two different trends in the observed Seebeck coefficient as the effective membrane thickness is increased – increasing the FKS thickness increases the thermoelectric potential because the membrane contribution is stronger than that from the solution. The trend is opposite for the FAD membrane because its contribution is weaker than that of solution. Since $t_w < 0$ for the FAD membrane, water is transported in the same direction as the anions carrying the current. In this context, this means that less work is required to drive Cl^- through the membrane, as co-transport of water occurs down the temperature gradient. This contributes to making the thermoelectric potential smaller. For the FKS membrane, on the other hand, co-transport of water occurs against the temperature gradient, which increases the thermoelectric potential. We conclude that at least 20 membranes should be used for this particular apparatus in order to obtain reasonably accurate results for η_S^{mem}. Halseid [62] used stacks of 55 NAFION membranes for his apparatus, while Felborg concluded from a subsequent investigation that the optimal number of such membranes lies somewhere between 10 and 45 [63].

In figure 3.9, we give plots of the estimated membrane contributions to the Seebeck coefficient against the concentration dependent terms of S_{NaCl}. We see that the contribution from the FKS membrane follows approximately a straight line, while that of the FAD membrane deviates somewhat. As previously discussed, the concentration dependence of the FAD contribution is expected to be mainly through changes in water activitiy, but it is the salt concentration that is most relevant for applications. Deviations from a straight line indicate changes in the transport numbers and/or the transported entropies. Since the FKS membrane contribution is reasonably close to a straight line, we conclude that the cationic transport number and the transported entropy of Na^+ in the FKS membrane are insensitive to the concentration changes. The dominant effect is therefore the change in molar entropy of NaCl. For the FAD membrane, the water transference coefficient varies a lot with concentration. The

Table 3.2: Observed Seebeck coefficients η_S^{obs} at different concentrations with stacks of 20 membranes, and estimates η_S^{∞} from extrapolation to an infinite membrane thickness at 0.03 mol/kg. We also report the corresponding membrane Seebeck coefficients, η_S^{mem}.

	FKS		FAD	
$\overline{m}$ (mol/kg)	η_S^{obs} (mV/K)	η_S^{mem} (mV/K)	η_S^{obs} (mV/K)	η_S^{mem} (mV/K)
0.03	0.86 ± 0.02	1.41 ± 0.02	0.015 ± 0.002	0.560 ± 0.002
0.10	0.67 ± 0.02	1.22 ± 0.02	-0.003 ± 0.002	0.542 ± 0.002
0.60	0.43 ± 0.01	0.98 ± 0.01	-0.063 ± 0.006	0.482 ± 0.006
	η_S^{∞} (mV/K)	η_S^{mem} (mV/K)	η_S^{∞} (mV/K)	η_S^{mem} (mV/K)
0.03	0.90 ± 0.02	1.45 ± 0.02	-0.004 ± 0.008	0.541 ± 0.008

deviation from a straight line indicates this, and also that the transported entropy of Cl^- in the FAD membrane has a significant concentration dependence. The relative insensitivity of the Seebeck coefficient of the FAD membrane to the concentration indicates, however, that these two effects are compensating. While the increase in magnitude of $\bar{t}_w$ with concentration indicates an increase in the work gained due to co-transport of water down the temperature gradient, the transported entropy of the Cl^- ions should also increase at a similar rate.

In all cases, we neglect the temperature dependence of the water activity, and estimate the transported entropies as

$$\begin{aligned} \overline{S}^*_{Na^+} &= S^0_{NaCl} - 2R\left(\ln\left(a_{NaCl}\right) + \xi_{NaCl}\right) + \bar{t}_w\left(S^0_w - R\ln\left(a_w\right)\right) - F\eta_S^{mem} \\ \overline{S}^*_{Cl^-} &= F\eta_S^{mem} - \bar{t}_w\left(S^0_w - R\ln\left(a_w\right)\right) \end{aligned} \tag{3.4.1}$$

for perfectly selective FKS and FAD membranes, respectively. The superscript 0 denotes standard state entropies. For these, we obtain from [25] values of $S^0_{NaCl} = 115.5$ J/mol K and $S^0_w = 69.95$ J/mol K, using 1 mol/kg as standard state for NaCl. The water transference coefficients were obtained by streaming potential measurements (not yet published). Water transference coefficients and estimated transported entropies are given in table 3.3. The magnitudes of the water transference coefficients indicate that, for each ion transported through the membrane, several water molecules are transferred on average. This means that a lot of work is gained or lost due to co-transport of water, depending on the direction of transport with respect to the temperature gradient. The estimates of the transported entropies are therefore highly sensitive to errors in the numerical values of $\bar{t}_w$. Since the errors in present estimates of $\bar{t}_w$ are large, then so are the errors in the estimates of the transported entropies. In order to improve estimates of the transported entropy, more precise methods for measuring the transference coefficients are required.

The apparent trend is that the transported entropy of Na^+ in the FKS membrane is insensitive to the composition of the aqueous solution, while the transported entropy

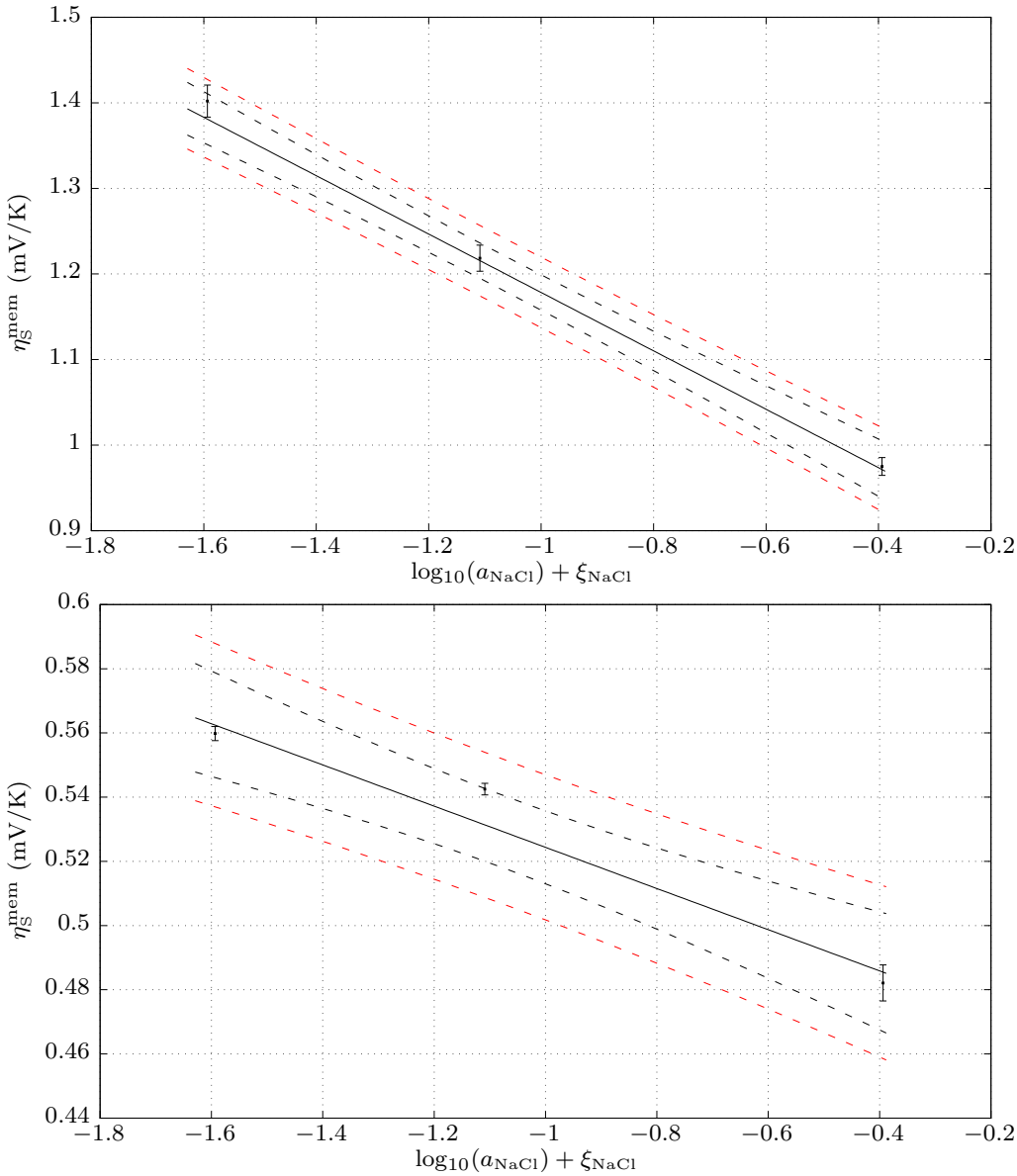

Figure 3.9: Plots of the observed Seebeck coefficients against the logarithm of electrolyte activity and the correction factor ξ_{NaCl} for stacks of 20 FKS (top) and FAD (bottom) membranes. The dashed lines indicate 95 % confidence.

Table 3.3: Water transference coefficients and estimated transported entropies of the charge carriers in ideally selective FUMASEP FKS PET-75 and FAD PET-75 ion exchange membranes.

	FKS		FAD	
$\overline{m}$ (mol/kg)	$\bar{t}_{\mathrm{w}}$	$\overline{S}^{*}_{\mathrm{Na^+}}$ (J/mol K)	$\bar{t}_{\mathrm{w}}$	$\overline{S}^{*}_{\mathrm{Cl^-}}$ (J/mol K)
0.03	3.9 ± 0.5	314 ± 35	-2.8 ± 1.0	251 ± 70
0.10	3.2 ± 0.9	266 ± 63	-4.9 ± 0.6	396 ± 42
0.60	4.2 ± 0.7	330 ± 49	-8.1 ± 4.9	608 ± 344
	$\bar{t}_{\mathrm{w}}$	$\overline{S}^{*(\infty)}_{\mathrm{Na^+}}$ (J/mol K)	$\bar{t}_{\mathrm{w}}$	$\overline{S}^{*(\infty)}_{\mathrm{Cl^-}}$ (J/mol K)
0.03	3.9 ± 0.5	310 ± 35	-2.8 ± 1.0	249 ± 70

of Cl^- in the FAD membrane appears to increase for higher salt concentrations. The error in $\bar{t}_{\mathrm{w}}$ dominates in all cases, and the Seebeck coefficients should be used to obtain new estimates of the transported entropies as soon as more accurate $\bar{t}_{\mathrm{w}}$ data is available. Ottøy [64] reported a transported entropy of 195 ± 14 J/mol K for protons in the NAFION 117 cation exchange membrane, which is about 50 % lower than has been found for Na^+ in the FKS membrane. Interestingly, Feldborg reported a transported entropy of Na^+ in NAFION 117 of 691 ± 2 J/mol K [63]. This is a very large value, and is likely connected to the large water transference coefficient of 9.2 ± 0.3 that was reported.

In both cases by Ottøy and Feldborg, the Thomson coefficient was found to be very similar in magnitude to the transported entropy, and we can expect the same behaviour for the FKS and FAD membranes. However, the data obtained in these experiments are generally too noisy to determine the Thomson coefficients, with the exception of the measurements made for the FAD membrane at 0.03 mol/kg. A plot of the observed Seebeck coefficient against the function f is given in figure 3.10. From this data, we obtain $\tau^{\mathrm{mem}} + \tau^{\mathrm{el}} = -1.30 \pm 0.44$ mV/K. Taking values of $c_{p,\mathrm{Ag}} = 25.4$ J/mol K, $c_{p,\mathrm{AgCl}} = 50.8$ J/mol K, and $c_{p,\mathrm{w}} = 75.3$ J/mol K [25], and neglecting the Thomson coefficient of electrons in platinum, this gives an estimate of $\overline{\tau}_{\mathrm{Cl^-}} = 111 \pm 86$ J/mol K, which is also a very uncertain number. It has, however, the expected order of magnitude. Application of noise reduction techniques and extending the measurements to larger temperature differences can improve such measurements drastically.

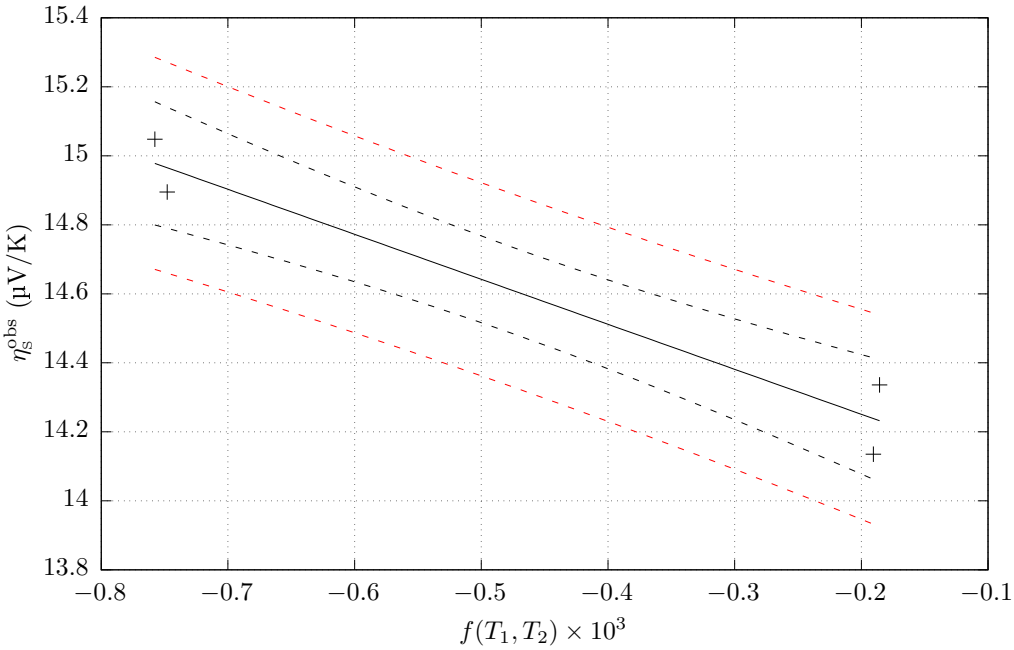

Figure 3.10: Plot of the observed Seebeck coefficient of a stack of 20 FUMASEP FAD-PET-75 anion exchange membranes in 0.03 mol/kg NaCl solution, against the logarithmic temperature function f, defined in equation (3.2.27).

Chapter 4
Conclusions and Future Perspectives

We conclude the thesis by summarizing the conclusions that can be made from the measurements and discussions in previous chapters, and also give pointers and suggestions for further work. In particular, we give suggestions for improvement of the experimental techniques, and also provide a sketch of a possible application in isothermal salt power generation. We show that the results in chapter 3 indicate that the electrical work retrieved by a salt power plant can be substantially increased by applying a temperature gradient in the correct direction. As an example, the Seebeck coefficient is estimated for a concentration cell with concentrations 0.03 and 0.60 mol/kg, with temperatures of 40°C and 0°C, respectively. It was found that the cell potential is increased by up to 50 % compared to the isothermal case.

4.1 Streaming Potential Measurements

The measurement of streaming potentials across membranes in aqueous alkali and alkali earth metal chlorides at 0.03 mol/kg allowed the estimation of water transference coefficients by means of Saxen's relation. The streaming potentials were found to be in the lower range of typical values found in earlier literature, and the water transference coefficients were found to be in the approximate range 3 - 14 in absolute value. In the cation exchange membranes, a tendency was found for the water transference coefficient to decrease with cation size, indicating that the principal mode of water transport is due to ion-dipole attraction. The water transport through the anion exchange membranes appears to be insensitive to the type of cation in solution, which supports the idea that the co-ion does not play a significant role in water transport. The sign of the coefficient was found to be positive for all cation exchange membranes, and negative for the anion exchange membranes, which indicates that water is in all cases transported in the direction of the principal charge carrier. The coefficient of the Fumasep FAD-PET-75 anion exchange membrane was found to increase significantly in magnitude with concentration of NaCl from 0.03 to 0.60 mol/kg, while that of the Fumasep FKS-PET-75 cation exchange membrane did not change significantly.

For all membranes, the water content was measured after equilibriation in the different salt solutions. The measurements were made both on new, unused membranes, and also on membranes that were used for streaming potential measurements, and thus deformed by the pressure difference. A general tendency for the water content to decrease after deformation was found, indicating possible structural collapse reducing the amount of water that can be accomodated in the matrix. A correlation was found between the water content of unused cation exchange membranes and their water transference coefficients. This suggests that part of the water transport is due to loosely bound water in the membrane matrix, and it is possible that the deformation leads to an underestimate of the true water transference coefficient by a value up to approximately 1. The water content of cation exchange membranes was found to decrease with cation size, indicating a volume exclusion effect. No particular correlation was found between cation type and water content of anion exchange membranes.

Water permeabilities were calculated from the time-dependent behaviour of the cell potential under the influence of the pressure difference. This property is sensitive to membrane deformations, and it is likely that an improved technique is required for measuring this property in the less elastic membranes. The results do, however, indicate that the permeability of cation exchange membranes tend to decrease as the cationic charge is increased, which is likely due to a structural effect of high-valence cations associating to several fixed charge groups in the membrane matrix at a time. The permeability of the Fumasep FAD-PET-75 anion exchange membrane was found to significantly increase with cation size and charge, though it is likely that

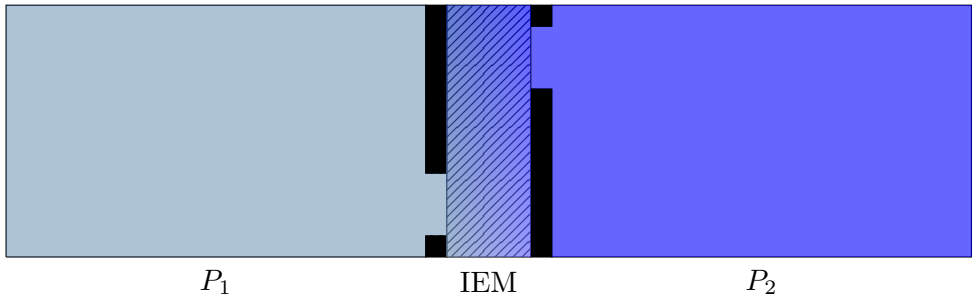

Figure 4.1: Suggested cell design concept for inducing a tangential pressure gradient in membrane samples.

these membranes were strongly affected by the pressure difference, and more reliable measurements with a different technique are needed. No significant concentration dependence of the permeabilities of the FUMASEP FKS-PET-75 and FAD-PET-75 membranes could be found for NaCl solutions from 0.03 to 0.60 mol/kg.

A correlation was found between the total number of water molecules transported per cation in the cation exchange membranes, and the Jones-Dole viscosity B-coefficients of the respective aqueous cations. The B-coefficients are known to correlate with the mass-corrected entropy of solvation in aqueous solution, indicating that the structural effect of the ion on the water pseudolattice correlates with the principal mode of water transport through these membranes. We suggest that this correlation is due to the ion-dipole interaction which is determined by the size and charge of the ion. The water transference coefficients were found to monotonously decrease with ion size for a given ion valence.

The streaming potentials were measured with a large error, at best a relative error on the order of 10 %. Occasionally, a measurement would be completely useless due to obvious membrane deformation disrupting the cell potential. While previous workers have used perforated support plates to minimize this effect, we suggest here a slightly different approach. A cell can be designed in such a way that the pressure gradient lies tangentially in the membrane structure, in order to minimize deformation. This cell design is inspired by the work of Scatchard et al [65], who used membranes as ribbons separating two chambers. A sketch of the suggested concept is given in figure 4.1.
Modelling the membrane as an isotropic medium with a diagonal pressure tensor, this essentially two-dimensional transport problem gives the same result for the total electric potential difference over the membrane, though dynamical contributions will be affected by the larger effective thickness due to the longer mean path through the material sample. Further work can e.g. relax the assumption of isotropy and/or investigate the functioning of such a cell experimentally. Such a design eliminates the

need for possibly disruptive support plates, and allows more freedom in the choice of exposed membrane area and length of tangential part. It also allows the application of tangential flow to reduce the effects of the diffusion layer as desired.

4.2 Thermoelectric Potential Measurements

Transported entropies of Na^+ and Cl^- in respectively the Fumasep FKS-PET-75 and FAD-PET-75 ion exchange membranes were calculated from measurements of their thermoelectric potentials in aqueous NaCl solution at 0.03, 0.10, and 0.60 mol/kg. It was found that stacking membranes together to increase the effective membrane thickness changed the observed Seebeck coefficient of the thermocell to converge to some limiting value. This value was interpreted as the sum of the membrane and electrode contributions to the total Seebeck coefficient, allowing us to neglect the effects of the diffusion layers. Calculation of the transported entropies requires knowledge about the water transference coefficients, and the currently estimated values of the entropies suffer from large errors due to the large errors in the measurements of the water transference coefficients. The Seebeck coefficients are, however, precise to the order of 1 %, and obtaining more precise measurements of the transference coefficients will therefore allow more precise estimates of the transported entropies.

For the experimental conditions considered here, no significant Thomson effect could be measured. An order of magnitude estimate suggests that the precision of the current measurements is one order of magnitude smaller than the expected precision required to measure the Thomson effect. It has thus been demonstrated experimentally that the Thomson effect operates on a relative scale smaller than 1 % compared to the first order Seebeck effect. The theoretical derivations in this thesis will be useful for future work with improved experimental techniques to increase the precision. It should be noted that more precise experimental work should probably neither neglect the transported entropy of electrons in external circuit, nor assume that the membranes are perfectly selective.

Although the errors in the transported entropy estimates are large, there are some general tendencies that can be deduced. The transported entropy of Na^+ in the FKS membrane appears to be insensitive to the concentration of electrolyte in the aqueous solution, remaining at a value around 300 J/mol K for all concentrations. The transported entropy of Cl^- in the FAD membrane, however, increases significantly with electrolyte concentration. Although the error in the water transference coefficient at 0.60 mol/kg is very large, and no real conclusion can be made on this value, the difference between transported entropies at 0.03 and 0.10 mol/kg is significant. The transported entropies of both ions in their respective membranes are definitely positive, which indicates that heat is in both cases transported along with the charge

carrier.

For improving future measurements on Seebeck coefficients, we suggest incremental improvements to the design developed in this project. An optimized flow pattern will probably lead to faster convergence of the Seebeck coefficient with respect to stack thickness, as it leads to more efficient mixing in the diffusion layers. Using thermocouples and electrodes with similar response times can allow the measurement of instantaneous Seebeck coefficients, which would lead to less noisy results than the practice of taking averages of the temperature difference and electric potential over an extended period of time. An important issue is the shielding of the thermocouples from viscous noise due to the flow in each compartment. This was done by encapsulating the thermocouples in glass tubes filled with glycerol, which did shield the thermocouples from noise, but also delayed their response. The averaging technique allowed the accurate determination of the steady state temperatures over extended periods of time, but bounded the variance estimates from below by the oscillatory behaviour of the thermostats. An improved technique would manage to obtain both shielding and fast response at the same time, such that the thermostatting oscillations could be eliminated in the calculations, and noise would be significantly reduced. A simple improvement for measuring Thomson coefficients is to simply extend the considered temperature differences to larger values, which will increase the significance of the Thomson effect.

4.3 Combining Salt Power and Waste Heat Harvesting

We now give what we consider to be the most important result in this thesis – the implications of the experimental results on applications in salt power. The calculated contribution of the membrane to the Seebeck effect is in both cases, FKS and FAD, positive, meaning that the electric potential increases on the hot side of both membranes. In both cases, the Seebeck coefficient also decreases with concentration, with the FKS membrane having the greatest concentration dependence. For a possible application, we consider a non-isothermal concentration cell, which might be realized in practice as a combined salt power plant and waste heat harvester. Whenever there is a concentration difference across such a membrane, the electric potential increases on the side with the lowest concentration of electrolyte. Therefore, a net increase in efficiency would be obtained by heating the brackish water, and keeping the more saline sea water at a lower temperature. A sketch of this suggestion is given in figure 4.2.
An estimate of the FKS-contribution to the thermoelectric potential would be

$$\eta_{\mathrm{S}}^{\mathrm{FKS}} = \frac{\left(T_2 - \hat{T}\right) S_{\mathrm{NaCl}}^{(2)} - \left(T_1 - \hat{T}\right) S_{\mathrm{NaCl}}^{(1)}}{F\Delta T} + \bar{t}_{\mathrm{w}} S_{\mathrm{w}}^{0} - \frac{\overline{S}_{\mathrm{Na}^+}^{*}}{F} \tag{4.3.1}$$

where we have used that the transported entropy of the sodium ions is insensitive to

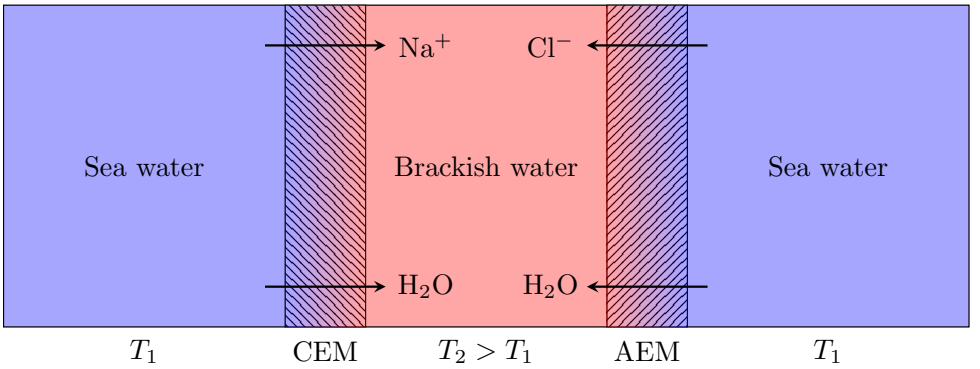

Figure 4.2: Suggestion for use of waste heat to improve the efficiency of a saline power plant.

the concentration gradient, and neglected the concentration dependence of S_w. Suppose we have a sea water temperature of 0°C, and we heat the brackish reservoir to a temperature of 40°C. If we use NaCl molalities of 0.03 mol/kg for brackish water, and 0.60 mol/kg for sea water, and use $\bar{t}_w = 3.8$, which is the average value over the concentration interval, we obtain a numerical value of around 1.15 mV/K. Since the FAD membrane was shown not to depend much on the electrolyte concentration, we apply a value of 0.5 mV/K for its contribution, giving a total of 1.65 mV/K. To top it off, both membranes contribute to maintain the concentration gradient through the electroosmotic transport of water from the sea water to the brackish reservoir, boosting the amount of work obtainable from the mixing potential even further. In this case, the total boost to the cell potential is 66 mV, which is added to the isothermal cell potential of approximately 142 mV, a nearly 50 % increase! Further work should attempt the explicit measurement of the nonisothermal concentration cell as a function of the temperature difference.

In a real salt power plant, several such membrane pairs separating sea water and brackish waters are put in series [8]. Maintaining such a temperature gradient by heating the brackish reservoir supplying all the brackish chambers in the power plant, the total thermoelectric power is boosted by a factor equal to the number of pairs in series. Supposing we have 20 such pairs in series, the total thermoelectric potential of the special case considered here would reach upwards of 33 mV/K, giving a total of 1.32 V boost for a 40 K temperature difference. These results indicate that the combination of salt power and harvesting of low-grade waste heat is feasible, given that the waste heat can easily be directed to the freshwater reservoir of the power plant.

List of Symbols

Symbol	Units	Explanation
U	J	Internal energy
T	K	Temperature
S	J K^{-1}	Entropy
P	Pa	Pressure
V	m^3	Volume
$\tilde{\mu}_j$	J mol^{-1}	Electrochemical potential
N_j	mol	Molar number
u	J m^{-3}	Internal energy density
s	J K^{-1} m^{-3}	Entropy density
c	mol m^{-3}	Concentration
$\mathbf{J}_s$	J $m^{-2}K^{-1}s^{-1}$	Entropy flux
σ	J $m^{-3}K^{-1}s^{-1}$	Entropy production
$\mathbf{J}_u$	J $m^{-2}s^{-1}$	Energy flux
$\mathbf{J}$	mol $m^{-2}s^{-1}$	Molar flux
r	mol m^{-2} s^{-1}	Reaction rate
ν_j	-	Stoichiometric coefficient
μ_j	J mol^{-1}	Chemical potential
ψ	J C^{-1}	Electric potential
F	C mol^{-1}	Faraday constant
z	-	Charge/valence number
H_j	J mol^{-1}	Partial molar enthalpy
S_j	J mol^{-1} K^{-1}	Partial molar entropy
$\mathbf{j}$	C m^{-2} s^{-1}	Electric current density
Γ	mol m^{-2}	Adsorption
G	J mol^{-1}	Molar Gibbs energy
ϕ	J C^{-1}	Total electric potential
L_{ij}, ℓ_{ij}	Varies	Generalized conductivity
t_j	-	Transference coefficient
ν	-	Electrolyte ion degrees of freedom

List of Symbols (cont.)

Symbol	Units	Explanation
R	J mol^{-1} K^{-1}	Universal gas constant
m_j	mol kg^{-1}	Molality
γ_j	-	Activity coefficient
α_j	-	Thermodynamic factor
V_j	m^3 mol^{-1}	Partial molar volume
M_j	kg mol^{-1}	Molar mass
β	J C^{-1} Pa^{-1}	Streaming potential
ε_j	J mol^{-1}	Chemical potential deviation
t	s	Time
L_p	m s^{-1} Pa^{-1}	Water permeability
D_j	m^2 s^{-1}	Diffusion coefficient
ε	F m^{-1}	Dielectric permittivity
e	C	Elementary charge
ρ_j	kg m^{-3}	Mass density
a	m	Debye-Hückel size parameter
S_j^*	J mol^{-1} K^{-1}	Transported entropy
$c_{p,j}$	J mol^{-1} K^{-1}	Isobaric heat capacity
τ_j	J mol^{-1} K^{-1}	Thomson coefficient
η_S	J C^{-1} K^{-1}	Seebeck coefficient
a_j	mol kg^{-1}	Activity
d	m	Membrane thickness
ξ_j	-	Activity temperature coefficient
κ	S	Electric conductivity
λ	J m^{-1} s^{-1} K^{-1}	Thermal conductivity
$\mathcal{F}$	K^{-1}	Figure of merit

Bibliography

[1] International Energy Agency. *Energy Efficiency Indicators*. 2017.

[2] *Study on the Energy Savings Potentials in EU Member States, Candidate Countries and EEA Countries - Final Report*. 2009.

[3] J. M. Cullen and J. M. Allwood. Theoretical efficiency limits for energy conversion devices. *Energy*, 35, 2010.

[4] C. Forman, I. K. Muritala, R. Pardemann, and B. Meyer. Estimating the global waste heat potential. *Renewable and Sustainable Energy Reviews*, 57, 2016.

[5] W. Xu, Q. Zhang, Y. Sun, and D. Zhu. Organic thermoelectric materials: Emerging green energy materials converting heat to electricity directly and efficiently. *Advanced Materials*, 26, 2014.

[6] T. Ikeda. Thermal membrane potential. *The Journal of Chemical Physics*, 28, 1958.

[7] K. D. Sandbakk, A. Bentien, and S. Kjelstrup. Thermoelectric effects in ion conducting membranes and perspectives for thermoelectric energy conversion. *Journal of Membrane Science*, 434, 2013.

[8] S. Kjelstrup and D. Bedeaux. *Non-Equilibrium Thermodynamics of Heterogeneous Systems*. World Scientific, 2008.

[9] S. R. de Groot and P. Mazur. *Non-Equilibrium Thermodynamics*. North-Holland Pub. Co., Amsterdam, 1962.

[10] D. N. Zubarev. *Nonequilibrium Statistical Thermodynamics*. Nauka Press, Moscow, 1971.

[11] T. S. Brun and D. Vaula. Correlation of measurements of electroosmosis and streaming potentials in ion exchanger membranes. *Berichte der Bunsengesellschaft für physikalische Chemie*, 71, 1967.

[12] G. Xie and T. Okada. Water transport behavior in Nafion 117 membranes. *Journal of the Electrochemical Society*, 142, 1995.

[13] G. Xie and T. Okada. Characteristics of water transport in relation to microscopic structure in Nafion membranes. *Journal of the Chemical Society, Faraday Transactions*, 92, 1996.

[14] G. Xie and T. Okada. Pumping effects in water movement accompanying cation transport across Nafion 117 membranes. *Electrochimica Acta*, 41, 1996.

[15] T. Okada, S. Møller-Holst, O. Gorseth, and S. Kjelstrup. Transport and equilibrium properties of nafion membranes with H^+ and Na^+ ions. *Journal of Electroanalytical Chemistry*, 442, 1998.

[16] T. Okada, N. Nakamura, M. Yuasa, and I. Sekine. Ion and water transport characteristics in membranes for polymer electrolyte fuel cells containing H^+ and Ca^{2+} cations. *Journal of the Electrochemical Society*, 144, 1997.

[17] T. Okada, G. Xie, O. Gorseth, S. Kjelstrup, N. Nakamura, and T. Arimura. Ion and water transport characteristics of Nafion membranes as electrolytes. *Electrochimica Acta*, 43, 1998.

[18] P. Trivijitkasem and T. Østvold. Water transport in ion exchange membranes. *Electrochimica Acta*, 25, 1980.

[19] T. Okada, S. K. Ratkje, and H. Hanche-Olsen. Water Transport in Cation Exchange Membranes. *Journal of Membrane Science*, 66, 1992.

[20] J. O. Bockris and A. K. N. Reddy. *Modern Electrochemistry: Volume 1*. Springer US, 1970.

[21] Y. Marcus. Evaluation of static permittivity of aqueous electrolytes. *Journal of Solution Chemistry*, 42, 2013.

[22] V. M. Barragán, C. Ruiz-Bauzá, and J. L. Imaña. Streaming potential across cation-exchange membranes in methanol-water electrolyte solutions. *Journal of Colloid and Interface Science*, 294, 2006.

[23] R. A. Fine and F. J. Millero. Compressibility of water as a function of temperature and pressure. *The Journal of Chemical Physics*, 59, 1973.

[24] W. B. Floriano and M. A. Chaer Nascimento. Dielectric constant and density of water as a function of pressure at constant temperature. *Brazilian Journal of Physics*, 34, 2004.

[25] *CRC Handbook of Chemistry and Physics, 96th edition.* CRC Press, 2015.

[26] B. B. Owen and S. R. Brinkley. Calculation of the effect of pressure upon ionic equilibria in pure water and in salt solutions. *Chemical Reviews*, 29, 1941.

[27] R. H. Stokes and R. A. Robinson. Ionic hydration and activity in electrolyte solutions. *Journal of the American Chemical Society*, 70, 1948.

[28] K. Giese, U. Kaatze, and R. Pottel. Permittivity and dielectric and proton magnetic relaxation of aqueous solutions of alkali halides. *Journal of Physical Chemistry*, 74, 1970.

[29] A. Maqsood, M. Anis ur Rehman, K. Kamran, and I. H. Gul. Thermophysical properties of AgCl in the temperature range 77-300 K. *Journal of Physics D: Applied Physics*, 37, 2004.

[30] A. Zlotorowicz, R. V. Strand, O. S. Burheim, Ø. Wilhelmsen, and S. Kjelstrup. The permselectivity and water transference number of ion exchange membranes in reverse electrodialysis. *Journal of Membrane Science*, 523, 2017.

[31] L. A. Dunn. Apparent molar volumes of electrolytes. *Transactions of the Faraday Society*, 64, 1968.

[32] T. Suzuki, Y. Takahashi, R. Kiyono, and M. Tasaka. Nonisothermal membrane phenomena across perfluorosulfonic acid-type membranes, Flemion S: Part I. thermoosmosis and transported entropy of water. *Colloid and Polymer Science*, 272, 1994.

[33] J. I. Calvo, A. Hernández, P. Prádanos, and F. Tejerina. Charge adsorption and zeta potential in cyclopore membranes. *Journal of Colloid and Interface Science*, 181, 1996.

[34] L. G. Longsworth. Transference numbers of aqueous solutions of potassion chloride, sodium chloride, lithium chloride and hydrochloric acid at 25°C by the moving boundary method. *Journal of the American Chemical Society*, 54, 1932.

[35] L. G. Longsworth. Transference numbers of aqueous solutions of some electrolytes at 25°C by the moving boundary method. *Journal of the American Chemical Society*, 57, 1935.

[36] D. G. Miller, J. A. Rard, L. B. Eppstein, and J. G. Albright. Mutual diffusion coefficients and ionic transport coefficients l_{ij} of $MgCl_2$-H_2O at 25°C. *Journal of Physical Chemistry*, 88, 1984.

[37] G. Jones and M. Dole. The transference number of barium chloride as a function of the concentration. *Journal of the American Chemical Society*, 51, 1929.

[38] H. S. Harned and C. L. Hildreth. The diffierential diffusion coefficients of lithium and sodium chlorides in dilute aqueous solution at 25°C. *Journal of the American Chemical Society*, 73, 1951.

[39] H. S. Harned. The diffusion coefficients of the alkali metal chlorides and potassium and silver nitrates in dilute aqueous solutions at 25°C. *Proceedings of the National Academy of Sciences*, 40, 1954.

[40] H. S. Harned and F. M. Polestra. The differential diffusion coefficients of magnesium and barium chlorides in dilute aqueous solutions at 25°C. *Journal of the American Chemical Society*, 76, 1954.

[41] H. S. Harned and H. W. Parker. The diffusion coefficient of calcium chloride in dilute and moderately dilute solutions at 25°C. *Journal of the American Chemical Society*, 77, 1955.

[42] R. H. Stokes. The diffusion coefficients of eight uni-univalent electrolytes in aqueous solution at 25°. *Journal of the American Chemical Society*, 72, 1950.

[43] B. F. Wishaw and R. H. Stokes. The diffusion coefficients and conductances of some concentrated electrolyte solutions at 25°. *Journal of the American Chemical Society*, 76, 1954.

[44] V. Vitagliano and P. A. Lyons. Diffusion coefficients for aqueous solutions of sodium chloride and barium chloride. *Journal of the American Chemical Society*, 78, 1956.

[45] G. Jones and M. Dole. The viscosity of aqueous solutions of strong electrolytes with special reference to barium chloride. *Journal of the American Chemical Society*, 51, 1929.

[46] R. A. Robinson and R. H. Stokes. *Electrolyte Solutions: Second Revised Edition.* Dover Publications, 2002.

[47] Jr. E. R. Nightingale. Phenomenological theory of ion solvation. effective radii of hydrated ions. *Journal of Physical Chemistry*, 63, 1959.

[48] V. M. Barragán and E. Pastuschuk. Viscoelastic deformation of sulfonated polymeric cation-exchange membranes exposed to a pressure gradient. *Materials Chemistry and Physics*, 146, 2014.

[49] M. Tasaka, S. Morita, and M. Nagasawa. Membrane potential in nonisothermal systems. *The Journal of Physical Chemistry*, 69, 1965.

[50] M. Tasaka, K. Ogawa, and T. Yamazaki. Thermal membrane potential across charged membranes in 2-1 and 1-2 electrolyte solutions. *Biophysical Chemistry*, 7, 1978.

[51] K. Hanaoka, R. Kiyono, and M. Tasaka. Thermal membrane potential across anion-exchange membranes in KCl and KIO_3 solutions and the transported entropy of ions. *Journal of Membrane Science*, 82, 1993.

[52] K. Hanaoka, R. Kiyono, and M. Tasaka. Thermal membrane potential across anion-exchange membranes in various electrolyte solutions and the transported entropy of ions. *Bulletin of the Chemical Society of Japan*, 67, 1994.

[53] K. Hanaoka, R. Kiyono, and M. Tasaka. Nonisothermal membrane phenomena across perfluorosulfonic acid-type membranes, Flemion S: Part II. thermal membrane potential and transported entropy of ions. *Colloid and Polymer Science*, 272, 1994.

[54] C. Ruiz-Bauzá and V. M. Barragán. Effect of unstirred solution layers on the thermal membrane potential through cation-exchange membranes. *Journal of Membrane Science*, 134, 1997.

[55] V. M. Barragán and C. Ruiz-Bauzá. On the dependence of the thermal membrane potential across cation-exchange membranes on the mean temperature. *Journal of Membrane Science*, 134, 1997.

[56] M. Jokinen, J. A. Manzanares, K. Kontturi, and L. Murtom ́aki. Thermal potential of ion-exchange membranes and its application to thermoelectric power generation. *Journal of Membrane Science*, 499, 2016.

[57] L. Yang, H. Sun, S. Wang, L. Jiang, and G. Sun. A solid state thermogalvanic cell harvesting low-grade thermal energy. *International Journal of Hydrogen Energy*, 42, 2017.

[58] J. N. Agar. *Electrochemistry and Electrochemical Engineering.* Interscience, New York, 1963.

[59] L. E. Bell. Cooling, heating, generating power, and recovering waste heat with thermoelectric systems. *Science*, 321, 2008.

[60] A. H. Truesdell. Activity coefficients of aqueous sodium chloride from 15° to 50°C measured with a glass electrode. *Science*, 161, 1968.

[61] I. N. Tang, H. R. Munkelwitz, and Ning Wang. Water activity measurements with single suspended droplets: The NaCl-H_2O and KCl-H_2O systems. *Journal of Colloid and Interface Science*, 114, 1986.

[62] R. Halseid. *Thermopotential Measurements on Nafion 117 Membranes and a Reversible Heat Balance for the Solid Polymer Electrolyte Fuel Cell.* Norwegian Institute of Technology, 1994.

[63] H. Feldborg. *Transportert Entropi i Solid Polymer Membraner.* Norwegian Institute of Technology, 1995.

[64] M. Ottøy. *Mass and Heat Transfer in Ion-Exchange Membranes - Applicable to Solid Polymer Fuel Cells.* Norwegian Institute of Technology, doctoral thesis, 1996.

[65] G. Scatchard and W. H. Orttung. The electromotive forces of NH_4Br and KBr concentration cells: Are the abnormalities in the freezing points of ammonium salts due to surface effects? *Journal of Colloid and Interface Science*, 22, 1966.

[66] D. Jou, J. Casas-Vàzquez, and G. Lebon. *Extended Irreversible Thermodynamics.* Springer, 2010.

[67] C. Cattaneo. Sulla conduzione del calore. *Atti Sem. Mat. Fis. Univ. Modena*, 3, 1948.

[68] N. G. van Kampen. *Stochastic Processes in Physics and Chemistry.* Elsevier, 2007.

[69] L. Fahrmeir, T. Kneib, S. Lang, and B. Marx. *Regression - Models, Methods and Applications.* Springer, 2013.

Appendix A
Microscopic Foundations of the Theory

Consider a system in statistical equilibrium, i.e. a state where all ensemble averages are constant, and the dynamical behaviour is due to fluctuations around the equilibrium state. We consider the classical, non-relativistic regime without external magnetic fields or coriolis forces. Let $\mathbf{a}$ be a vector containing the values of all state variables of the system, and define their fluctuations $\boldsymbol{\alpha} := \mathbf{a} - \langle \mathbf{a} \rangle$, where brackets denote ensemble averages. Following Boltzmann's principle, the distribution function to second order in $\boldsymbol{\alpha}$ is

$$f_{\boldsymbol{\alpha}}(\boldsymbol{\alpha}) = \sqrt{\frac{|\mathbf{A}|}{(2\pi k_{\mathrm{B}})^n}} \exp\left(-\frac{1}{2k_{\mathrm{B}}} \boldsymbol{\alpha}^{\mathrm{T}} \mathbf{A} \boldsymbol{\alpha}\right) \tag{A.1}$$

i.e. a multivariate Gaussian with covariance matrix $k_{\mathrm{B}}\mathbf{A}^{-1}$, where $\mathbf{A}$ satisfies [9]

$$\Delta S = S(\boldsymbol{\alpha}) - S(\mathbf{0}) = -\frac{1}{2} \boldsymbol{\alpha}^{\mathrm{T}} \mathbf{A} \boldsymbol{\alpha} + \mathcal{O}(\boldsymbol{\alpha}^3) \tag{A.2}$$

which means that $\mathbf{A}$ is a tensor containing the second derivatives of the entropy S with respect to the fluctuations. Since the entropy function is concave in the neighborhood of equilibrium, $\mathbf{A}$ is positive definite. The definiteness of $\mathbf{A}$ can also be noted as a sufficient condition for the integrability of $f_{\boldsymbol{\alpha}}$. By Schwarz' theorem on the symmetry of mixed derivatives, $\mathbf{A}$ is also symmetric. In this treatment, we will consider stationary states, and thus neglect inertia effects or fluctuations of fluxes. For discussions on e.g. heat inertia, see [66] and [67]. We define the fluxes $\mathbf{J}_j$ and their conjugate driving forces $\mathbf{X}_j$

$$\mathbf{J}_j := \frac{\mathrm{d}\boldsymbol{\alpha}_j}{\mathrm{d}t} \qquad\qquad \mathbf{X}_j := \frac{\partial \Delta S}{\partial \boldsymbol{\alpha}_j} = -\sum_i A_{ji} \boldsymbol{\alpha}_i \tag{A.3}$$

From the time-reversal symmetry of the Hamiltonian dynamics of the microscopic system, one can prove that the system obeys detailed balance. For an elegant proof, see [68]. Let $W(\boldsymbol{\alpha}'; t|\boldsymbol{\alpha})$ be the probability of finding the system in state $\boldsymbol{\alpha}'$ at time t, given that it was initially in state $\boldsymbol{\alpha}$. Since the state variables under consideration are even with respect to microscopic time reversal, detailed balance then means that

$$f_{\boldsymbol{\alpha}}(\boldsymbol{\alpha}) W(\boldsymbol{\alpha}'; t|\boldsymbol{\alpha}) = f_{\boldsymbol{\alpha}}(\boldsymbol{\alpha}') W(\boldsymbol{\alpha}; t|\boldsymbol{\alpha}') \tag{A.4}$$

this property is also known as microscopic reversibility. We now introduce the conditional mean values

$$\overline{\mathbf{X}}_j = -\sum_i A_{ji}\overline{\boldsymbol{\alpha}}_i = -\sum_i A_{ji}\int \boldsymbol{\alpha}_i' W(\boldsymbol{\alpha}_i';t|\boldsymbol{\alpha}_i)\mathrm{d}\boldsymbol{\alpha}_i' \tag{A.5}$$

The most important assumption imposed on the theoretical foundations is then the linear regression hypothesis, which reads

$$\frac{\mathrm{d}\overline{\boldsymbol{\alpha}}_j}{\mathrm{d}t} =: \overline{\mathbf{J}}_j = \sum_i L_{ji}\overline{\mathbf{X}}_i \tag{A.6}$$

i.e. the fluxes are expanded to first order in all the thermodynamical driving forces, where the conductivity tensor $\mathbf{L}$ satisfies [9]

$$\mathbf{L} = -\frac{1}{k_\mathrm{B}}\lim_{\Delta t\to 0}\frac{1}{\Delta t}\iint \Delta\boldsymbol{\alpha}'\boldsymbol{\alpha}^\mathrm{T} f_{\boldsymbol{\alpha}}(\boldsymbol{\alpha})W(\boldsymbol{\alpha}';\Delta t|\boldsymbol{\alpha}_j)\mathrm{d}\boldsymbol{\alpha}'\mathrm{d}\boldsymbol{\alpha} \tag{A.7}$$

where $\Delta\boldsymbol{\alpha}' := \boldsymbol{\alpha}' - \boldsymbol{\alpha}$. In other words, the elements of $\mathbf{L}$ are correlation functions between the fluxes and fluctuations. One such example is the correlation between a temperature fluctuation and the heat flux, which is essentially the thermal conductivity of the system. Relabelling the integration variables in (A.7) and imposing (A.4), it is straightforward to show that

$$\mathbf{L} = \mathbf{L}^\mathrm{T} \qquad \text{i.e.} \qquad L_{ij} = L_{ji} \tag{A.8}$$

which are the famous Onsager reciprocal relations. These relations will be used for deriving experimental expressions for various transport coefficients. It follows trivially that

$$\mathbf{L} = \frac{1}{2}\left(\mathbf{L} + \mathbf{L}^\mathrm{T}\right) =: \mathbf{L}^\mathrm{s} \tag{A.9}$$

and since for stationary processes, we impose translation symmetry along the time axis

$$\langle\boldsymbol{\alpha}\boldsymbol{\alpha}^\mathrm{T}\rangle = \langle\boldsymbol{\alpha}'\boldsymbol{\alpha}'^\mathrm{T}\rangle \tag{A.10}$$

such that for an arbitrary vector $\mathbf{x}$

$$\begin{aligned}\mathbf{x}^\mathrm{T}\mathbf{L}\mathbf{x} = \mathbf{x}^\mathrm{T}\mathbf{L}^\mathrm{s}\mathbf{x} &= -\frac{1}{k_\mathrm{B}}\lim_{\Delta t\to 0}\frac{1}{2\Delta t}\mathbf{x}^\mathrm{T}\left\langle\Delta\boldsymbol{\alpha}'\boldsymbol{\alpha}^\mathrm{T} + \boldsymbol{\alpha}\Delta\boldsymbol{\alpha}'^\mathrm{T}\right\rangle\mathbf{x}\\ &= -\frac{1}{k_\mathrm{B}}\lim_{\Delta t\to 0}\frac{1}{2\Delta t}\mathbf{x}^\mathrm{T}\left\langle\Delta\boldsymbol{\alpha}'\boldsymbol{\alpha}^\mathrm{T} + \boldsymbol{\alpha}\Delta\boldsymbol{\alpha}'^\mathrm{T} + \boldsymbol{\alpha}\boldsymbol{\alpha}^\mathrm{T} - \boldsymbol{\alpha}'\boldsymbol{\alpha}'^\mathrm{T}\right\rangle\mathbf{x}\\ &= \frac{1}{k_\mathrm{B}}\lim_{\Delta t\to 0}\frac{1}{2\Delta t}\mathbf{x}^\mathrm{T}\left\langle\left(\Delta\boldsymbol{\alpha}'\right)^2\right\rangle\mathbf{x} \geq 0\end{aligned} \tag{A.11}$$

so that $\mathbf{L}$ is also restricted to be positive definite. In accordance with the local equilibrium hypothesis, the local mean entropy production must be positive, and thus

the determinant of $\mathbf{L}$ and all its principal minors must also be positive. Considering single and pairwise flux-force pairs, we obtain the restrictions

$$\forall\, i \;\; L_{ii} \geq 0 \qquad\qquad \forall\, i \;\forall\, j \;\; L_{ii}L_{jj} \geq L_{ij}L_{ji} = (L_{ij})^2 = (L_{ji})^2 \tag{A.12}$$

which are useful for deriving bounds on the coupling coefficients imposed by the second law and the local equilibrium hypothesis. The entropy production σ is obtained by taking the time derivative of the local entropy fluctuation

$$\sigma = \frac{\mathrm{d}\Delta S}{\mathrm{d}t} = -\overline{\boldsymbol{\alpha}}^{\mathrm{T}}\mathbf{A}\frac{\mathrm{d}\overline{\boldsymbol{\alpha}}}{\mathrm{d}t} = \sum_j \overline{\mathbf{J}}_j \cdot \overline{\mathbf{X}}_j = \overline{\mathbf{X}}^{\mathrm{T}}\mathbf{L}\overline{\mathbf{X}} \geq 0 \tag{A.13}$$

where the last equality was used to demonstrate that the positive-definiteness of $\mathbf{L}$ was in fact a statement of the second law. The second to last equality gives the ubiquitous bilinear form of the entropy production as the sum over the dot products between all fluxes with their conjugate driving forces. The intuitive notion that the system is indifferent as to whether a driving force in the system arises due to an equilibrium fluctuation or an external perturbation is the physical content of the fluctuation-dissipation theorem, see e.g. [10]. Applying this theorem, we confirm that all relations derived here, which govern the system's response to its equilibrium fluctuations, are also valid for external perturbations, and thus yields a strong framework for a general transport theory. Of course, these relations are only valid for perturbations to weakly non-equilibrium states. A stronger theory is obtained by invoking the local equilibrium hypothesis, which supposes that the system can be divided into small volume elements, each acting as an equilibrium system. This allows the local equilibrium theory to describe systems in strongly non-equilibrium global states, given that small enough volume elements may be chosen. For a discussion on tests of the validity of the theory by means of molecular dynamics simulations, see [8, 66].

To summarize this section, we have

- The linear force-flux relations, $\overline{\mathbf{J}}_j = \sum_i L_{ji}\overline{\mathbf{X}}_i$.
- The reciprocal relations, $L_{ij} = L_{ji}$.
- Positivity of diagonal elements, $L_{ii} \geq 0$.
- Constraints on off-diagonal elements, $L_{ii}L_{jj} \geq L_{ij}L_{ji}$.
- The bilinear form of the entropy production, $\sigma = \sum_j \overline{\mathbf{J}}_j \cdot \overline{\mathbf{X}}_j$.

Appendix B
Streaming Potential Regression Model

B.1 Analytical Solution

In order to develop a model for fitting the time-dependent streaming potential data, we need to consider the dynamics of the electrolyte flux through the membrane. Our starting point is the set of flux equations describing flux of water, electrolyte, and electric current in the electrolyte solution. Eliminating the electric potential difference and the chemical potential of water, the electrolyte flux $\mathbf{J}_\mathrm{e}$ at zero electric current and temperature T is

$$\mathbf{J}_\mathrm{e} = -\frac{\Lambda_\mathrm{ee}}{T}\nabla\mu_\mathrm{e} + \frac{\ell_\mathrm{ew}}{\ell_\mathrm{ww}}\mathbf{J}_\mathrm{w} \tag{B.1.1}$$

with μ_e the chemical potential of electrolyte, $\mathbf{J}_\mathrm{w}$ the water flux, and

$$\ell_{ij} = L_{ij} - \frac{L_{i\phi}L_{\phi j}}{L_{\phi\phi}}, \qquad \Lambda_{ij} = \ell_{ij} - \frac{\ell_{i\mathrm{w}}\ell_{\mathrm{w}j}}{\ell_\mathrm{ww}} \tag{B.1.2}$$

with L_{ij} being the generalized conductivities of the full set of flux equations, as prescribed by the linear regression hypothesis. For the first term, we use that

$$\nabla\mu_\mathrm{e} = \frac{\partial\mu_\mathrm{e}}{\partial c}\nabla c = \frac{\nu RT}{c}\left(1 + \frac{\partial\ln(\gamma)}{\partial\ln(c)}\right)\nabla c \tag{B.1.3}$$

where c is the electrolyte concentration, R the universal gas constant, γ the mean activity coefficient, and ν the number of ions per molecule of electrolyte. We then assign the diffusion coefficient

$$D = \frac{\nu\Lambda_\mathrm{ee}R}{c}\left(1 + \frac{\partial\ln(\gamma)}{\partial\ln(c)}\right) \tag{B.1.4}$$

and also obtain from the flux equations that

$$\frac{\ell_\mathrm{ew}}{\ell_\mathrm{ww}} = \left(\frac{\mathbf{J}_\mathrm{e}}{\mathbf{J}_\mathrm{w}}\right)_{\mathbf{j}=\mathbf{0}} \approx V_\mathrm{w}c \tag{B.1.5}$$

where the last approximation is due to the water making up most of the volume in the system, so that flux of water is essentially the flux of volume, so that electrolyte is dragged along in proportion to its concentration. We set the volume flux $\mathbf{J}_\mathrm{v} = V_\mathrm{w}\mathbf{J}_\mathrm{w}$. The electrolyte flux is then

$$\mathbf{J}_\mathrm{e} = -D\nabla c + c\mathbf{J}_\mathrm{v} \tag{B.1.6}$$

We now assume that neither the molar volume of water nor the diffusion coefficient vary throughout the system, and that the concentration of water changes negligibly compared to that of electrolyte. Conservation of mass gives then

$$\nabla \cdot \mathbf{J}_{\mathrm{V}} = -V_{\mathrm{w}} \frac{\partial c_{\mathrm{w}}}{\partial t} \approx 0, \qquad \nabla \cdot \mathbf{J}_{\mathrm{e}} + \frac{\partial c}{\partial t} = 0 \tag{B.1.7}$$

Taking the divergence of (B.1.6) then gives

$$\frac{\partial c}{\partial t} + \mathbf{J}_{\mathrm{V}} \cdot \nabla c = D \nabla^2 c \tag{B.1.8}$$

which we confine to one dimension

$$\frac{\partial c}{\partial t} + J_{\mathrm{V}} \frac{\partial c}{\partial x} = D \frac{\partial^2 c}{\partial x^2} \tag{B.1.9}$$

with the membrane surface at the origin. Assuming that the system begins initially at a uniform concentration c_0, the initial condition to the equation becomes

$$c(0, x) = c_0 \tag{B.1.10}$$

while the continuity of the electrolyte flux gives the boundary condition

$$\left.\frac{\partial c}{\partial x}\right|_{x=0} = \frac{c J_{\mathrm{V}} - J_{\mathrm{e}}}{D} \tag{B.1.11}$$

and we finally establish the other boundary condition by requiring that the concentration far away from the membrane surface remains constant, i.e.

$$\lim_{x \to \pm\infty} c(t, x) = c_0 \tag{B.1.12}$$

Furthermore, we simplify by rescaling to dimensionless form

$$X := \frac{J_{\mathrm{V}}}{4D} x, \qquad \tau := \frac{J_{\mathrm{V}}^2}{4D} t, \qquad C := \frac{c}{c_0}, \qquad J := \frac{J_{\mathrm{e}}}{c_0 J_{\mathrm{V}}} \tag{B.1.13}$$

and the problem reads

$$\begin{aligned} \frac{\partial C}{\partial \tau} + \frac{\partial C}{\partial X} &= \frac{1}{4} \frac{\partial^2 C}{\partial X^2} \\ C(0, X) &= 1 \\ \lim_{X \to \pm\infty} C(\tau, X) &= 1 \\ \left.\frac{1}{4} \frac{\partial C}{\partial X}\right|_{X=0} &= C - J \end{aligned} \tag{B.1.14}$$

To solve this equation, we apply a Laplace transform with respect to T. Letting s be the independent variable in Laplace space, we obtain

$$s\mathcal{L}C - 1 + \frac{\partial \mathcal{L}C}{\partial X} = \frac{1}{4} \frac{\partial^2 \mathcal{L}C}{\partial X^2} \tag{B.1.15}$$

which has the general solution

$$\mathcal{L}C(s,X) = \frac{1}{s} + C_1 \exp\left(2\left(1+\sqrt{1+s}\right)X\right) + C_2 \exp\left(2\left(1-\sqrt{1+s}\right)X\right) \quad \text{(B.1.16)}$$

Depending on whether the surface is oriented towards the negative or positive X-direction, the boundary condition at infinity gives that the respective divergent term must vanish. We treat the case where $C_1 = 0$. Applying the boundary condition at the membrane surface gives

$$C_2 = 2\frac{\mathcal{L}J - s^{-1}}{1+\sqrt{1+s}} = \frac{2}{s^2}\left(1 - s\mathcal{L}J\right)\left(1-\sqrt{1+s}\right) \quad \text{(B.1.17)}$$

such that the solution at $X = 0$ is

$$\mathcal{L}C(s,0) = \frac{1}{s} + \frac{2}{s^2}\left(1 - s\mathcal{L}J\right)\left(1-\sqrt{1+s}\right) \quad \text{(B.1.18)}$$

while the result for the opposite membrane surface is

$$\mathcal{L}C(s,0) = \frac{1}{s} + \frac{2}{s^2}\left(1 - s\mathcal{L}J\right)\left(1+\sqrt{1+s}\right) \quad \text{(B.1.19)}$$

We will assume that there is no open circuit electrolyte flux. Then, $\mathcal{L}J = 0$. Taking the inverse transform of the two solutions gives

$$C_{\pm}(t) = (1+2\tau)\left(1 \mp \frac{2}{\sqrt{\pi}}\int_0^{\sqrt{\tau}} e^{-s^2}\mathrm{d}s\right) \mp \frac{2}{\sqrt{\pi}}\sqrt{\tau}e^{-\tau} \quad \text{(B.1.20)}$$

Where the subscripts $+$ and $-$ denote the values at the membrane surface in compartment 2 and 1, respectively. In the regression models, we will be interested in the prefactor $A := J_{\mathrm{V}}/2\sqrt{D}$ to the dimensionful time t.

B.2 Linear Regression Model

We begin by expanding the exponential functions in the expression for the concentration profile

$$\int_0^{\sqrt{\tau}} e^{-s^2}\mathrm{d}s = \int_0^{\sqrt{\tau}} \sum_{n=0}^{\infty} (-1)^n \frac{s^{2n}}{n!}\mathrm{d}s = \sum_{n=0}^{\infty} \frac{(-1)^n}{2n+1}\frac{\tau^{\frac{2n+1}{2}}}{n!} \quad \text{(B.2.1)}$$

After a bit of algebra, expansion of (B.1.20) gives

$$C_{\pm} = 1 + 2\tau \mp \frac{4}{\sqrt{\pi}}\left(\sqrt{\tau} + \sum_{n=0}^{\infty}\frac{(-1)^n}{(2n+1)(2n+3)}\frac{\tau^{\frac{2n+3}{2}}}{(n+1)!}\right) \quad \text{(B.2.2)}$$

Rewriting

$$\frac{C_+}{C_-} = \frac{C_+ - C_-}{C_-} + 1 \quad \text{(B.2.3)}$$

we can make the expansion

$$\ln\left(\frac{C_+}{C_-}\right) = \ln\left(\frac{C_+ - C_-}{C_-} + 1\right) = \sum_{k=1}^{\infty} \frac{(-1)^{k+1}}{k}\left[\frac{C_+ - C_-}{C_-}\right]^k \tag{B.2.4}$$

which converges when the bracketed term has an absolute value lower than unity, which will always be the case with the appropriate choice of reference frame. Inserting (B.2.2), we obtain

$$\ln\left(\frac{C_+}{C_-}\right) = \sum_{k=1}^{\infty} \frac{(-1)^{k+1}}{k}\left[\frac{-\frac{8}{\sqrt{\pi}}\left(\sqrt{\tau} + \sum_{n=0}^{\infty}\frac{(-1)^n}{(2n+1)(2n+3)}\frac{\tau^{\frac{2n+3}{2}}}{(n+1)!}\right)}{1 + 2\tau + \frac{4}{\sqrt{\pi}}\left(\sqrt{\tau} + \sum_{n=0}^{\infty}\frac{(-1)^n}{(2n+1)(2n+3)}\frac{\tau^{\frac{2n+3}{2}}}{(n+1)!}\right)}\right]^k \tag{B.2.5}$$

We can then apply the expansion

$$\frac{1}{1-x} = \sum_{\ell=0}^{\infty} x^{\ell} \tag{B.2.6}$$

for

$$x = -2\tau - \frac{4}{\sqrt{\pi}}\left(\sqrt{\tau} + \sum_{n=0}^{\infty}\frac{(-1)^n}{(2n+1)(2n+3)}\frac{\tau^{\frac{2n+3}{2}}}{(n+1)!}\right) < 1 \tag{B.2.7}$$

where it can be shown that the inequality holds because the concentration is non-negative. We thus obtain

$$\begin{aligned}\ln\left(\frac{C_+}{C_-}\right) = \sum_{k=1}^{\infty}\frac{(-1)^k}{k}\left(\frac{8}{\sqrt{\pi}}\left(\sqrt{\tau} + \sum_{n=0}^{\infty}\frac{(-1)^n}{(2n+1)(2n+3)}\frac{\tau^{\frac{2n+3}{2}}}{(n+1)!}\right)\right)^k \times \\ \left[\sum_{\ell=0}^{\infty}\left(-2\tau - \frac{4}{\sqrt{\pi}}\left(\sqrt{\tau} + \sum_{n=0}^{\infty}\frac{(-1)^n}{(2n+1)(2n+3)}\frac{\tau^{\frac{2n+3}{2}}}{(n+1)!}\right)\right)^{\ell}\right]^k\end{aligned} \tag{B.2.8}$$

which is the basic expression from which polynomial expressions in time can be extracted, by appropriate truncation of the sums and neglection of terms of higher order than is needed. By inspection, one can observe that the lowest order term is proportional to the square root of time. This is the successful simple linear model used by Okada et al. [19]. The square root model works very well for a wide array of membranes. For some membranes, however, the pressure response is significantly non-linear with respect to the square root of time. This problem can hopefully be solved by including higher order terms from the above expansion. The time-dependent perturbation to the electric potential is

$$(\Delta\phi)_t = -\left(\bar{t}_{\mathrm{a}} - t_{\mathrm{a}}\right)\frac{\Gamma\nu RT}{F}\ln\left(\frac{C_+}{C_-}\right) \tag{B.2.9}$$

The first few terms of the Taylor series around $\tau = 0$ are

$$\begin{aligned}\ln\left(\frac{C_+}{C_-}\right) &\approx -\frac{8}{\sqrt{\pi}}\sqrt{\tau} - \frac{1}{3\sqrt{\pi}}\left(\frac{128}{\pi} - 40\right)A^3 t^{\frac{3}{2}} - \frac{1}{3\sqrt{\pi}}\left(80 - \frac{640}{\pi} - \frac{24576}{5\pi^2}\right)A^5 t^{\frac{5}{2}} \\ &= a_1 A\sqrt{t} + a_2 A^3 t^{\frac{3}{2}} + a_3 A^5 t^{\frac{5}{2}}\end{aligned} \tag{B.2.10}$$

where we observe that the coefficients for integer powers vanish. The first term reproduces the result obtained by Okada et al [19]. We have introduced a parameter A such that $\tau = A^2 t$, where t is the physical time. To this order in time, a straightforward linear model is then

$$\Delta\boldsymbol{\phi} = \mathbb{A}\boldsymbol{\alpha} + \boldsymbol{\varepsilon} \tag{B.2.11}$$

where $\Delta\boldsymbol{\phi}$ is a vector containing the observed potential, $\boldsymbol{\varepsilon}$ are the errors, the deviations from the model. Also

$$\mathbb{A} = \begin{bmatrix} 1 & \sqrt{t}_1 & t_1^{\frac{3}{2}} & t_1^{\frac{5}{2}} \\ 1 & \sqrt{t}_2 & t_2^{\frac{3}{2}} & t_2^{\frac{5}{2}} \\ \vdots & \vdots & \vdots & \vdots \\ 1 & \sqrt{t}_N & t_N^{\frac{3}{2}} & t_N^{\frac{5}{2}} \end{bmatrix} \qquad \boldsymbol{\alpha} = \begin{bmatrix} \alpha_0 \\ \alpha_1 \\ \alpha_2 \\ \alpha_3 \end{bmatrix} \tag{B.2.12}$$

where the α_i are coefficients related to the above expressions in a straightforward manner. The columns of $\mathbb{A}$ tend to be numerically close to linear dependence, so that the numerical properties are notoriously bad. This problem can be alleviated by transformations. We transform the problem to the unit interval by the rescaling

$$\mathbf{y} := \left|\left|\sqrt{\mathbf{t}}\right|\right|_\infty^{-1} \sqrt{\mathbf{t}} = \gamma^{-1}\sqrt{\mathbf{t}} \tag{B.2.13}$$

where $||\cdot||_\infty$ is the supremum-norm, taken to equal the maximum. Assigning

$$M := -\left(\bar{t}_\mathrm{a} - t_\mathrm{a}\right)\frac{\Gamma\nu RT}{F} \tag{B.2.14}$$

we obtain the theoretical expression for the electric potential in terms of $\mathbf{y}$

$$\Delta\boldsymbol{\phi} = a_0 + \gamma MA\left(a_1\mathbf{y} + a_2 A^2\gamma^2\mathbf{y}^3 + a_3 A^4\gamma^4\mathbf{y}^5\right) \tag{B.2.15}$$

and we can now identify the monomial coefficients α_i' in $\mathbf{y}$ as rescaled versions of the a_i

$$\begin{aligned}\alpha_0' &= a_0 \\ \alpha_1' &= \gamma MA a_1 \\ \alpha_2' &= \gamma^3 MA^3 a_2 \\ \alpha_3' &= \gamma^5 MA^5 a_3\end{aligned} \tag{B.2.16}$$

We now set up the continuous inner product

$$\langle f(y), g(y) \rangle := \int_0^1 f(y) g(y) \mathrm{d}y \tag{B.2.17}$$

and we say that two functions are orthogonal iff their inner product vanishes. We can now orthonormalize our constrained basis with respect to this inner product, such that our basis polynomials $P'_n(y)$ satisfy

$$\langle P'_n(y), P'_k(y) \rangle = \delta_{nk} \tag{B.2.18}$$

By Gram-Schmidt orthonormalization, we obtain the set

$$\begin{aligned} P'_0(y) &= 1 \\ P'_1(y) &= \sqrt{12}\left(y - \frac{1}{2}\right) \\ P'_2(y) &= \frac{\sqrt{7}}{3}\left(10y^3 - 9y + 2\right) \\ P'_3(y) &= \frac{1191}{38}\left(y^5 - \frac{100}{81}y^3 + \frac{25}{63}y - \frac{32}{567}\right) \end{aligned} \tag{B.2.19}$$

We can then set up the matrix and the corresponding coefficients

$$\mathbb{A}' = \begin{bmatrix} P'_0 & P'_1(y_1) & P'_2(y_1) & P'_3(y_1) \\ P'_0 & P'_1(y_2) & P'_2(y_2) & P'_3(y_2) \\ \vdots & \vdots & \vdots & \vdots \\ P'_0 & P'_1(y_N) & P'_2(y_N) & P'_3(y_N) \end{bmatrix} \qquad \boldsymbol{\alpha}'' = \begin{bmatrix} \alpha''_0 \\ \alpha''_1 \\ \alpha''_2 \\ \alpha''_3 \end{bmatrix} \tag{B.2.20}$$

We then wish to find the $\boldsymbol{\alpha}''$ which minimizes

$$||\boldsymbol{\varepsilon}||^2 = ||\Delta\boldsymbol{\phi} - \mathbb{A}'\boldsymbol{\alpha}''||^2 \tag{B.2.21}$$

the optimal least squares result gives the coefficient vector related to the orthogonal projection of $\Delta\boldsymbol{\phi}$ onto the columns of $\mathbb{A}'$

$$\hat{\boldsymbol{\alpha}}'' = \left(\mathbb{A}'^{\mathrm{T}}\mathbb{A}'\right)^{-1}\mathbb{A}'^{\mathrm{T}}\Delta\boldsymbol{\phi} \tag{B.2.22}$$

where the projection onto the orthogonal completement yields an estimate for the errors, the residuals

$$\hat{\boldsymbol{\varepsilon}} = \Delta\boldsymbol{\phi} - \mathbb{A}'\hat{\boldsymbol{\alpha}}'' \tag{B.2.23}$$

which can be made independent by calculating them instead in a leave-one-out fashion

$$\hat{\varepsilon}'_i = \frac{\hat{\varepsilon}_i}{S_i\sqrt{1 - h_{ii}}} \tag{B.2.24}$$

where S_i is an estimate of the regression standard deviation excluding data point i, and h_{ii} is the ith diagonal element of the projection matrix $\mathbb{A}'\left(\mathbb{A}'^{\mathrm{T}}\mathbb{A}'\right)^{-1}\mathbb{A}'$. The regression mean square error is

$$S^2 = \frac{\hat{\boldsymbol{\varepsilon}}^{\mathrm{T}}\hat{\boldsymbol{\varepsilon}}}{N - df_R} \tag{B.2.25}$$

where df_R is the number of regression degrees of freedom, i.e. the rank of $\mathbb{A}'$. Finally, the covariance matrix of the coefficients is

$$\mathrm{Cov}\left(\hat{\boldsymbol{\alpha}}''\right) = \left(\mathbb{A}'^{\mathrm{T}}\mathbb{A}'\right)^{-1}\mathbb{A}'^{\mathrm{T}}\mathbb{A}'\left(\mathbb{A}'^{\mathrm{T}}\mathbb{A}'\right)^{-1}\widehat{\mathrm{Var}\left(\Delta\boldsymbol{\phi}\right)} = S^2\left(\mathbb{A}'^{\mathrm{T}}\mathbb{A}'\right)^{-1} \tag{B.2.26}$$

which is expected to be close to diagonal due to the orthogonal basis used. The monomial coefficients are related to the orthonormalized coefficients by an upper triangular matrix

$$\boldsymbol{\alpha}' = \mathbb{T}\boldsymbol{\alpha}'', \qquad \mathbb{T} = \begin{bmatrix} 1 & -\sqrt{3} & \frac{2\sqrt{7}}{3} & -\frac{375}{212} \\ 0 & \sqrt{12} & -3\sqrt{7} & \frac{4863}{391} \\ 0 & 0 & \frac{10\sqrt{7}}{3} & -\frac{10873}{281} \\ 0 & 0 & 0 & \frac{1191}{38} \end{bmatrix} \tag{B.2.27}$$

If the independent residuals can be shown to be distributed according to a student t-distribution, then it can be shown that $\boldsymbol{\alpha}''$ is multinormally distrubuted. Since we are using an orthonormalized basis, we expect the covariance matrix to be close to diagonalized, and we argue that we can to a good approximation factorize the distribution of $\boldsymbol{\alpha}''$ into a product of univariate distributions for each coefficient. The estimates are therefore statistically independent, and can be used to obtain independent estimates of the generally unknown factors of M. One should be aware, however, that this constitutes a nonlinear set of equations where uniqueness is an unresolved issue that should be approached with care. If such a method is employed, variance estimates are most easily found by a bootstrapping method, such as pseudorandom residual resampling.

B.3 Choosing the Regression Interval

Another problem arising in the data treatment is how to choose the interval for the regression. The physical considerations on which the advection-diffusion equation is based are valid for short time scales. A too long regression interval might force the regression model to account for effects not covered by the simplified model, and therefore give erroneous estimates. On the other hand, starting the interval too early might lead to inclusion of points where the system has not yet reached steady state, and an overall too short regression interval leads to unreliable and imprecise estimates. The correct interval should therefore begin a short time after application of

the pressure gradient, and then go on for a period long enough to provide precise results, but short enough that we still have confidence in the applied model.

To decide on the first point of the regression interval, we start with the exact moment the pressure is applied as the first candidate. The linear model is then fitted up until the moment the pressure is relieved. The residuals are calculated, and we observe the differences

$$\widehat{\Delta\varepsilon}_i = \hat{\varepsilon}_{i+1} - \hat{\varepsilon}_i \tag{B.3.1}$$

and form the criterion that the first difference should be smaller than the variance of the remaining residual differences. If this criterion is not met, we increment the initial regression point and repeat the procedure until the criterion is satisfied. We are thus saying that the most abrupt changes in potential, characterized by very large residual differences, are excluded from the interval. We identify these points as belonging to the transient period where the theory is not applicable, and the linear model has a very bad fit where these points are included. We now fix the initial point to the first which satisfied the difference criterion, and apply a similar procedure to find the end point. We begin with the last point before the pressure is relieved as the first candidate, and then fit the linear model. We then calculate the streaming potential by extrapolating to the initial time when the pressure was applied (not the initial regression point). We then repeat this procedure for all possible end points until we reach a minimum interval length. We want the calculated streaming potential to be as independent as possible of the choice of end point. We therefore calculate the differences

$$\Delta\left(\Delta\phi\right)_i = \Delta\phi_{i+1} - \Delta\phi_i \tag{B.3.2}$$

where the ith value is the value calculated with i more points in the regression interval than the minimum interval length. The criterion for accepting the end point is as follows: we locate the first interval for which the sum of the absolute values of 4 consequtive differences is smaller than the standard deviation of the later points. If the next 4 consequtive points fulfill the same criterion, then the 4th point of the first interval is chosen as the candidate end point. Once this criterion is fulfilled, we impose yet another criterion - goodness of fit. Once a point has been found which satisfies both the aforementoned difference criterion and the criterion that the distribution of residuals is not significantly different from normal according to the Anderson-Darling goodness-of-fit test, this point is finally accepted as the regression end point. The rationale for this choice is that this end point is in the middle of an interval where the estimated streaming potential is insensitive to the choice of end point, while at the same time the model has a good fit in that the residuals represent normally distributed noise.

We summarize how the regression interval was chosen. We choose the first point deemed not to be a part of the transient period as the initial point, and we choose the end point such that the estimated streaming potential is insensitive to the choice,

and that the residuals are significantly normal.

B.4 Choice of Model Order

Adding more fitting parameters always gives a better fit, whether the parameters belong in the actual model or not. If the deterministic effects modeled by the higher order terms are insignificant in the presence of the lower order terms, the model is at risk of overfitting the data. It is therefore often desirable to choose a more parsimonious model to ensure that the estimates are of the highest possible quality, and insensitive to the noise present in the physical system. The Runge phenomenon is also more pronounced for higher order polynomials, so that careless application of higher order models can lead to wildly inaccurate extrapolation results. We therefore implement the fitting procedure for models of all 3 orders in time, and compare the successful models to one another. We choose our model according to the Akaike Information Criterion, which is, for normally distributed residuals [69]

$$N \ln\left(\frac{\hat{\boldsymbol{\varepsilon}}^{\mathrm{T}}\hat{\boldsymbol{\varepsilon}}}{N}\right) + 2df_R \tag{B.4.1}$$

where the first term is the logarithm of the maximum likelihood estimate of the regression variance, and the second term is simply the number of parameters in the model. While the first term is smaller for any model with better fit to the data, the second term is added as a punishment for having more parameters. The criterion for best model is then to have the lowest value of this sum. This criterion can be shown to be asymptotically optimal, given the assumptions we have made on the residuals, see e.g. [69] for a discussion. We add this functionality because for many membranes, the simple model used by Okada et al in their work is sufficient, and adding more parameters is only of detriment in such a situation.

B.5 Variance Estimation and Robustness

Once the model satisfying the aforementioned criteria has been found, we simulate new data by drawing at random with replacement from the residuals, and adding them to the fitted values. The best model is then refitted to the simulated data to gain a new estimate of the regression coefficients, which are then used to gain a new estimate of the streaming potential. The bootstrapping algorithm is repeated until a satisfactory number of estimates are made, and the mean and variance are calculated as the sample mean and variance of the bootstrap samples. The mean value estimated from the bootstrapping procedure is taken to be the best estimate of the streaming potential, and the variance is added to the experimental error. A low bootstrap variance indicates that the chosen model gives a robust estimate of the streaming potential.

Appendix C
Thermocell Design

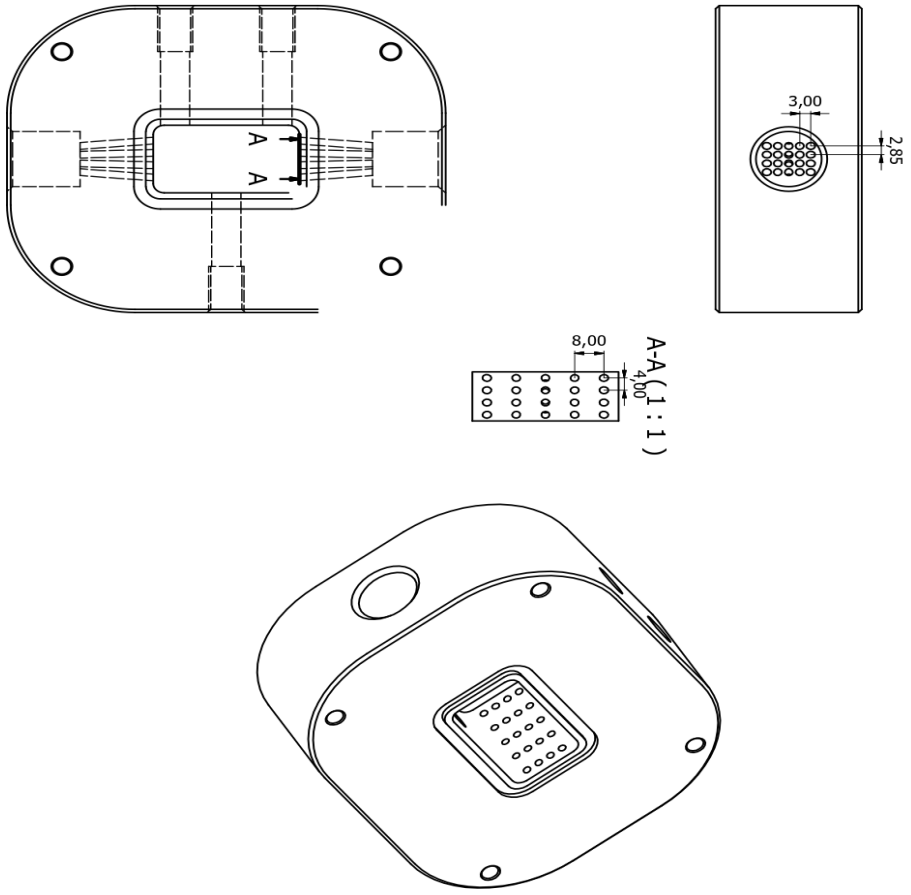

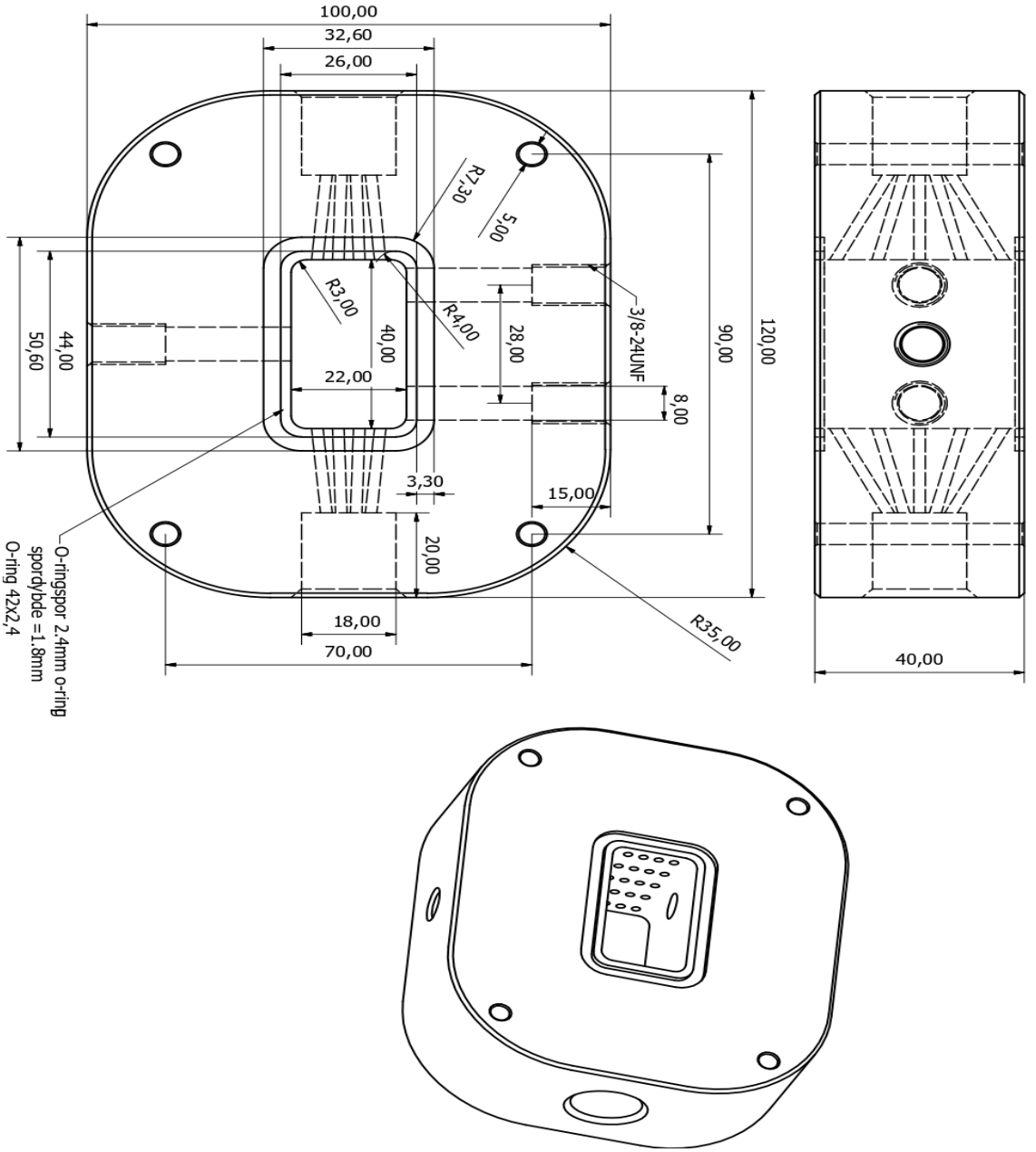
100,00
32,60
26,00
R2,30
5,00
R3,00
R4,00
40,00
28,00
22,00
3/8-24UNF
8,00
90,00
120,00
50,60
44,00
3,30
15,00
20,00
18,00
70,00
R35,00
O-ringspor 2.4mm o-ring
spordybde =1.8mm
O-ring 42x2,4
40,00